



No. 101 – September 2000

## Successful Completion of an Ambitious Project – A Midwinter Night’s Dream

CATHERINE CESARSKY, *Director General of ESO*

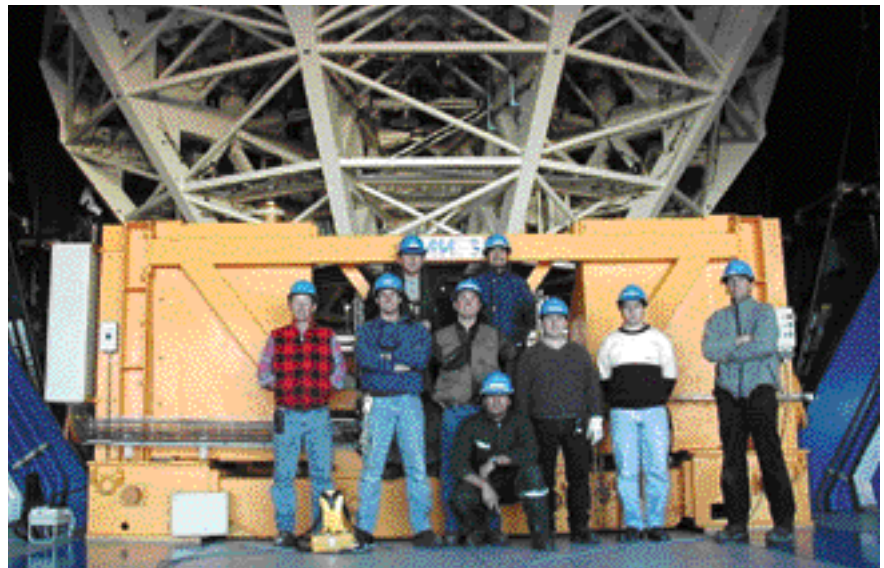
At 21:44 hours on the night of September 3, the test camera at the Cassegrain focus was opened for 30 seconds, and the fourth VLT Unit Telescope, Yepun, saw First Light. A historic event in the life of ESO; this first light marks the successful conclusion of the important period which started with the approval of the VLT project by the ESO Council in December 1987. Exceptionally for such a complex and expensive project, the four VLT telescopes have come into operation ahead of schedule. The VLT is no longer only a project, it is now also an Observatory. The first challenge has been met, thanks to the skill and dedication of astronomers, engineers and technicians at ESO and its collaborating institutes and of many industrial firms throughout Europe: four 8.2-m telescopes of exceptional quality are standing on Cerro Paranal.

The primary mirror arrived at Paranal on April 11, received an aluminium coating in early June, and by the end of July was installed in its cell, ready for use. The secondary mirror followed rapidly; it arrived on August 25th, was coated on the 26th and set in its mount on the 27th. The primary mirror of Yepun is the best of all the large astronomical mirrors polished by REOSC to date, with a surface precision of only 8.5 nanometres. To fully exploit its outstanding optics, we will install the adap-

tive optics instruments, NAOS CONICA and SINFONI, as well as our first laser guide star, on Yepun, rather than on Melipal (UT3) as we had originally planned.

By virtue of becoming ESO’s Director General at the right time, I had the priv-

ilege of actually being in the observing hut of Yepun at the crucial moment, sharing the excitement of the VLT Manager, Massimo Tarenghi, of the Director of Paranal Observatory, Roberto Gilmozzi, and of the members of the commissioning team, Jason Spyromilio,



*Most of the crew that put together Yepun is here photographed after the installation of the M1 mirror cell at the bottom of the mechanical structure (on July 30, 2000). Back row (left to right): Erich Bugueno (Mechanical Supervisor), Erito Flores (Maintenance Technician); front row (left to right) Peter Gray (Mechanical Engineer), German Ehrenfeld (Mechanical Engineer), Mario Tapia (Mechanical Engineer), Christian Juica (kneeling – Mechanical Technician), Nelson Montano (Maintenance Engineer), Hansel Sepulveda (Mechanical Technician) and Roberto Tamai (Mechanical Engineer).*

Krister Wirenstrand and Rodrigo Amestica. It was a cold night, appropriate to the late Chilean winter, and we could hear the wind howling outside. We had chosen our first light target in advance: the planetary nebula He 2-428. In a few minutes, the guide star was acquired, the position and shape of the mirrors were actively corrected, and we could see on the computer screen the unmistakable shape of the source, with an image quality limited only by the atmospheric seeing (0.9 arcsec at the time). The rest of the evening was

spent in the VLT Control room in the appropriate celebratory manner, taking more images, attending to the PR requirements, and drinking champagne with the teams observing on the other telescopes.

Everyone present felt the sense of accomplishment, triumph and elation that always accompanies the culmination of a great human adventure.

Thus did I celebrate the beginning of my second year at ESO. I cannot imagine any better way.

Two important challenges remain for

ESO and for the numerous laboratories throughout Europe with which it collaborates: the completion of the ambitious instrumental programme and of the corresponding data-acquisition, flow and reduction tools, and the development of the VLT Interferometer, the next project on the mountain. Already underway, these will both come to fruition in the next few years.

Finally, the whole ESO scientific community faces the biggest challenge: to make momentous and original discoveries with the VLT!

## ISAAC: 18 Months of Paranal Science Operations

*J.G. CUBY, C. LIDMAN and C. MOUTOU*

### 1. Introduction

ISAAC was offered to the ESO astronomical community on April 1st, 1999, as one of the first two VLT instruments installed at UT1-Antu.

ISAAC (Infrared Spectrometer And Array Camera) is a 1–5  $\mu\text{m}$  imager and spectrometer and has been fully developed by ESO (P.I. Alan Moorwood). Figure 1 shows it mounted on the adaptor/rotator of the Nasmyth B focus. Following integration and extensive testing in Garching, ISAAC was de-

livered to the Paranal Observatory in June 1998, where it was re-assembled and re-tested in the Integration Laboratory prior to installation on the telescope as scheduled. There were two commissioning periods, in November 1998 and in February 1999 (Moorwood et al., 1998; Moorwood et al., 1999).

ISAAC weighs 1.5 tons, is 2 m in diameter and required 3000 drawings for its design. It is made of 15,000 pieces, which were shipped in 40 boxes (30 tons) to Paranal (including laboratory equipment). Its cost amounted to 4.5

MDM, and 50 man-years were needed to build it. It has had, up to now, more than 40 cool-downs, operates at 70 K and uses 11 cryogenic functions. In some operational situations, the telescope field stabilises (i.e. M2 tip-tilt) at 70 Hz with full active optics control, while chopping every second (in the Long Wavelength (LW)), nodding every minute, synchronising M2 and detector while reading out  $10^6$  pixels every 70 ms, and can deliver images as good as, or better than, 0.3 arcsec.

From this, let us make an obvious statement: getting ISAAC to run on sky was a challenge. The instrument and the telescope have to work, the thousands of parameters controlling this complex system have to be fine-tuned. This would not have been possible to achieve without the prior success of the instrument design, development and integration, and the incontestable success of the VLT.

The first year of ISAAC operations was punctuated by a number of technical failures, mainly related to the cryogenic functions (gears, motors, bearings). Fortunately, the impact on the Science Operations could be limited to a minimum. On one hand, most of the problems were temporarily fixed by immediate interventions on the instrument by people from the Instrument Division and/or from Paranal Engineering, and, on the other hand, the flexibility offered by the service mode allowed to run FORS1 instead, hence preserving telescope time. A few visitor runs had however to be re-scheduled, or transferred to service, or cancelled, and only one visitor run (ironically with the visitor being one of the authors of these lines) was affected in real time by a technical failure. In total, no more than about 10 ISAAC nights were lost in one year, the most affected programmes being in the LW domain. In the meantime, the Instrument Division in Gar-

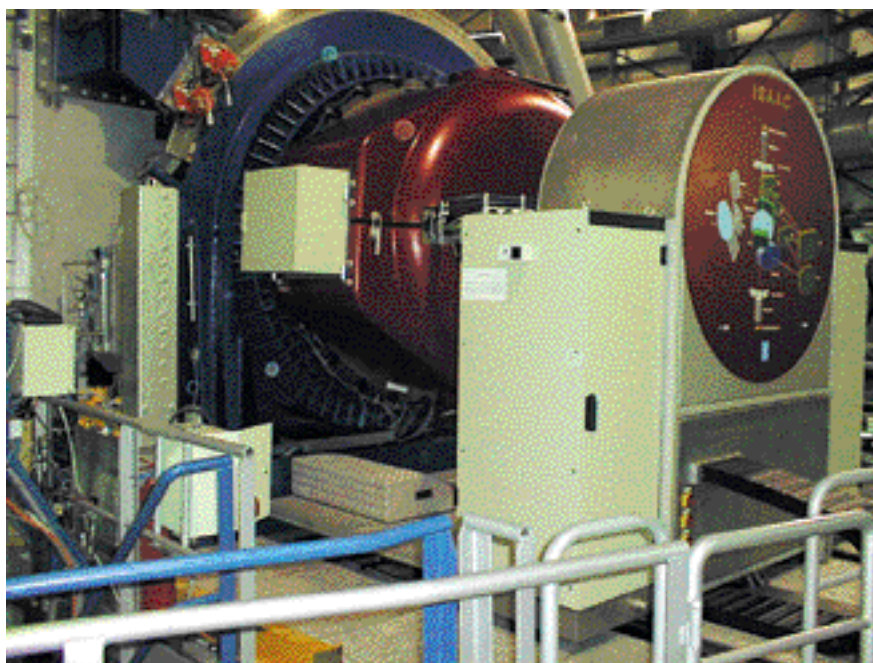


*Figure 1: ISAAC at the Nasmyth B focus of the VLT UT1. The instrument is attached to the adaptor/rotator system and has a total weight of around 1.5 tons. The box at the left contains some of the electronics required for controlling and reading the two infrared array detectors. To the right is the co-rotator system that transfers all the electrical cables and gas hoses for the closed-cycle coolers to the instrument and rotates with it and the adaptor. At each side of the co-rotator are cabinets containing electronics for controlling and monitoring the instrument functions and the vacuum and cryogenic system. Under the vacuum vessel, one can see part of the platform to which the instrument is attached for installation, removal and maintenance activities.*

ching spent tireless efforts to investigate and understand the cause of the problems, and eventually ended up with a new design for the faulty mechanical parts. In February 2000, a major overhaul took place, and these parts were replaced. In addition, the LW detector was upgraded from a  $256 \times 256$  array to an Aladdin  $1024 \times 1024$ , together with a new detector acquisition system. Since then, ISAAC has run quietly without any need for further interventions.

Operating ISAAC is yet another challenge. The performance, as it reaches unprecedented levels, has to be assessed, understood and monitored, scientific needs have to be anticipated, users have to be offered simple, yet powerful, tools, unanticipated situations have to be dealt with, experience from real observations and data reduction has to be fed back as soon as possible while preserving configuration control, and this can only be achieved if the various people involved in the operation chain work together.

In practice, Science Operations started on D-day; many science programmes were completed in visitor and service modes in the very first weeks of operations. Still, many things have been improved since the start of the operations, and the steep learning curve of the first months has now stabilised towards a flatter one. We have learned a lot, optimised accordingly, developed tools to ease the operations and data reduction. All of our first visitors, whenever the weather was on their side, left Paranal enthusiastic about the observatory, the VLT, ISAAC and their data.

We will summarise in this *Messenger* article where we are with ISAAC, from a Paranal perspective, after about 18 months of operations.

## 2. Characteristics and Performance

The main characteristics of ISAAC are summarised in Table 1. There are two channels, one covering the  $[1-2.5]$   $\mu\text{m}$  range (SW) and one covering the  $[2-5.5]$   $\mu\text{m}$  range. In spectroscopy, there are 2 gratings providing low ( $R_s \sim 500$ ) and medium ( $R_s \sim 3000$ ) resolution spectroscopy with a 1-arcsec slit. The highest achievable resolution is  $\sim 10,000$  with a 0.3 arcsec slit. The interested reader can find more information on the capabilities of ISAAC at <http://www.eso.org/instruments/isaac>.

### Sky backgrounds and emissivity

The telescope emissivity was measured in Medium Resolution Spectroscopy at  $\sim 2.5 \mu\text{m}$ , in Narrow-Band imaging at  $3.28 \mu\text{m}$  and in broad band L. With a freshly coated mirror the emissivity is 17%.

Typical backgrounds in  $\text{mag}/\text{arcsec}^2$  are given in Table 2.

**Table 1: Main characteristics of ISAAC**

	Short Wavelength (SW)	Long Wavelength (LW)
Detector	Hawaii $1024 \times 1024$ $2.5 \times 2.5$ arcmin, 0.147 arcsec/pixel	Aladdin $1024 \times 1024$ $1.2 \times 1.2$ arcmin, 0.07 arcsec/pixel
Imaging	21 filters (5 BB, 16 NB) 1 Wollaston prism (+ mask)	6 filters (5 NB, 1 BB (L))
Spectroscopy	$R_s \approx 500$ (Low Resolution, 1 arcsec slit) $R_s \approx 3000$ (Medium Resolution, 1 arcsec slit) 4 slit widths (s): 0.3, 0.6, 1.0 and 2.0 arcsec	

The background between the OH lines was measured and its dependence with the Moon phase was assessed during an eclipse of the Moon (January 2000). The main results are, pending more careful analysis to be described elsewhere:

- In J, the background at  $1.19 \mu\text{m}$  is  $1200 \text{ phot s}^{-1} \text{ arcsec}^{-2} \mu\text{m}^{-1} \text{ m}^{-2}$ , corresponding to a magnitude of  $\sim 18$  in dark sky conditions.

- In H, the background at  $1.70 \mu\text{m}$  is  $2300 \text{ phot s}^{-1} \text{ arcsec}^{-2} \mu\text{m}^{-1} \text{ m}^{-2}$ , corresponding to a magnitude  $\sim 16.5$  in dark sky conditions. This value is 4 times higher than the value reported by Mairaha et al., 1993 as measured in Hawaii.

- At  $\sim 30^\circ$  distance from the Moon, the background between the OH lines increases by a factor 4 to 5 depending on phase.

- At more than  $70^\circ$  from the Moon, there is little dependence on the phase, meaning that the background is almost at its minimum, within a factor of 2.

Background-limited observations between the OH lines require long integration times, above 10–15 minutes of time, and low readout noise. With long integration times, the density of hot pixels increases significantly, and a compromise has to be found between data integrity and purely background-limited performances.

### Efficiency

The overall efficiency, measured as detected electrons to photons incident at the top of the atmosphere varies from  $\sim 20\%$  at  $1 \mu\text{m}$  to  $\sim 30\%$  in K or L, in imaging. In spectroscopy, the efficiency is further modulated by the grating diffraction efficiency, and varies from  $\sim 8\%$  to  $20\%$ , from top of the atmosphere to the detector.

### Image quality, distortion

The image quality in the LW and SW channels is extremely good, from 1 to 1.5 pixels (0.147 arcsec/pixel) all over the array. The field distortion in SW amounts to 2 pixels at the edges and 3.5 pixels at the very corners of the field of view.

### Detector performance

The Hawaii array equipping the SW channel is used in Double Correlated

Readout mode in imaging, and in Non-Destructive Readout mode in spectroscopy. The readout noise varies from less than  $10 e^-$  rms in non-destructive mode to  $\sim 15 e^-$  rms in DCR mode, the dark current is as low as  $0.01 e^- \text{ s}^{-1}$ . The Aladdin array equipping the LW channel is used in Uncorrelated or Double Correlated reads depending on application. The readout noise varies accordingly between 50 and  $100 e^-$  rms. See Finger et al., 2000, for a more detailed description of the ISAAC detectors.

### Spectroscopic detection limits

As a guideline, a detection limit of  $10^{-17} \text{ ergs s}^{-1} \text{ cm}^{-2}$  for emission lines between the OH lines is achievable in just a few hours of time in Medium-Resolution Spectroscopy, depending on wavelength, line width, slit width, etc.

### 2.1 Miscellaneous performance issues

During the course of the first year of operation, we had to live with, or discover a number of issues, most of them intrinsic to the detectors and/or to a cryogenic instrument, for which procedures have been implemented (SW) or are being investigated (LW).

### Short Wavelengths (SW)

- Electrical ghost with the Hawaii array. A feature of this detector is to generate on each line and on the line 512 lines away a bias of constant intensity proportional to the number of counts integrated along the line. This effect has been characterised, and a reduction routine has been implemented (*is\_ghost*, in the *eclipse data* reduction package, Devillard, 1997) and allows to accurately correct for it.

- Persistence effects with the Hawaii array. These persistence effects have some operational consequences (see section 3.1).

**Table 2: Typical backgrounds ( $\text{mag}/\text{arcsec}^2$ )**

Band	J	H	Ks	L	M_NB
Magnitude	16.5	14.4	13.0	3.9	1.2

- The Hawaii array suffers from bias variations with detector integration time and flux. The latter behaviour (together with persistence effects) limits the ability to use dark subtraction techniques as in the visible, but rather encourages one, as usual in the IR, to resort to sky-subtraction data-reduction techniques.

- Some low level (1 to 2 e<sup>-</sup>) 50 Hz pickup noise is occasionally seen, mostly visible in spectroscopy where the background levels are the lowest.

- The Hawaii array also shows fringing, with well-defined Fabry-Perot rings, originating from the sapphire substrate on top of the array. Although very stable, this fringing has a secondary effect, related to the reproducibility of the grating in spectroscopy. If the grating does not reproduce well between consecutive set-ups (even at the level of a fraction of a pixel), the fringing pattern will be slightly displaced, and will not flat field out perfectly, leaving some residuals on the array. In order to circumvent this potentially limiting factor for high S/N observations, we implemented special procedures to take, if deemed necessary, night-time spectroscopic flat fields at the end of the spectroscopic observations.

#### *Long Wavelengths (LW)*

- Aladdin electrical ghosts. Like the Hawaii array, the Aladdin detector, or its associated electronics, also presents some electrical ghosts that are being investigated.

- For still non understood reasons, there is a 'scattering feature' in the LW spectroscopic modes, generating scattered light depending on where the object spectrum lies on the array. Until further evaluation, the problem is simply circumvented by acquiring the target asymmetrically along the slit so as to avoid this scattering feature.

- For the same reason as above regarding the reproducibility of the functions, it is not desirable to move from imaging to spectroscopy during a night. The objective wheel, bearing the 2 objectives in use in these LW modes, will not perfectly reposition, and hence affect the calibrations that can be done at the end or beginning of night.

### **3. Operations**

#### *3.1 General aspects*

ISAAC shares Antu with FORS1, a visible imager and multi-object spectrograph. The observing time at Antu is therefore roughly split between FORS1 in dark time and ISAAC in bright time, pending the arrival of another instrument at the Nasmyth A focus.

ISAAC is operated in service and visitor modes with slightly more time allocated in service mode. The full process of data flow operation is performed by an Instrument Operation Team, gather-

ing people from the various groups involved in Paranal and Garching. The VLT is operated within the Data Flow System (Quinn et al., 2000), and an overview of VLT science operations is given in Gilmozzi et al., 2000.

Operations in visitor mode only involve Paranal, save for data archiving. The high satisfaction of the visitors is in itself a demonstration of the effectiveness of the Paranal Science Operation (PSO) scheme.

A specific aspect of the service-mode operations is that the front and back ends are in Garching (User Support Group (USG) and Quality Control Group (QCG) from the Data Management Division), Paranal Science Operations (PSO) being at the core of the chain. This chain therefore includes persons from different Divisions, 12,000 km away, and working in different time zones. Keeping the information synchronised all along the chain requires constant efforts, and heavy e-mail traffic.

The regular operations on Paranal involve, at minimum, (i) one night astronomer per telescope performing the observations in both visitor and service modes, (ii) one day astronomer for 2 telescopes in charge of supporting the visitors, performing the daytime calibrations, checking the data, and of many other miscellaneous duties, (iii) one Telescope and Instrument Operator per telescope, (iv) one data-flow operator in charge of handling/packing the data and maintaining data flow operations.

In service mode, the users interact with USG and prepare their Observation Blocks (OBs) in advance at their home institute using the Phase II Proposal Preparation tool (P2PP). In addition, users provide readme files and finding charts. The importance of carefully preparing this material cannot be overstated: imagine a long winter night, when the astronomer on duty will typically work 15 hours per night, 10 nights in a row, execute up to 10 service programmes in a night, execute the Calibration Plan accordingly, check the OBs, read the proposals and associated material, perform the acquisitions, start the observations and monitor them all during their execution, check the pipeline reduced data, report on their quality, while writing down in the night log everything happening for any single executed OB, all of that not mentioning possible problems to deal with. In these conditions, the winning User will be the one who has carefully prepared his material and provided the clearest explanations and finding charts. Observations insufficiently prepared are usually returned to the User via the User Support Group, resulting in a waste of time for all, and reducing the chances for this programme to be executed.

The User Support Group generates the queues for every scheduled service period (Medium Term Schedule). The material is then sent to Paranal a few days before the start of the service period. The staff astronomer on duty then browses through the monthly queue and in real time during the night selects the programmes that can be executed. The selection is a human-based process, and essentially relies on common sense, taking into account:

- The priority of the programme. There are three categories of programmes, from A to C, reflecting the ranking given by the OPC. Class A programmes have the highest priority, and all efforts are made to execute and complete them within the constraints specified by the user.

- Distance to the Moon and phase of the Moon constraints as specified by the user. In most cases, the constraints on the Moon are irrelevant in the infrared. There are, however, 2 cases where the Moon constraints are to be taken into account: (i) distance to the Moon is too small, preventing active optics (performed in the optical) to work, (ii) medium-resolution spectroscopy, with increased background between the OH lines.

- Air mass constraint as specified by the user.

- Seeing (understood as the actual image quality) constraint as specified by the user. The seeing, as measured by the Paranal Astronomical Site Monitor (see e.g. Sandrok, 2000, or <http://www.eso.org/gen-fac/pubs/astclim/paranal/asm>) can vary during a night. The seeing variations, although dimmed in the IR, forces one to adapt in real time the Short Term Schedule during a night, and occasionally to abort the running observations if the user-specified constraints are not met.

- Sky transparency constraint as specified by the user (choices are photometric, clear, thin cirrus, thick cirrus).

- Time critical observations (e.g. Targets of Opportunity like Gamma Ray Bursts, Supernovae follow up, monitoring programmes,...)

- Status of a programme. Clearly, the aim is to complete and finish programmes rather than starting them all. Since time allocated in service is over-subscribed (for obvious reasons intrinsic to service observations), this criterion of choice is particularly important and calls for a timely preparation of the observations by the users..

- Persistence effects. The Hawaii array suffers from persistence effects when it is strongly illuminated (see section 2.1). This prevents one from observing in Medium-Resolution Spectroscopy at low flux between the OH lines after imaging of bright, saturated stars (e.g. acquisition of bright standard stars for spectroscopy). This particular problem has led us to enforce

rules regarding the brightness of the targets.

In addition to executing the observations, Paranal Science Operations also performs on-line quality control on the service data: the executed observations are classified as "Completed within constraints", "Not completed within constraints but should not be repeated", "Not completed within constraints and should be repeated". Note that this classification is usually done with ISAAC on the pipeline reduced images, (see section 3.5) or, if not available in case of non supported templates, on the raw images. The Quality Control Group in Garching performs the final Quality Control on fully processed and calibrated frames (see Amico & Hanuschik, 2000).

In visitor mode, the users interact exclusively with Paranal Science Operations for the preparation and execution of their observations, and may also request calibration frames maintained in Garching. They arrive on site two days in advance of their observing run, discuss the observation strategy and prepare their Observation Blocks with the daytime astronomer. They receive their data as tapes or CD-Roms upon their departure from Paranal the day following their last night.

### 3.2 Exposure Time Calculator

Exposure Time Calculators (ETCs) have been developed for all modes of operation of ISAAC, for imaging and spectroscopy, SW and LW.

These exposure time calculators reflect the performance of the instrument. They include an accurate modelling of the sky emission and absorption, including the thermal background above 2.0  $\mu\text{m}$ . Note that we are currently working at compiling a Paranal atmospheric absorption spectrum, whereas the current spectrum used by the ETC comes from a model and is not accurate in terms of depth of the atmospheric features.

The ETC allows simulating objects of different spectral types (continuum, black body, single emission line). It is the entry point to the Phase I Proposal Preparation, and users are requested to use it beforehand to estimate the required exposure time.

These ETCs are available on line at <http://www.eso.org/observing/etc>.

### 3.3 Templates

All observations are executed via templates. ISAAC is equipped with a variety of templates, providing for most observing needs. Excluding the calibration templates (flats, darks, arcs, etc.) the offered ISAAC templates are:

- Imaging. The 'AutoJitter' template automatically generates a random pattern of telescope offsets within a box width that is defined; the

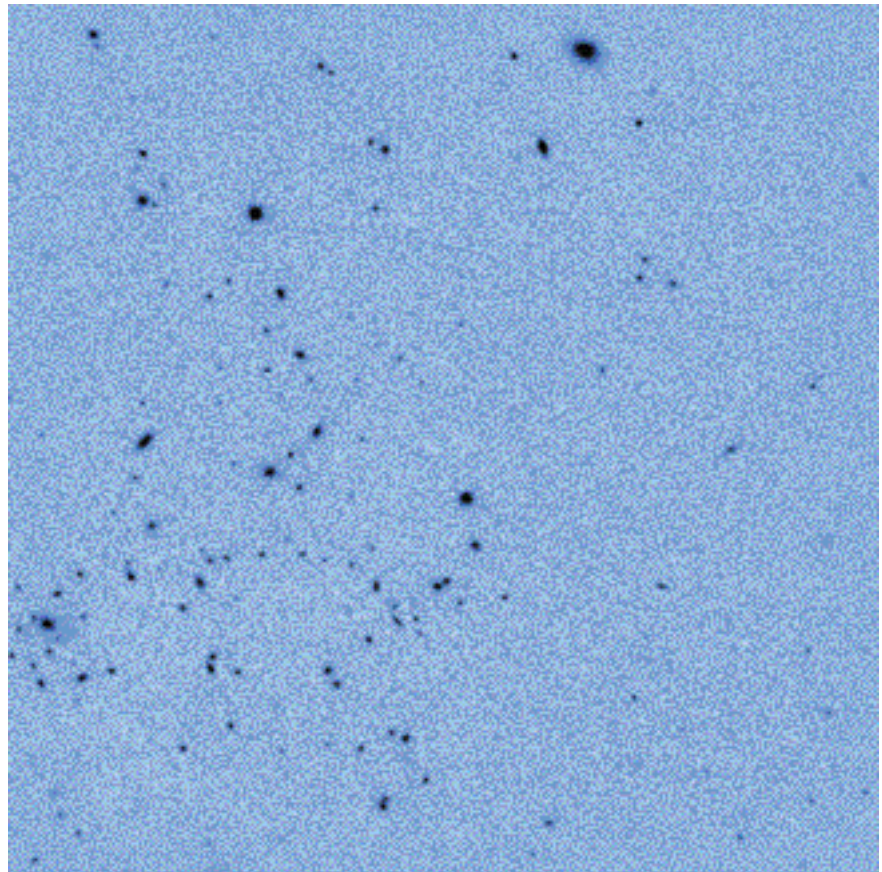


Figure 2: Illustration of the imaging pipeline. A full ISAAC frame resulting from a jitter sequence of 30 images corresponding to 1/2 hour integration on sky in the Ks filter. This is a partial image from a public deep-imaging survey (Franx, 2000). This image is the raw image delivered in a fully automatic way by the pipeline at the telescope a few minutes after the observations were finished.

- 'AutoJitterOffset' template, executes Object-Sky-Sky-Object sequences; the 'GenericOffset' template, allows the user to define any telescope offset sequence either in sky or detector co-ordinates. Note that these templates are constrained so that the Detector Integration Time (DIT) and the filter are fixed for the whole template.

- Spectroscopy. The 'AutoNodOnSlit' template nods the telescope along the slit between two positions separated by a throw defined, with the choice of additional jittering around each position of the nod; the 'GenericOffset' template allows to define any sequence of offsets, along or perpendicular to the slit.

- LW templates combine telescope nodding and chopping in both imaging and spectroscopy for a cancellation of the sky residuals left by the chopping.

Additionally, there is a variety of acquisition templates allowing one to move objects interactively to a particular position on the array, or to centre them in the selected slit. Most of the acquisition procedures rely on subtracting an offset sky image.

### 3.4 Calibration plan

In addition to the scientific observations, calibrations are regularly performed. On a daily/nightly basis (only

when the instrument is used at night), the calibrations are:

- Twilight flat fields in imaging, usually 1 or 2 filter(s) per twilight (broadband only, the narrow-band twilight flats are performed as these filters are used).

- Zero points of the night. At least one standard star is observed nightly in imaging for zero point determination.

- Spectroscopic flat fields. They are performed at the end of the night according to the set-ups used during the night. Flat fields are occasionally taken during the night.

- Arcs. Same as spectroscopic flat fields. In most cases, arcs (at least below 2.2  $\mu\text{m}$ ) are not needed for wavelength calibration, the OH lines providing *in-situ* references for this purpose (see Rousselot et al., 2000, for a detailed atlas of the OH lines measured with ISAAC).

- Darks. They are taken with the Detector Integration Times (DITs) used during the night.

On a less frequent basis, other calibrations are performed, such as:

- Star trace. A star is stepped along the slit, in imaging first, then in spectroscopy for both Low and Medium resolutions. This is used to calibrate the distortion of the spectra as a position along the slit, and to calibrate the geo-

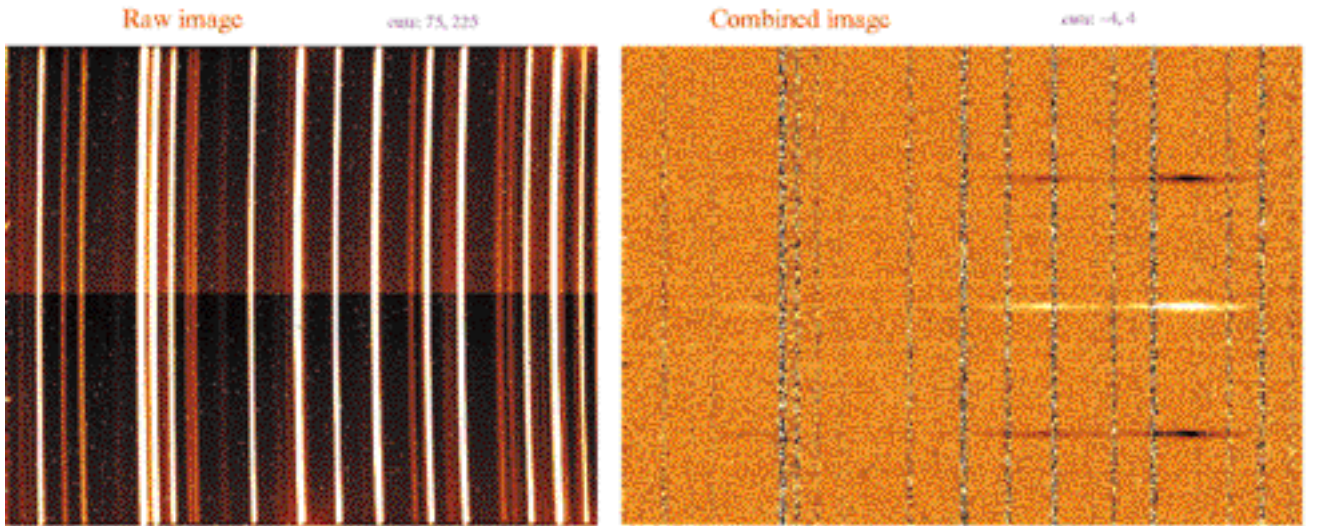
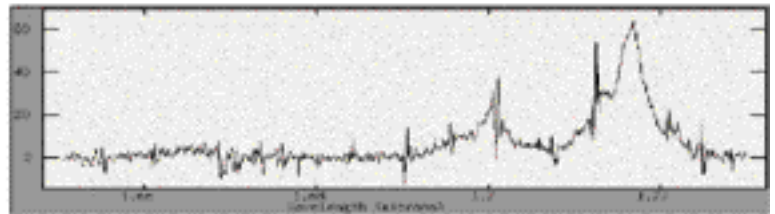


Figure 3: This figure illustrates the ISAAC spectroscopic pipeline 'AutoNodOnSlit' template. This is the spectrum of [OIII]5007/4959 in the  $z = 2.4$  radio galaxy MRC 0406-244. Left: raw image (Medium Resolution Spectroscopy), showing the curved OH lines. Right: fully processed image, showing how well 'double' subtraction works. The OH lines are perfectly subtracted, leaving on the image only the photon shot noise. Bottom: extracted spectrum, showing the variation of the noise where OH lines are present.



metrical transformation between imaging and spectroscopy.

- Illumination frame. A star is imaged at different locations across the array, allowing one to remove low-frequency variations which are not removed by using sky flats.

### 3.5 Data Reduction – Pipeline

Pipelines are supported for the most commonly used templates (non-'generic' ones). The ISAAC pipeline has been developed as a library of C routines, which are available under the eclipse package (Devillard, 1997; see also <http://www.eso.org/eclipse>). The package is also available for off-line data reduction. In the pipeline mode, the frames are classified with a data organiser as they are delivered from the instrument workstation to the pipeline workstation. Whenever a template has finished, the pipeline automatically starts reducing all frames belonging to the template, according to a pre-established recipe.

The aim of these tools is not to provide in all cases ready to publish results. E.g., in spectroscopy, wavelength calibration is not as accurate as it could be. In most cases, the users will need to refine their wavelength calibrations. Still, these tools allow to generate reduced frames to be then analysed with other standard reduction packages (e.g. iraf, midas), for e.g. aperture photometry, accurate wavelength calibration, spectrum extraction, etc.

In imaging, the 'AutoJitter' template is the most common template used. The pipeline performs:

- Dark subtraction, flat fielding and bad pixel correction on each input image if requested.
- Running sky subtraction.  $N$  (user defined) images around each image in the stack are filtered and averaged to produce a running sky which is then subtracted from each input image.
- Sky subtracted images are then shifted and added. The offsets between images are either taken from the image headers, as a user defined list, or automatically found by cross-correlating frames. If offsets are provided, the cross-correlation is run to refine them. The input objects for the offset determination are either user defined, or automatically found. The shift and add process includes image resampling. Various interpolation kernels are available.
- The final image is then averaged, with rejection.

Figure 2 illustrates the capabilities of the imaging pipeline. This image is the absolutely raw pipeline result obtained at the telescope from a jitter sequence of 30 images, and shows how efficient the tool is in reducing data in fully automatic manner.

In spectroscopy ('AutoNodOnSlit' template), the pipeline performs:

- Dark subtraction, flat fielding and bad pixel correction on each input image if requested.
- Grouping and subtraction of images within one AB or BA cycle.

- Distortion correction in the spatial and spectral directions. In the spatial direction, an input calibration file is needed. This file comes from another routine which reduces and calibrates the 'star traces', i.e. the profile of the spectra across the array as a function of the position along the slit. In the spectral direction, the pipeline performs automatically a correction of the slit curvature as measured on the OH lines in the input images. Conversely, an arc frame can be given as input for the slit curvature correction.

- Wavelength calibration from the OH lines automatically found in the input images. Conversely, the wavelength calibration can be performed either from an arc given as input frame, or from a model of the instrument dispersion.

- Combination of A-B and B-A images within one cycle, based on the offset between A and B positions as reported in the image headers. This 'double subtraction' perfectly subtracts out the sky line residuals present on individual A-B or B-A images, thanks to the slit curvature distortion correction that was done in the previous step.

- Averaging with rejection of all doubly subtracted frames belonging to the template.

- Extraction of the brightest spectrum in the image. Optionally, a spectrum can be extracted at some user-defined position.

Figure 3 illustrates the principle of the spectroscopic pipeline.

In addition to the above-mentioned pipeline recipes for the scientific data,

the pipeline also performs a number of tasks related to calibration: dark frame creation and computation of the read-out noise, creation of flat field frames from twilight cubes, automatic computation of the imaging zero points, automatic calibration of the spectroscopic spatial distortions (star trace), automatic computation of the response functions in spectroscopy, etc.

The pipeline has many applications on site, such as faint object identification prior to spectroscopy, on-line quality control, etc. The pipeline is re-run off-line in Garching by the Quality Control Group to reduce the service data (and all calibration data) prior to shipment to the service users. The main difference between the on-line and off-line versions running on the mountain and in Garching is with the calibration data (flat fields, arcs, darks, etc.) that are used.

### 3.6 Miscellaneous facts

After 18 months of operational experience, a few facts emerge.

- The Image Quality with ISAAC is very frequently better than 0.6 arcsec, and often below 0.4 arcsec. The latter allows one to execute programmes in service mode that require superb image quality.

- The on-target overheads (i.e. excluding pre-setting operations) range from ~ 30% in imaging to less than 10% in spectroscopy.

- The open shutter time as a fraction of the night time varies from ~ 40% (imaging, many sources) to more than 80% (spectroscopy, few targets).

### 4. Pending Issues

Nothing is perfect. We still have a few pending issues which are not entirely satisfactory with ISAAC, and we will address them as time and resources permit.

#### Instrument and telescope

- Improvement of the positioning reproducibility of the cryogenic functions.

- The polarimetric mode is for the time being basically non operational. This needs intervention on the instrument.

- There is some vignetting in both imaging and spectroscopic modes, needing to re-align the optical train.

- The image quality across the dispersion correction is not constant, degrading the highest spectral resolution that can be achieved.

- Two filters need to be replaced.

- Residual pick-up noise with the Hawaii array. Occasionally, some 50 Hz pick-up noise pops up in spectroscopic data, with so far no tool to get rid of it.

- The image quality in chopping mode is not stable and occasionally exhibits image elongation. This is under investigation.

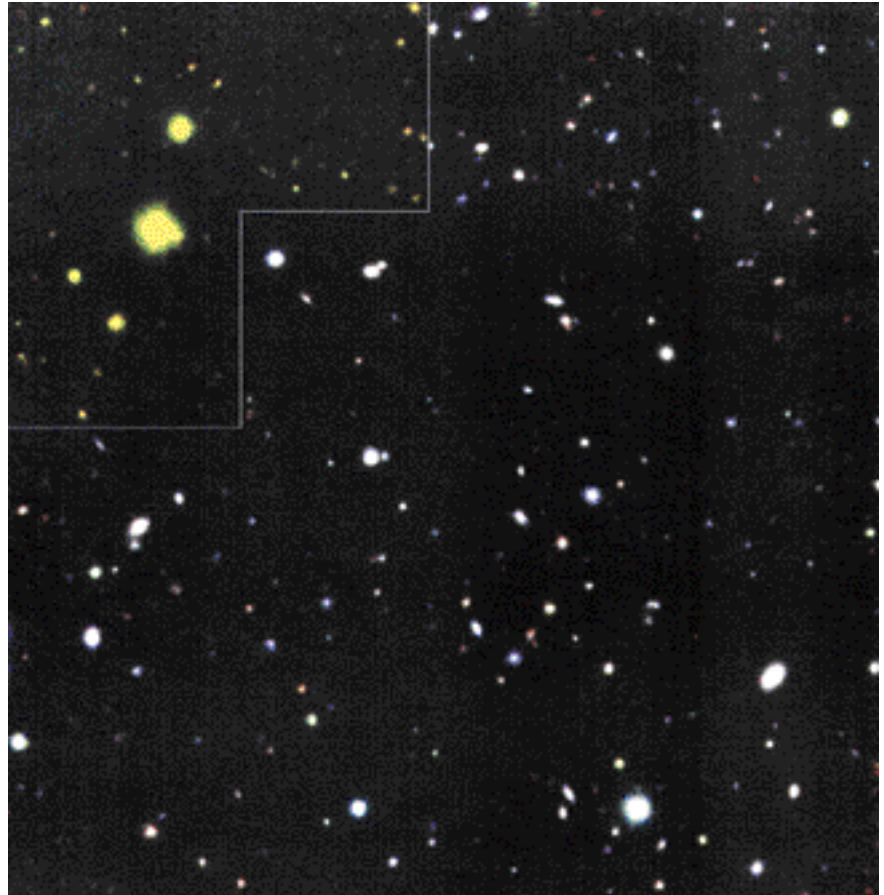


Figure 4: Deep HDFS image from a public survey (Franx et al., 2000). Field is  $2.5 \times 2.5$  arcmin. This is a combined image of HST I images and ISAAC Js (4.7 hrs) and K images (7.45 hrs). Limiting AB magnitudes are  $J \sim 26$ ,  $K_s \sim 25.5$  at  $3\sigma$  (see *The Messenger* No. 99, p. 20).

#### Operations and tools

- Finalise the LW pipeline. The pipeline group in Garching is actively working at developing new recipes, this should be implemented very soon, both on Paranal in pipeline mode and in Garching for data processing of the service data.

- Spectrophotometric calibration of standard stars in spectroscopy. So far, we resorted to existing material available elsewhere. More compilation is needed, as well as dedicated observations if deemed necessary.

- Monitoring statistics. With the implementation of the so-called QC1 (Quality Control 1), it will become easier in the near future to log parameters measured by the pipeline (e.g. Image Quality, Background values in imaging), monitor these parameters and their variations with external parameters (e.g. outside seeing, temperature, etc.) and perform trend analysis.

- Reducing the number of calibrations. Within the execution of the Calibration Plan, we have been so far

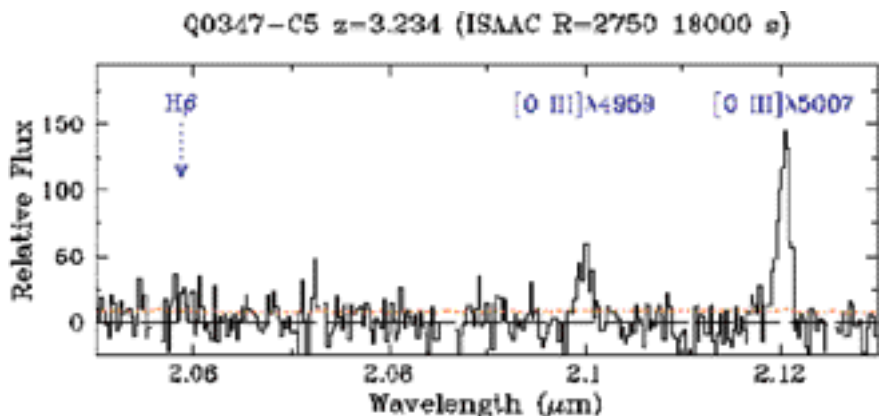


Figure 5: Example of an [OIII] line detection on a galaxy at redshift 3.2. The intensity of the [OIII]/5007 is  $7.10^{-17}$  ergs  $s^{-1} cm^{-2}$ . See Cuby et al., 2000, and Pettini et al., 2000.

very conservative regarding the obtainment of calibration frames. We are aiming at reducing the number of daytime calibration frames produced, e.g., the number of dark frames, usually not of very much use for data reduction, still interesting to monitor instrument performance like readout noise.

- LW operations resumed in June 2000 with a new detector. We are still in a learning curve for optimising the operation and assessing the performance and the calibration needs of this mode, in imaging and spectroscopy. The difficulty is here to carry out this exercise while keeping the instrument fully operational.

## 5. Main Achievements

After almost 18 months of operations, we believe that our main achievements regarding ISAAC operations are:

- Template operations. All templates seem to cover the main requirements from the users. Only in exceptional cases did we have to develop specific templates. The control system is powerful and flexible enough that exceptional requests (e.g. occultation) can usually be accommodated, provided that this is anticipated long enough in advance and iterated upon with Paranal staff. The philosophy adopted for these templates was to hard wire as many parameters as possible (e.g. detector readout mode), so as to limit the number of parameters to be defined by the users, and to simplify the calibrations.

- Calibration Plan. The calibration plan fulfils the needs for the calibration of the instrument and of the science data.

- Automatic generation of daytime calibrations. Sequences of daytime calibrations are automatically generated at the end of the night, based on the FITS header information of the images taken during the night.

- Miscellaneous material provided to the users. Beyond the User Manual, we provide lists of standard stars, atlas of OH and arc lines (to be complemented soon by an atlas of atmospheric absorption lines), library of available IR spectra, etc.

- ETC. The ETC has proved to be reasonably reliable in estimating the performance of the instrument, and all major modes are now supported.

- Pipeline and Data Reduction Tools. Most of the ISAAC modes and/or templates are supported by data reduction tools, running in pipeline, fully automatic mode on Paranal, and available off-line for data reduction. The usefulness of these tools cannot be overstated, both from the user point of view and from the Paranal Operations view. Reduced frames in imaging or spectroscopy allow to assess in real time the quality of the data and determine whether the science goals of the observations are reached.

With the forthcoming addition of some more material for the LW channel in the next months, we believe that we are providing the user community with a self-consistent set of tools and documentation allowing them to use ISAAC in the best of its capabilities for any particular scientific observation.

## 6. Conclusion

After its first year and a half of successful operation at the VLT, ISAAC

has already provided a vast amount of first-class scientific results. See Cuby, 2000, for a presentation of some scientific results obtained in the past year. Figure 4 shows a partial image from a deep, wide-field public imaging programme carried out in service mode with image quality below 0.5 arcsec on the HDFS field, which is described in Franx et al., 2000. Figure 5 shows a Medium Resolution spectrum of a galaxy at redshift 3, illustrating the line detection capabilities between the OH lines.

## References

- Amico P., Hanuschik R., 2000, SPIE 4010 proceedings.
- Cuby J.G., Barucci A., de Bergh C., Emselfem E., Moorwood A., Petr M., Pettini M., Tresse L., 2000, SPIE 4005 proceedings.
- Devillard N., 1997, *The Messenger* No. **87**.
- Finger G., Mehrgan H., Meyer M., Moorwood A., Nicolini G., Stegmeier J., 2000, SPIE 4005 proceedings.
- Franx M., Moorwood A., Rix H.W., Kuijken K., Röttgering H., van der Werf P., van Dokkum P., Labbe I., Rudnick G., 2000, *The Messenger*, No. **99**.
- Gilmozzi R., Leibundgut B., Silva D., 2000, SPIE 4010 proceedings.
- Malhara T., Iwamuro F., Yamashita T., Hall D., Cowie L., Tokunaga A., Pickles A., 1993, *PASP* **105**, 940-944.
- Moorwood A., Cuby J.G., Biereichel P., et al., 1998, *The Messenger*, No. **94**.
- Moorwood A., Cuby J.G., Ballester P., et al., 1999, *The Messenger*, No. **95**.
- Pettini et al., 2000, in preparation.
- Quinn P., Albrecht A., Leibundgut B., Grosbøl P., Peron M., Silva D., 2000, SPIE 4010 proceedings.
- Rousselot, P., Lidman, C., Cuby, J.-G., Moreels, G., Monnet, G., 2000, *A&A*, **354**, p.1134-1150.

# MESSAGE TO THE ESO COMMUNITY: Opening of the VLT Visitor Focus

ESO plans to open on 1 April 2002 a Visitor focus located at a Nasmyth Focus of UT3 (Melipal).

The Visitor Focus has been reserved to permit innovative observations by teams stand-alone instruments, free from a substantial fraction of the requirements for fully automated VLT general-use instruments.

The instruments will be provided by institutes or consortia, and they can be temporarily mounted at the Visitor focus. In addition, this could provide a powerful scientific/technical test bench for new instrumental concepts, eventually incorporated later in standard VLT instruments. The set of guidelines on how to propose and carry out this type of observations can be found at: [http://www.eso.org/instruments/visitor\\_focus/](http://www.eso.org/instruments/visitor_focus/)

Note that the side port of NAOS could also hold a small visitor instrument.

Interested parties should contact the VLT Programme Scientist ([arenzini@eso.org](mailto:arenzini@eso.org)), Instrumentation ([gmonnet@eso.org](mailto:gmonnet@eso.org)) and Paranal ([rgilmozz@eso.org](mailto:rgilmozz@eso.org)).



# The La Silla News Page

*The editors of the La Silla News Page would like to welcome readers of the sixteenth edition of a page devoted to reporting on technical updates and observational achievements at La Silla. We would like this page to inform the astronomical community of changes made to telescopes, instruments, operations, and of instrumental performances that*

*cannot be reported conveniently elsewhere. Contributions and inquiries to this page from the community are most welcome.*

## 2p2 Team News

### Personnel Movements

In June we welcomed José Cortes and Mauricio Martínez to our Operations Team. José was previously a mechanical engineer with a local firm, while Mauricio worked with the US Naval Observatory survey telescope at CTIO.

### Decontamination Monitoring Programme

In May we concluded our Decontamination Monitoring Programme at the Wide-Field Imager (WFI). This campaign was initiated in November 1999, following dismantling of the dewar and cleaning of contaminants on the CCDs. The programme consisted of the weekly collection and measurement of dome flats in UBVRIZ. An analysis of those frames found no decline in the sensitivity of the CCDs, as had been seen during 1999 before the cleaning episode. None of the flat-fields obtained during the 6 months of monitoring show a return of the ring around the mosaic perimeter that is characteristic of contamination.

Furthermore, a comparison of the ratios for consecutive flat-fields in each of B- and R-bands indicates no change in the relative sensitivity to a particular colour. The original contamination problem caused a diminished CCD response in the blue and this is not seen now.

A by-product of this analysis was the confirmation that dome flat-fields for the 2.2-m are quite often non-reproducible. Both high- and low-frequency

structures are seen in roughly two-thirds of all cases when two flat-fields (consecutive in time) are divided. Recent tests indicated some light leakage from the sides of the camera, which has subsequently been made light tight. Observers who take dome flats are urged to compare them to twilight flat-fields to verify their integrity. A full description of the post-decontamination monitoring is posted on the 2p2 Team Web Pages at <http://www.ls.eso.org/lasilla/Telescopes/2p2T/E2p2M/WFI/documents/Decontam/FFofWFI.ps.gz>.

### Servicing of 2.2-m Telescope

In June, the 2.2-m telescope underwent a comprehensive servicing effort that saw improvement in many key areas of its performance. Micrometers were installed in three locations on M1 to see whether movements in M1 position are responsible for the astigmatism seen previously at large zenith distances. The preload gearbox for the right-ascension drive was serviced and a replacement vacuum gauge was mounted in the CCD dewar. At the same time, a new version of the DAISY+ image acquisition software (v. 1.0) was installed, tested and accepted. Elsewhere, software efforts concentrated upon testing the first components of the BOB (Broker for Observation Blocks) interface. An important milestone in this was first movement of the 2.2-m telescope using VLT-compliant commands. The five days of technical time saw a stream of activity on

our telescope by many members of La Silla Teams for Instrumentation, Optics, Mechanics and Software. We are grateful to all of them for their extensive efforts.

### WFI Data Characteristics

Team member F. Selman recently calibrated some images from the WFI camera in terms of their spatial and photometric qualities. The astrometric solution he has derived for the camera shows negligible change in pixel areas on the sky from centre to edge of the mosaic. The colour terms are stable compared to the chip to chip variations seen in all filters. Variations result in photometric errors less than 1 per cent. In terms of the size of the colour terms, the best filter appears to be R, followed by V, U, I, and B. The zero points show systematic variations across all chips, of approximately 8 per cent (peak-to-valley). This study is continuing with additional observations.

### Upcoming Developments

In the coming months, we are looking forward to the commissioning of a new CCD in DFOSC at the Danish 1.54-m. For the 2.2-m, development of the BOB observing interface by members of the La Silla Software and Communications Team continues. The first completed version of this software will commence testing (and usage on a trial basis) during the first few months of Period 66, later this year.

# COSMIC SHEAR WITH ANTU/FORS1: An Optimal Use of Service Mode Observation

R. MAOLI<sup>1,2,3</sup>, Y. MELLIER<sup>2,3</sup>, L. VAN WAERBEKE<sup>2,4</sup>, P. SCHNEIDER<sup>5,6</sup>, B. JAIN<sup>7</sup>,  
T. ERBEN<sup>6</sup>, F. BERNARDEAU<sup>8</sup>, B. FORT<sup>2</sup>, E. BERTIN<sup>2,3</sup>, M. DANTEL-FORT<sup>3</sup>

<sup>1</sup>Dipartimento di Fisica, Università di "Roma La Sapienza", Italy; <sup>2</sup>Institut d'Astrophysique de Paris, France;  
<sup>3</sup>Observatoire de Paris, DEMIRM, France; <sup>4</sup>Canadian Institute for Theoretical Astrophysics, Toronto, Canada;  
<sup>5</sup>Institut für Astrophysik und Extraterrestrische Forschung, Bonn, Germany; <sup>6</sup>Max-Planck-Institut für  
Astrophysik, Garching, Germany; <sup>7</sup>Department of Physics, Johns Hopkins University, Baltimore, USA;  
<sup>8</sup>Service de Physique Théorique, C.E. de Saclay, France.

The measurement of weak gravitational lensing induced by large-scale structures is one of the most challenging programmes for imaging with ground-based telescopes. The VLT, used in Service Mode, offers an exceptional technical configuration which in principle guarantees high-quality data for demanding programmes. The first attempt done in Period 63 turned out to work very well and provides a remarkable data set on a short time-scale as well as first constraints on cosmological models. It demonstrates that the VLT is a perfectly suited telescope for cosmic shear measurements. Moreover, when it is operated in service mode, this is the most competitive ground-based tool which could make a major breakthrough in the field.

## 1. Introduction

At the beginning of 2000, four groups have announced the detection of a "cosmic shear" signal in deep field images. Among those works, one resulted of VLT observations we obtained on UT1/ANTU during its first year of operation. These results produced a strong excitement in the community who realised the fantastic interest of cosmic shear for cosmology.

Light beams emitted by distant galaxies can be altered by the gravitational field of groups, clusters or filaments of (dark) matter they cross during their propagation through the universe. The weak gravitational lensing effects accumulated along a line of sight result in a small distortion of the shape of background galaxies which can be observed on CCD images as a correlated ellipticity distribution of the lensed sources (the cosmic shear).

The properties of these gravitational lensing effects are characterised by an anisotropic deformation (a vector, the gravitational shear,  $\gamma$ ) and an isotropic rescaling (a scalar, the gravitational convergence,  $\kappa$ ). The convergence is

directly related to the projected mass density accumulated along a line of sight. It turns out that in the weak lensing regimes, the shear and the convergence are linearly related.

The analysis of the cosmic shear signal as function of angular scales (between 10 arcseconds to about one degree) has an important scientific potential for cosmology (see Mellier 1999; Bartelmann and Schneider 2000 and references therein). The cartography of the distortion field traced by lensed galaxies can be used to reconstruct the projected mass density and the shape of the power spectrum of the dark matter, without regard to the light distribution. When these mass maps are cross-correlated with galaxy redshift surveys, one can also probe the evolution of the biasing as function of angular scale and its evolution with look-back time. Moreover, the normalisation of the power spectrum and the cosmological parameters can be inferred from the second and third moments of the gravitational convergence,  $\kappa^2(\theta)^{1/2}$  and  $S_3(\kappa)$ , which are also sensitive to cosmological models (Bernardeau et al. 1997):

$$0.01 \kappa_g \approx 0.8 \left( \frac{\theta}{1 \text{ deg.}} \right)^{-\frac{n+2}{2}} z_s^{0.75}, \quad (1)$$

and

$$S_3(\kappa) \approx 40 \kappa_g^{-0.8} z_s^{-1.35}, \quad (2)$$

where  $\kappa_g$  is the normalisation of the power spectrum of density fluctuations, the density parameter and  $z_s$  the redshift of the lensed sources<sup>1</sup>. Therefore, by measuring these two quantities, one can recover  $\kappa_g$  and the normalisation of the power spectrum independently. Setting aside the technical difficulties,

<sup>1</sup>This is the averaged redshift of the lensed sources. Since it is not necessary to get a precise measure of it, one can get a reasonable estimate from photometric redshift of galaxies.

the measurement of the second moment looks in particular an easy task because in the weak lensing regime the variance of the convergence is the variance of the gravitational shear. So, in principle it can be measured directly from the measurement of ellipticities of galaxies.

The expected amplitude of the gravitational distortion is extremely small (the ellipticity induced by weak lensing is only a few per cent) which makes the observations among the most challenging in optical astronomy. Because this programme needs high image quality, the HST seems well suited to study cosmic shear. However, its small field of view cannot realistically survey many fields of view as large as 10 arcminutes over a large fraction of the sky. In contrast, ground-based telescopes can easily observe wide fields and are indeed efficient tools to carry out this type of surveys, provided the data fulfil the following criteria:

- high image quality in order to accurately measure shapes of very faint galaxies,
- deep observations in order to get a high galaxy number density and to minimise Poisson noise on small angular scales,
- a large number of fields spread over a large fraction of the sky, in order to minimise the field-to-field fluctuations produced by cosmic variance,
- a homogeneous data set which permits to obtain the shape of about 100,000 galaxies observed in almost the same conditions and to measure statistical quantities from a homogeneous sample,

which require an optimised design of the observing strategy. Unfortunately, it turns out that classical observing modes of ground-based telescopes are inefficient in providing large amounts of data on a short time-scale. Experienced visitor observers are aware that weather conditions are never stable

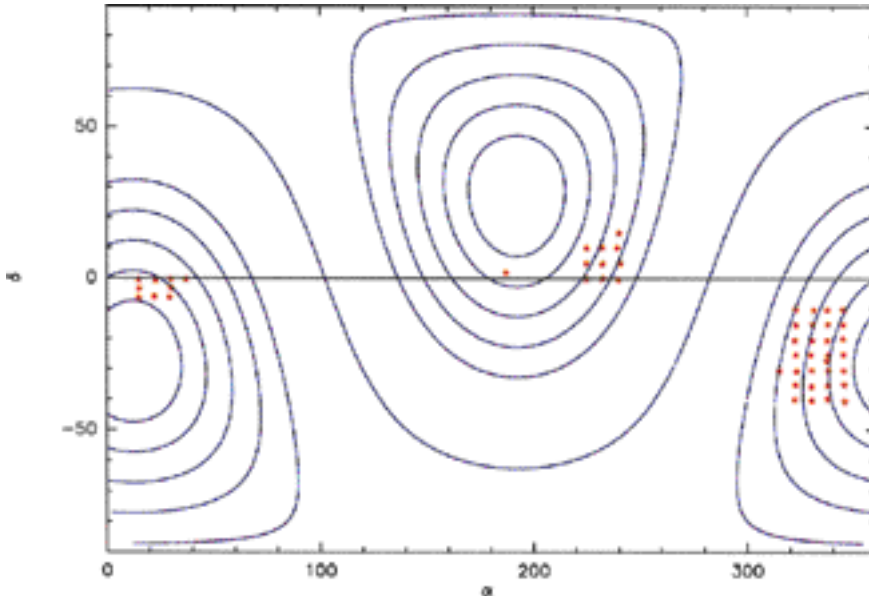


Figure 1: Distribution on the sky of the 50 VLT fields. Continuous lines are for galactic latitudes  $b = 0, \pm 30, \pm 40, \pm 50, \pm 60, \pm 70$ . Contrary to the apparent distribution shown on this figure, the fields are not selected on a regular grid.

enough over a long period to succeed in a survey with demanding constraints. The best strategy is probably Service Mode, where observations are done by a staff of astronomers in charge of scheduling each night depending on the weather conditions and the recommendations of the OPC. When this mode is coupled with a very large telescope and an instrument with high image quality like FORS1, the constraints enumerated above are no longer critical. In fact, this configuration looks perfectly suited for a cosmic shear survey.

## 2. Selection and Observations of the Fields

In Period 63, we proposed to observe  $0.6 \text{ deg}^2$  with FORS1 spread over  $2000 \text{ deg}^2$  of the sky in order to measure the cosmic shear on many uncorrelated fields. Our scientific goals were<sup>2</sup> (1) the detection of cosmic shear on scales below 10 arcminutes, (2) the analysis of the variance of the gravitational shear as a function of angular scale and (3) the acquisition of a very large number of fields in order to minimise the noise contribution due to cosmic variance. We were granted 32 hours in Service Mode and Priority A (programme 63.O-0039A; PI: Mellier). Our specifications were the following:

- observation of a sample of 50 FORS1 fields totalising an area of  $0.6 \text{ deg}^2$ , which is a minimum request in order to get a signal-to-noise ratio higher than 3 on the cosmic shear signal;

- a selection of fields, free of bright stars, over a large part of the sky in order to provide targets for any period during the semester. We pre-selected 120 fields with no bright star or bright/big galaxies. Note that “empty fields” is not a good selection criterion since it would bias the sample towards low-density regions instead of sampling the full mass range of structures in the universe;

- observation in I-band in order to keep the image quality as good as possible. Since we were informed that FORS1 has no fringes with the common broad band filter, I-band was the best choice for the programme. The I-band also offers the possibility to observe during grey or dark time;

- exposure time of 36 minutes per field, split in  $6 \times 6$  minutes individual frames. Each was offset in order to remove bad pixels, cosmic rays, and to produce many different frames for the master flat field. The total exposure time was chosen in order to reach  $l = 24.5$  (5, 3 arcseconds aperture) for the lensed galaxies. We then expected a galaxy number density of about  $40 \text{ arcmin}^{-2}$  per field and an effective redshift distribution with  $z \approx 1$ ;

- observations acceptable during non-photometric nights, since the photo-

metric stability is not critical for the measurement of cosmic shear;

- image quality with seeing lower than 0.8 arcsecond for all exposures.

From an observational point of view, the request for images acceptable during grey time and non-photometric nights, with targets covering the whole semester, eases the scheduling and the set-up of the instrument. The seeing specification is also reasonable when compared to the average seeing on Paranal. Paradoxically, although this programme looks very difficult to implement on ground-based telescopes in visitor mode, it can be easily scheduled and completed by astronomers in charge of service observations.

The preparation of the Observing Blocks (OBs) of  $6 \times 50$  observations was also a new experience and a bit of concern since no one prepared such a large number of targets before. Fortunately, we had experienced most of the problems one year earlier, when we expected to make these observations in service mode with the NTT. For technical reasons this never happened but we had to prepare our targets with a very first version of the Phase II Proposal Preparation interface (P2PP) which forced us to interact with the User Support Group of the Data Division Management (DMD) in charge of P2PP. In order to work closely with the User Support Group, we prepared the files at ESO in Garching, which turned out to be the most efficient way to learn and to improve this interface for survey cases. All our requests and the problems we faced were immediately addressed and fixed very quickly by the DMD. When Period 63 started, the improvements done in P2PP made the preparations of the OBs an easy task. The final sample defined on the OBs is plotted in Figure 1.

Observations were done between May and September 1999 with FORS1. During the semester, we were continu-

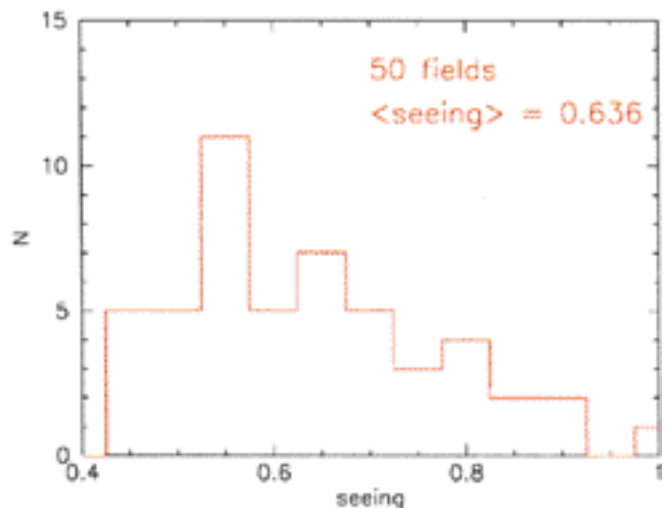


Figure 2: Histogram of the seeing for the 50 final coadded fields.

<sup>2</sup>See a detailed description of our project DESCART at <http://terapix.iap.fr/Descart/Descart-english.html>

ously informed on the status of the observations by monitoring the progress of the observations on the ESO web pages<sup>3</sup>. The comments made for each observation provide some details on the conditions with respect to our specifications, so we had a rather good idea of the success of the programme prior to proceed to thorough investigations at the TERAPIX data centre at the Institut d'Astrophysique de Paris (IAP). The programme was completed in due time by September 1999, and the CD-ROMs containing the data were received at IAP by the end of November 1999.

### 3. Analysis of VLT/FORS1 Data

Each image was overscan corrected, bias subtracted and flatfielded with a superflat computed with the exposures taken during the same night. The FORS1 images are read through four ports readout, so we processed separately the image subsets coming from the four quadrants of the CCD. Then we normalised the gain of each quadrant to obtain an image with a homogeneous background. Finally, we aligned the six individual exposures to produce the final stacked image. An example of one of the 50 FORS1 fields is given in Figure 3.

At this stage, the images are ready for weak lensing analysis. It consists in measuring the ellipticity of all galaxies, correcting their apparent shape for the atmospheric and optical distortions, and then recovering the lensing signature.

The corrections are done assuming that the smearing and the circularisation produced by the atmosphere and the instrument are small. Kaiser et al. (1995, hereafter KSB) have developed an efficient algorithm which expresses the linear corrections and permits to recover easily the lensing signal. If one defines the ellipticity of the source as function of the second moments of the image

$$\mathbf{e} = \left( \frac{I_{11} - I_{22}}{\text{Tr}(I)}, \frac{2I_{12}}{\text{Tr}(I)} \right) \text{ with} \quad (3)$$

$$I_{ij} = \int d^2\beta W(\beta)\beta_i\beta_j f(\beta),$$

then the observed ellipticity can be expressed by the KSB formalism,

$$\mathbf{e}^{\text{obs}} = \mathbf{e}^{\text{source}} + P_\gamma \boldsymbol{\gamma} + P^{\text{sm}} \mathbf{p} \quad (4)$$

where  $\mathbf{e}^{\text{source}}$  is the intrinsic ellipticity of the source,  $P^{\text{sm}}$  is the *smear polarisability tensor* associated with the effects produced by the anisotropic part of the PSF, expressed by  $\mathbf{p}$ , and  $P$  is the *shear polarisability tensor* which expresses the effect of the response of

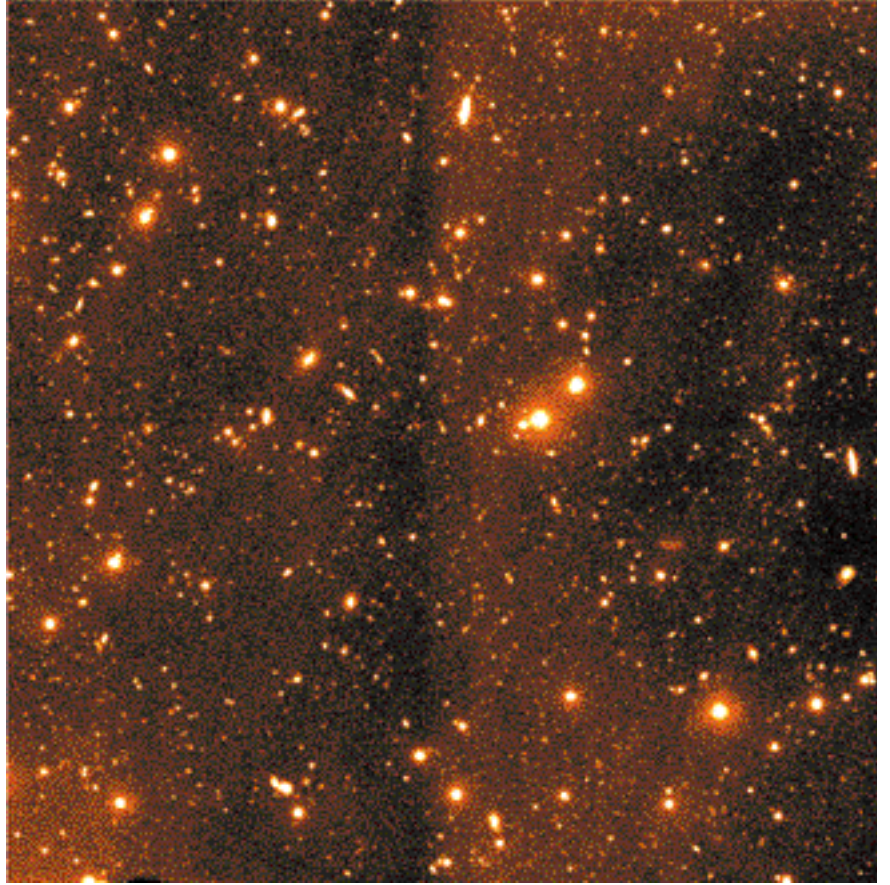


Figure 3: Final coadded image of a VLT field. In this case the FWHM of the stellar images is  $0.53''$ , the source density is  $35.3 \text{ galaxies/arcmin}^2$ , with a  $6.5' \times 6.5'$  field and with 67 unsaturated stars.

a source to a gravitational shear. These tensors are complicated functions which depend on the profile of the light distribution. They can be calculated directly from the image profiles.

Both  $\mathbf{p}$  and  $\boldsymbol{\gamma}$  can be deduced from the data. The former is determined from the field stars, which are not gravitationally distorted and which must be circular objects once corrected for atmospheric and instrumental effects. On the other hand, if we assume that there is no preferred direction for the intrinsic ellipticity of the sources (i.e. the galaxies), then the averaged ellipticity of the sources is  $\mathbf{e}^{\text{source}} = 0$ , and the mean shear at a given angular scale is

$$\boldsymbol{\gamma} = P^{-1} \cdot \mathbf{e}^{\text{obs}} - P^{\text{sm}} \mathbf{p} \quad (5)$$

where the average (and therefore its variance) is computed over the angular scale  $\theta$ .

The selection of stars for PSF correction and the selection of galaxies for the measurement of the gravity-induced ellipticity are obtained by the following sequence (for details, see Figure 4 and van Waerbeke et al. 2000):

1. *Masking*: on each image, we remove the boundaries of the CCD as well as the central cross delineating the four quadrants. Areas around bright

stars, bright galaxies and satellite traces are also removed;

2. *Star selection*: we use a radius<sup>4</sup> vs. magnitude diagram to select unsaturated stars (see Fig. 4). Note that the stars in a given image have all the same radius given by the seeing. Thus, in the diagram, they fall along a thin vertical line (indicated by a red arrow). In the example in Figure 4, their radius  $r_h = 2$  corresponds to a FWHM of 0.8 arcsec with a detector having a scale of 0.2 arcsec per pixel. The stars are selected along the central domain of the thin vertical branch of the diagram where there is no confusion with galaxies and no saturated stars;

3. *Fit of the stellar polarisability tensors*: using stars, we map the PSF by fitting their shape over the CCD with a third-order polynomial;

4. *Shear estimate computation*: using the stellar fits, we compute Eq. 5 for all the sources;

5. *Source selection*: finally, galaxies are selected using the star/galaxy classification defined in SExtractor (Bertin & Arnouts 1996). All objects with ambiguous classification and close pairs of galaxies are removed from the sample.

<sup>3</sup><http://www.eso.org/observing/dfo/p63/vlt/63O0039A.html>

<sup>4</sup>The radius is defined as the radius of stars which includes half the flux,  $r_h$ .

## CORRECTION OF PSF ANISOTROPY FROM STARS

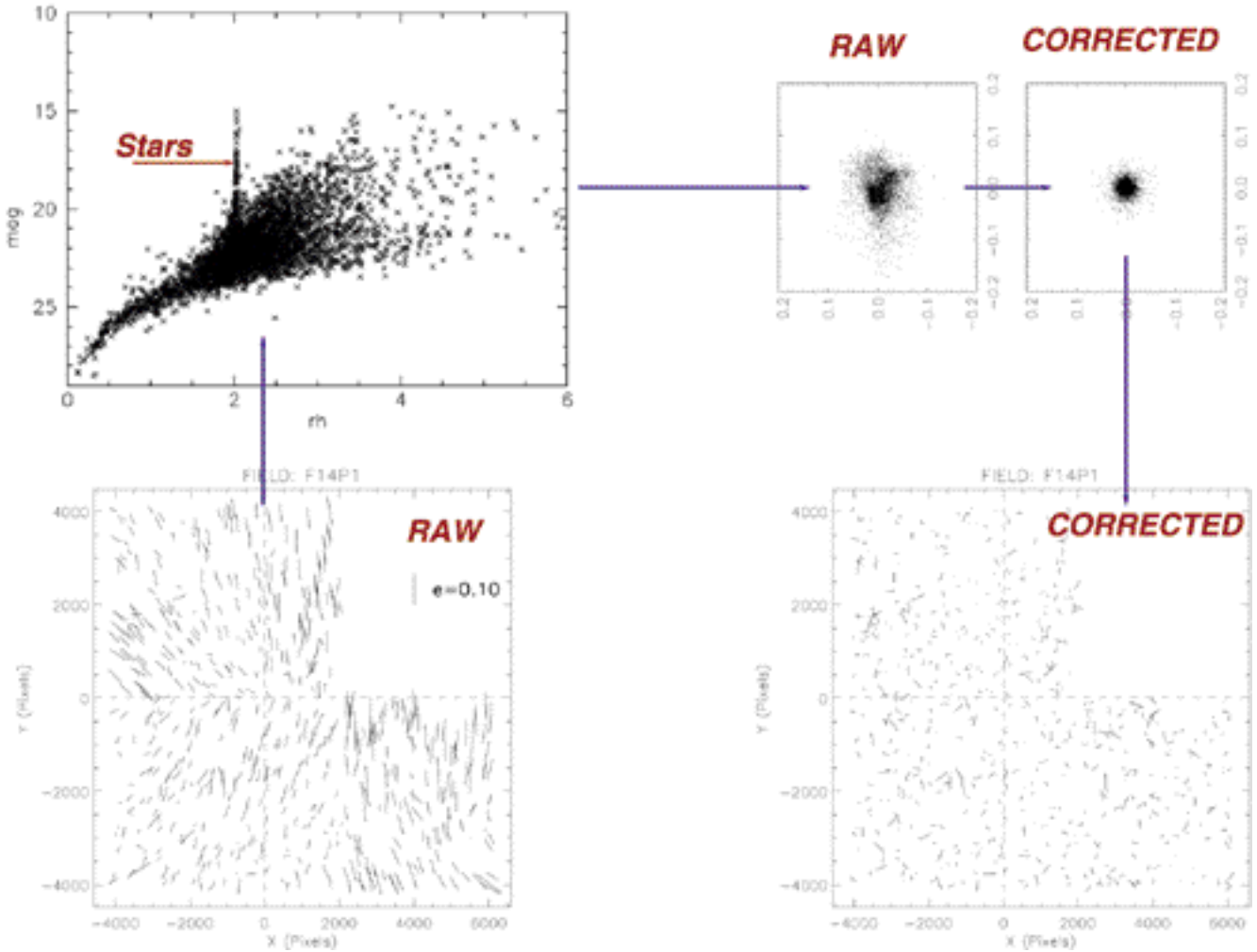


Figure 4: The PSF correction procedure using the stars selected from the  $rh$  vs.  $mag$ . diagram. The bottom-left panel shows the ellipticity of the stars before correction. The lines indicate the position, the elongation and the orientation of each object (this is an example, not a FORS1 field). The automatic identification of the stars is done using the  $rh$  vs.  $mag$ . diagram shown on the top-left panel. The stars can be easily identified from their location along the vertical line. Using the stars, the PSF can be estimated anywhere in the CCD, from which one can recover the corrections to apply. The top-right panel shows the ellipticities of the uncorrected and corrected stars. We usually characterise the shape of objects in the  $(e_1 = e \cos(2\beta), e_2 = e \sin(2\beta))$  plane, where  $e$  is the amplitude of the ellipticity and  $\beta$  the orientation with respect to the horizontal axis. If the correction is well determined, the final distribution should be isotropic with respect to the central position of the panel. The bottom-right panel shows the shape of the stars, once corrected, on the CCD.

In Figure 5 we plot the star ellipticities for all VLT fields before and after the PSF correction. The procedure works very well, except for a few cases which correspond to fields where the image quality is far from our specifications (seeing significantly altered by strong wind). We ended up with 45 fields with in average 60 stars/field (a minimum of 20 and a maximum of 120) and a total number of 58,700 galaxies for 1900 arcmin<sup>2</sup>, that is  $\sim 31$  galaxies/arcmin<sup>2</sup> and 1300 galaxies/field. It is worth noticing that 45 of 50 fields turn out to be very good for the cosmic-shear analysis, which means that the efficiency of the programme in service mode is 90% after 32 hours of service observing. For comparison, in visitor mode on a 4-metre telescope

and assuming 50% of good weather condition (clear night and seeing below 0.8 ), one would need about 25 nights...

### 4. Cosmology with Cosmic Shear

For each final corrected image, we computed the variance of the shear,  $\sigma^2$ , using a top-hat window function with angular diameter varying from one to five arcminutes. Then we averaged  $\sigma^2$  over the 45 fields. In this way we can associate an error to the value of  $\sigma^2$  at a given angular scale. It is important to stress that with 45 fields, we also have a fairly good estimate of the field-to-field fluctuation produced by the cosmic variance.

In Figure 6 we plot our results together with the recent measurements of other cosmic shear surveys. Note the remarkable agreement between the results of the VLT and the results of other programmes conducted with different observational strategies and different instruments. This is a strong indication that the signal is of cosmological nature and not produced by systematic effects.

Prediction from different cosmological models are also plotted in the figure. The joint use of all the data sets puts very tight constraints on the shear amplitude on those scales, in particular with respect to theoretical expectations of the COBE-normalised standard CDM, which is ruled out at a 5- confidence level. This ex-

ample illustrates the potential of cosmic shear for cosmology. The data fit also most popular models, in particular in the range 2–10 arcminutes, where the averaged signal obtained by the various surveys provides a cosmic shear amplitude with very high signal-to-noise ratio. We are indeed very close to be able to constrain also these models.

The observations done with ANTU provide many more random fields than any other cosmic shear surveys done so far, which for the first time permits to beat the noise distribution generated by the cosmic variance. However, the errors are still too large to give precise estimates for the cosmological parameters and for the normalisation of the power spectrum of primordial density fluctuations. Only a larger amount of data will allow to reach this important goal. We have simulated the amount of data one would need in order to increase the signal-to-noise ratio by a factor of 3. It turns out that with 300 FORS1 fields obtained in service mode (that is 250 more fields than what we got, or 160 hours) we could separate the three other models plotted in Figure 6. This number of fields can be reduced to 150 if we use jointly the CFHT data and the other surveys going on at other telescopes.

On a longer time-scale, the observation of weak gravitational distortion of galaxies will be used to reconstruct the power spectrum of the dark matter up to 100 Megaparsec scales.

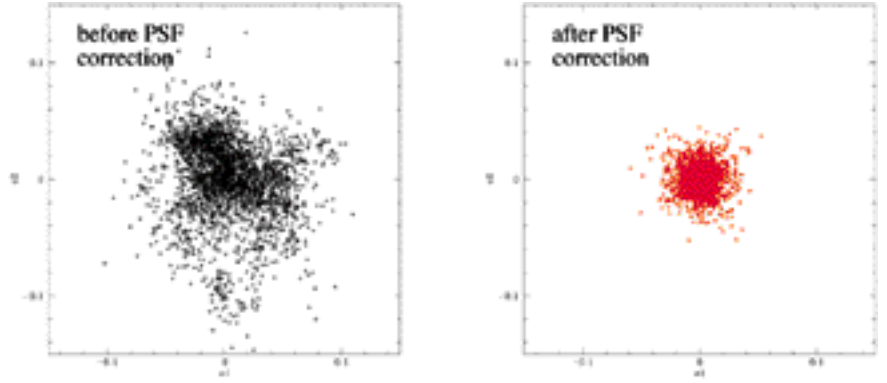


Figure 5: Star ellipticities before (at left) and after (at right) the PSF correction, for all the 45 selected VLT fields. A good PSF correction implies a zero mean value for  $e_1$  and  $e_2$  with small symmetric deviations.

This is a much more difficult project which in particular demands to map angular scales up to few degrees (Figure 6 shows that beyond 10 arcminutes there are discrepancies between the surveys, which express that the signal is very weak). This is beyond the reach of FORS1 which has a rather small field of view. But the WFI at the 2.2-m and maybe VIMOS on UT3, are excellent instruments for such a project. The image quality and performance of VIMOS for a weak lensing survey will be known this fall<sup>5</sup>. If the tests are positive, then this instrument could

<sup>5</sup>see <http://www.astrsp-mrs.fr/vimos/vimos.htm> for preliminary tests.

easily cover degree-scale fields and provide superb data for cosmic shear, if the survey is carried out in service mode.

## Acknowledgements

We thank the team in charge of the service observing at the VLT for performing the observations for us and the DMD for its help to produce the 300 OBs with P2PP. We thank the TERAPIX data centre for providing its facilities to process the FORS1 data. This work was supported by the TMR Network “Gravitational Lensing: New Constraints on Cosmology and the Distribution of Dark Matter” of the EC under contract No. ERBFMRX-CT97-0172.

## References

- Bacon, D., Réfrégier, A., Ellis, R.S. *MNRAS*, submitted (2000).
- Bartelmann, M., Schneider, P. *Phys. Rep.*, in press (2000).
- Bernardeau, F., van Waerbeke, L., Mellier, Y., *Astr. & Astrophys.* **322**, 1 (1997).
- Bertin, E., Arnouts, S., *Astr. & Astrophys.* **117**, 393 (1996).
- Kaiser, N., Squires, G., Broadhurst, T., (KSB), 1995, *Astrophys. J.* **449**, 460.
- Kaiser N., Wilson G. & Luppino G., 2000, *Astrophys. J. submitted*, astro-ph/0003338.
- Maoli, R., Mellier, Y., van Waerbeke, L., Schneider, P., Jain, B., Erben, T., Bernardeau, F., Fort, B., 2000, astro-ph/0008179.
- Mellier, Y., *Ann. Rev. Astr. & Astrophys.* **37**, 127 (1999).
- van Waerbeke, L., Mellier, Y., Erben, T., et al., *Astr. & Astrophys.* **358**, 30 (2000).
- Wittman, D.M., Tyson, A.J., Kirkman, D., Dell’Antonio, I., Bernstein, G. (2000), *Nature* **405**, 143.

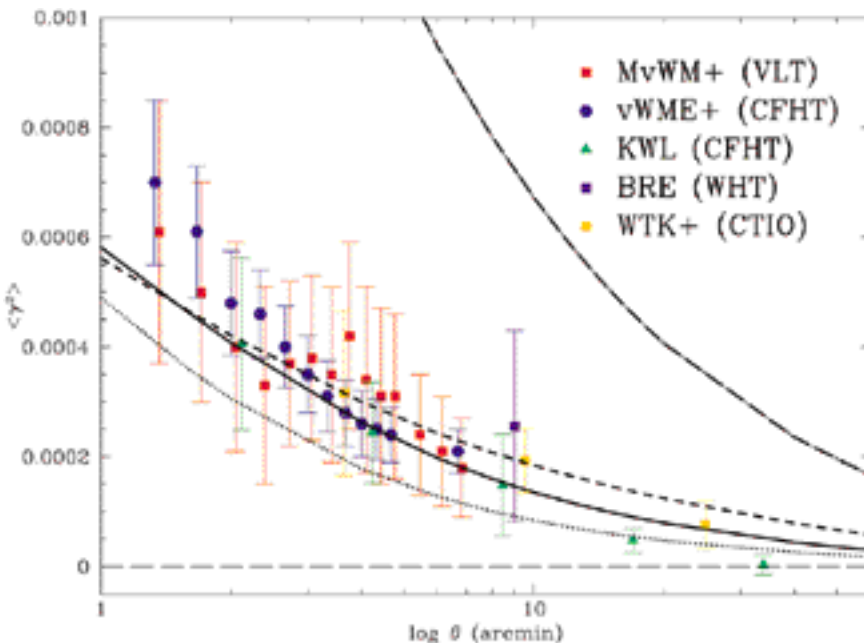


Figure 6: Summary of cosmic shear measurements plotted as function of the angular scale  $\theta$ . The work described here is referred to as MvWM+ (Maoli et al. in preparation; see Maoli et al. 2000), the other results are from van Waerbeke et al. 2000 (vWME+), Kaiser et al. 2000 (KWL), Bacon et al. 2000 (BRE) and Wittman et al. 2000 (WTK+). Some predictions of cosmological models are also plotted, assuming sources at  $z_{eff} = 1$ . The solid line corresponds to  $\lambda$ CDM, with  $\Omega_m = 0.3$ ,  $\Omega_\Lambda = 0.7$ ,  $\Gamma = 0.21$ ; the dot-dashed line corresponds to COBE-normalised SCDM; the dashed line corresponds to cluster-normalised SCDM and the dotted line corresponds to cluster-normalised Open CDM with  $\Omega_m = 0.3$ .

# VLT/ISAAC Images of Quasar Hosts at $z \sim 1.5$

R. FALOMO, Osservatorio Astronomico di Padova, Italy  
 J. KOTILAINEN, Tuorla Observatory, Finland  
 A. TREVES, Università dell'Insubria, Como, Italy

## 1. Introduction

Our present knowledge of quasar host galaxies is essentially limited to  $z < 1$ . Fundamental data come specifically from observations obtained using both Hubble Space Telescope (HST, e.g. Disney et al. 1995; Bahcall et al. 1997; Boyce et al. 1998; McLure et al. 1999) and ground-based 4-m-class telescopes (e.g. McLeod & Rieke 1994, 1995; Taylor et al. 1996; Kotilainen, Falomo & Scarpa 1998; Hutchings et al. 1999; Kotilainen & Falomo 2000; Percival et al. 2000).

Present data indicate that radio-loud quasars (RLQ) are almost exclusively found in galaxies dominated by the bound (spheroidal) component. These luminous ellipticals exceed by  $\sim 2\text{--}3$  mag the typical galaxy luminosity ( $M_H^*$ ,  $\sim -25$ ; Mobasher, Sharples & Ellis 1993), and are close to the brightest cluster galaxies ( $M_H \sim -26$ ; Thuan & Puschell 1989). For radio-quiet quasars (RQQ), the situation is less clear, with both types of hosts found.

The characterisation of the properties of the galaxies hosting the most luminous active nuclei is traditionally hindered by the presence of the very bright nucleus that outshines the faint starlight from its host galaxy. Significant improvements for the detection and the study of the surrounding nebulosities have been obtained with the use of CCD detectors on large telescopes and with a "narrow" point spread function

(PSF) that greatly helps to increase the contrast of the host light superposed to the nucleus.

Moving to high redshift makes the optical light of the nucleus even brighter with respect to the galaxy because of the different intrinsic spectral distributions of host and nucleus while the host galaxy becomes also progressively fainter because of the cosmological dimming of the surface brightness.

In order to cope with these problems, one needs to obtain observations in the NIR with high efficiency and good resolution capabilities. In spite of its superior spatial resolution, HST, with its relatively small throughput with respect to the 8–10-m ground telescopes, may fail to detect faint extended emission with reasonable exposure times. Eight-metre-class telescopes, like the VLT with ISAAC, combine high throughput and (during good seeing conditions) sufficiently narrow PSF to detect and study the underlying nebulosity of quasars. Further improvements are expected to come from the common use of adaptive optics (see e.g. Hutchings et al. 1999) on large telescopes.

In this report we present the results of a pilot study aimed at investigating high  $z$  quasar hosts of a sample of radio-loud and radio-quiet quasars with redshift  $1.0 < z < 2.0$ , and  $-25.5 < M_V < -28$ . High-resolution images, obtained with the VLT and ISAAC of three RLQs at  $z \sim 1.5$  are shortly discussed (see Falomo, Kotilainen and Treves 2000 for more details). We use  $H_0 = 50$  km s $^{-1}$  Mpc $^{-1}$  and  $q_0 = 0$ .

## 2. Observations, Data Analysis, and Results from Individual Objects

NIR  $H$ -band ( $1.65 \mu\text{m}$ ) images of the quasars were obtained at Paranal, using ISAAC (Infrared Spectrometer And Array Camera; Moorwood et al. 1998) mounted on the VLT unit telescope ANTU (UT1). The SW arm of ISAAC is equipped with a  $1024 \times 1024$  px Hawaii Rockwell array, with pixel scale  $0.147$  px $^{-1}$ , giving a field of view  $150 \times 150$  arcsec (corresponding to  $\sim 1.8$  Mpc at  $z = 1.5$ ). The observations were performed in service mode during the nights of 20 and 21 October 1999. Each quasar was observed for a total integration time of 1 hour using a jitter procedure and individual exposures of 2 minutes per frame. The jittered obser-

vations were controlled by an automatic template (see Cuby 2000), which produced a set of frames slightly offset in telescope position from the starting point. The seeing was excellent during the observations, resulting in stellar FWHM of 0.50, 0.41 and 0.38 in the fields of PKS 0000-177, PKS 0348-120 and PKS 0402-362, respectively.

In order to determine the amount of extended emission around the quasars, one needs to perform a detailed study of the PSF. The relatively large field of view of ISAAC ( $\sim 2.5$ ) allowed us to perform a reliable characterisation of the PSF. For each field, we analysed the shape of many stellar profiles and constructed a composite PSF, whose brightness profile extends down to  $\mu_H = 24.5$  mag arcsec $^{-2}$ . This warrants a reliable comparison between the luminosity profile of the quasars and of the stars without requiring extrapolation of the PSF. The shape of the PSF profile was found to be stable across the field of the images (see Figure 1).

For each quasar, we have derived the azimuthally averaged fluxes excluding all regions around the quasars contaminated by companion objects. This procedure yielded the radial luminosity profile out to a radius where the signal became indistinguishable from the background noise (typically  $\mu(H) \sim 24$  mag arcsec $^{-2}$ , reached at  $\sim 2$  distance from the nucleus). Modelling of the luminosity profile was then carried out using an iterative least-squares fit to the observed profile, assuming a combination of a point source (PSF) and an elliptical galaxy convolved with the proper PSF.

Absolute magnitudes have been K-corrected (at this  $z$  K-corr is  $< 0.2$  mag in  $H$ ), using the optical-NIR evolutionary synthesis model for elliptical galaxies (Poggianti 1997).

In Figure 2, we show the final images of the three quasars together with their PSF-subtracted images. The PSF scaling factor was adjusted in order to prevent strong negative values in the few central pixels of the residual image. Although this method tends to over-subtract the point source, it gives us a model-independent way to analyse the surrounding nebulosity. After subtraction of the scaled PSF, two out of the three quasar images exhibit clearly extended emission and suggest the presence of knotty structure. For one quasar (PKS 0402-362), only marginal extended emission is detected.

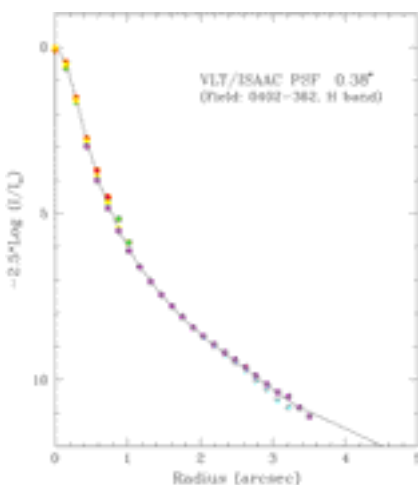


Figure 1: The azimuthal averaged brightness profiles of stars in the field of PKS 0402-362 compared with the PSF model used. The seeing in this frame (UT1+ISAAC, 1 hour total integration,  $H$  filter) is  $0.38''$ .

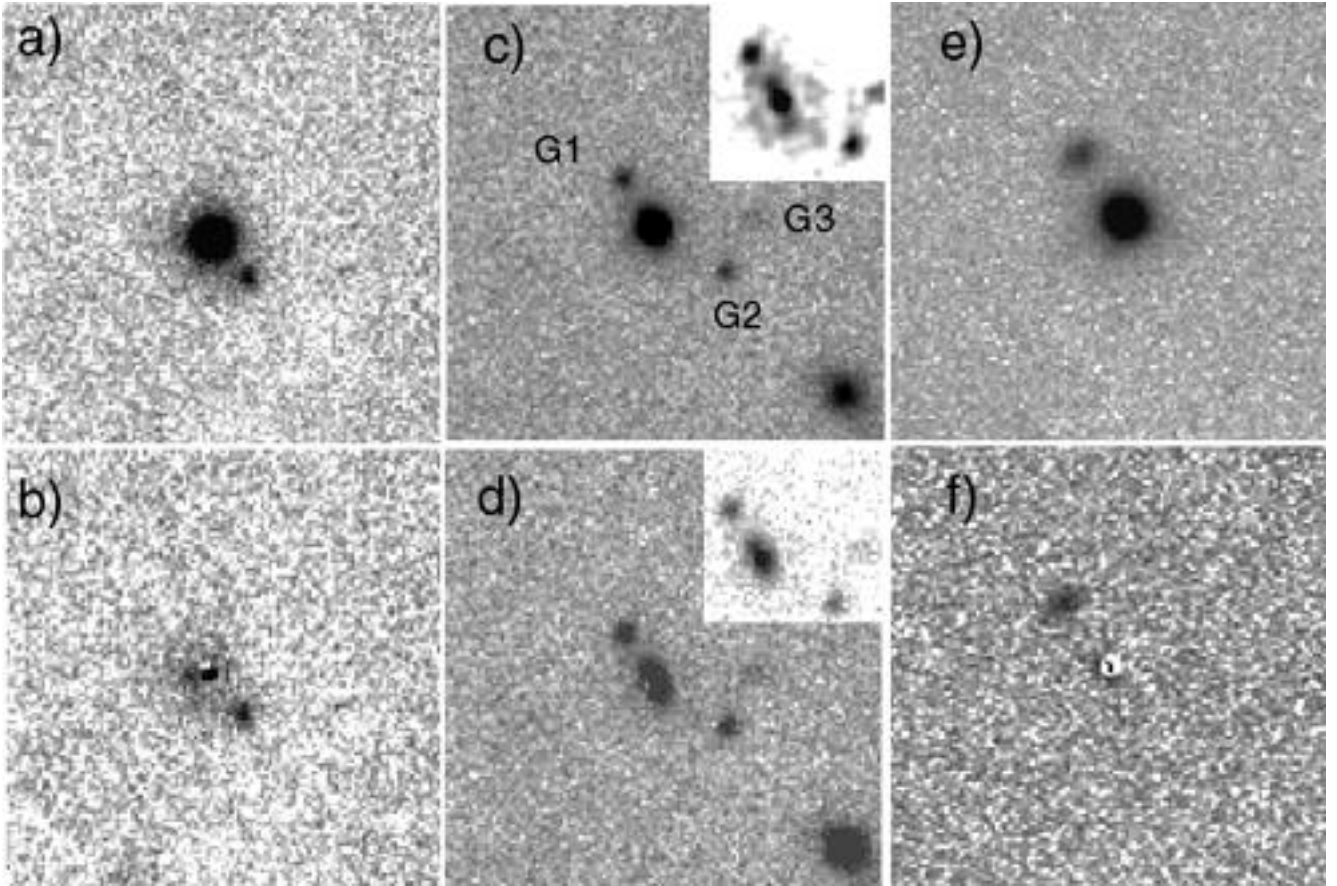


Figure 2: H-band images of the three quasars before (top) and after (below) subtraction of a scaled PSF (see text). From left to right: a), b) PKS 0000-177, c), d) PKS 0348-120 and e), f) PKS 0402-362. The full size of the images in each panel is  $\sim 17''$ . North is to the top and east to the left. The inset in panel c) shows the result of a deconvolution of the image. The inset in the panel d) yields a different grey-scale of the central portion of the PSF subtracted image in order to enhance the knot structure.

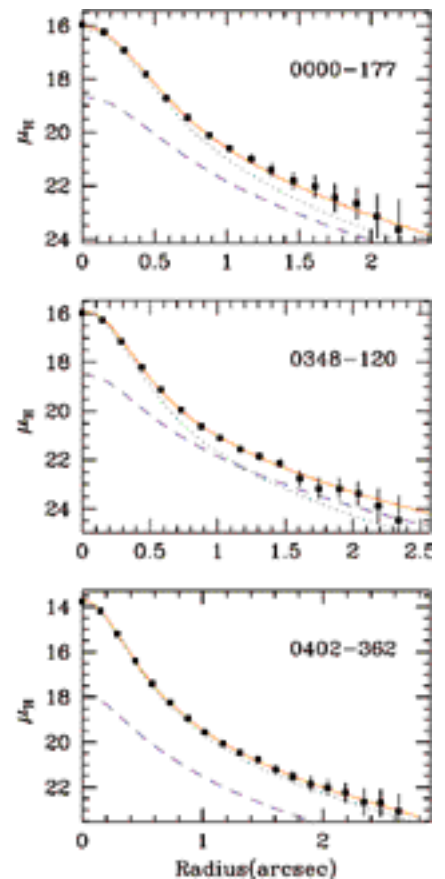
**PKS 0000-177** ( $z = 1.465$ ) is located at  $\sim 4''$  NW from a  $m_H \sim 14.5$  mag star which, although well separated from the quasar, has been subtracted from the final image to avoid confusion. In our H-band image (Fig. 2a), the QSO appears round and compact with a companion object ( $m_H = 20.3$ ) at  $1.8''$  SW. After removing this companion, we note faint “arc-like” structures to the NE and SW at  $\sim 1.5''$  from the nucleus. After subtraction of a scaled PSF at the position of the quasar nucleus (Fig. 2b), some extended nebulosity is clearly detected together with a faint knot at  $\sim 0.6''$  E of the nucleus. After masking the companion,  $1.5''$  SW of the nucleus, we derived the brightness profile (Fig. 3) that exhibits a significant excess over the PSF, starting at  $\sim 1''$  ( $12$  kpc) radius from the nucleus. Model fit of the profile yields  $M_H = -27.4$  and effective radius  $R_e \sim 3.5$  kpc for the elliptical host. Assuming the redshift of the companion is that of the quasar, the projected distance of the companion galaxy is  $\sim 21$  kpc while its absolute magnitude is  $M_H = -25.8$ .

**PKS 0348-120** is a flat-spectrum radio quasar at  $z = 1.520$  (Wright et al. 1983). The H-band image of the quasar (Fig. 2c) is clearly extended and elongated approximately along the NE-SW

direction. A resolved companion galaxy (G1) with  $m_H = 20.5$  lies at  $2.2''$  NE from the quasar. The projected distance of this galaxy, if at the redshift of the quasar, is  $27$  kpc. Other fainter galaxies, G2 and G3 respectively ( $m_H = 21.1$  and  $m_H = 22.2$ ), are located at  $3.2''$  ( $39$  kpc) SW, and at  $3.9''$  ( $43$  kpc) W of the quasar.

From fitting the radial brightness profile (Fig. 3) we obtain a very luminous ( $M_H = -27.6$ ) and compact ( $R_e = 4.9$  kpc) host galaxy. The profile is not smooth, suggesting the presence of substructures in the host that are revealed in the PSF subtracted image. A knot at  $0.7''$  ( $8.6$  kpc) from the nucleus along the direction of G1 is visible in Figure 2d. This feature is clearly seen in the deconvolved image of the quasar (see inset in Fig. 2d) using a Lucy-Richardson algorithm implemented in IRAF (Lucy 1991) with 15 iterations.

Figure 3: The observed radial brightness profiles in the H band of the three quasars (filled squares), superimposed to the fitted model consisting of the PSF (short-dashed line) and the elliptical galaxy (long-dashed line). The red solid line shows the total model fit.



With the present data, it is not possible to clarify the nature of this circumnuclear emission knot. Most likely, it is another small companion galaxy projected onto the envelope of the quasar host.

**PKS 0402-362** is at about the same redshift ( $z = 1.417$ ) as the other quasars in this study, but the nucleus is  $\sim 2$  mag brighter. The H-band image of this quasar is shown in Figure 2e. The nuclear luminosity is very high,  $M_H = -30.6$ , and it out-shines the light from the host galaxy. Using azimuthally averaged radial brightness profile, we substantially improved the signal-to-noise and found a small excess of light over the PSF starting from 1 distance from the nucleus (Fig. 3). Modelling of this profile suggests a host luminosity of  $M_H = -27.7$  and scale-length  $R_e \sim 4$  kpc. However, since it is small, we consider this only a marginal host detection.

Also in this case we detect a companion galaxy ( $m_H = 19.5$ ; 2.8 NE) close to the quasar. Its projected distance is 34 kpc, and if at the redshift of the quasar it would be very luminous ( $M_H = -26.6$ ; only 1 mag fainter than the quasar host). Note, however, that the optical spectrum of the quasar exhibits a weak absorption system tentatively identified as MgII 2800 Å at  $z = 0.797$  (Surdej & Swings 1981) which, if associated with the companion galaxy, would lead to a reduced  $M_H = -24.5$ .

### 3. Discussion and Conclusions

We have shown that NIR high-resolution imaging obtained with VLT/ISAAC is able to detect extended emission around the active nucleus of distant quasars. These images allow us to characterise the host properties and to investigate their close environment.

The derived NIR host luminosities of these quasars ( $M_H \sim -27.5$ ) are very bright and correspond to galaxies  $> 2$  mag brighter than  $M^*$  ( $M_H = -25$ ; Mobasher et al. 1993). The nuclei are  $\sim 1.5$  mag ( $\sim 3$  mag for PKS 0402-362) more luminous than their host galaxies. The scale-length of the hosts ranges from 3 to 5 kpc and appears to be smaller than those observed in low ( $z < 0.5$ ) and intermediate ( $0.5 < z < 1$ ) redshift quasar hosts (e.g. McLeod & Rieke 1994; Taylor et al. 1996; McLure et al. 1999; Kotilainen et al. 1998; Kotilainen & Falomo 2000), which typically have scale-lengths of  $\sim 10$  kpc.

The luminosities of the host galaxies of our three RLQs are very similar to those of high-redshift 6C radio galaxies (RG) studied by Eales et al. (1997). In their Hubble diagram, RGs at  $z \sim 1.5$  have K-band magnitude  $\sim 18.5$ , while we find  $\langle m_K(\text{host}) \rangle \sim 18.3$  (assuming  $H-K = 0.2$ ). The similarity with high  $z$  RGs is also supported by the knotty structure observed in the hosts of two of the quasars and in the density of the immediate environment (e.g. Best, Longair and Röttgering 1997).

These results underline an evolutionary scenario for RLQ and RG hosts that appears significantly different from that of RQQ hosts. In fact, a recent study of RQQs at  $z \sim 1.8$  and  $z \sim 2.7$ , performed with HST and NICMOS in the H-band, was able to resolve 4 out of 5 RQQs (Ridgway et al. 2000). The deduced host luminosities appear 1–2 mag fainter than those found in our RLQ hosts and in the 6C RGs (Eales et al. 1997), and are similar to  $M^*$ . This suggests that the systematic difference of host luminosity between RLQs and RQQs, already noted at low redshift (e.g. Bahcall et al. 1997 and references therein), is even more significant at higher redshift, indicating a different formation and/or evolutionary history of the two types of AGNs.

Some models of galaxy formation and evolution based on hierarchical clustering (e.g. Kauffmann & Haehnelt 2000) predict progressively less luminous host galaxies for quasars at high redshift. This seems to be in agreement with the observations of high  $z$  RQQ hosts (Ridgway et al. 2000; Hutchings 1995), which may still be undergoing major mergers to evolve into the low redshift giant ellipticals but contrasts with our results on high  $z$  RLQs and with previous indications that RLQ hosts at  $z = 2-3$  are extremely luminous (Lehnert et al. 1992).

The large-scale environments of the three quasars observed do not appear particularly rich in galaxies with respect to the background. There is no evidence of a rich cluster of galaxies around any of the quasars. However, in all three cases we have detected a companion galaxy of  $m_H \sim 20 \pm 1$  at a distance from the quasar  $< 3$  (40 kpc). Close companion galaxies around quasars have been noted since the first systematic imaging studies of quasars (e.g. Hutchings & Neff 1990; Hutchings 1995; Bahcall et al. 1997; Hutchings et al. 1999) and spectroscopic investigations have shown that, at least in the case of the closest companions, they are often galaxies at the

redshift of the quasars (e.g. Heckman et al. 1984; Ellingson et al. 1994; Canalizo & Stockton 1997). These companions are often taken as evidence for interactions with the host and possible trigger of the nuclear activity but their effective role on the QSO phenomenon is far from being understood.

### References

- Bahcall, J.N., Kirhakos, S., Saxe, D.H., Schneider, D.P., 1997, *ApJ* **479**, 642.  
 Best P.N., Longair M.S. and Röttgering H.J.A. 1997 *MNRAS* **292**, 758.  
 Boyce, P.J., Disney, M.J., Blades, J.C. et al., 1998, *MNRAS* **298**, 121.  
 Canalizo, G., Stockton, A., 1997, *ApJ* **480**, L5.  
 Cuby, J.G., 2000, ISAAC user manual, ESO.  
 Disney, M.J., Boyce, P.J., Blades, J.C., et al., 1995, *Nature* **376**, 150.  
 Eales, S., Rawlings, S., Law-Green, D., Cotter, G., Lacy, M., 1997, *MNRAS* **291**, 593.  
 Ellingson, E., Yee, H.K.C., Bechtold, J., Dobrzycki, A., 1994, *AJ* **107**, 1219.  
 Falomo R., Kotilainen J., and Treves A. 2000, *ApJ*, in press.  
 Heckman, T.M., Bothun, G.D., Balick, B., Smith, E.P. 1984, *AJ*, **89**, 958.  
 Hutchings, J.B., Neff, S.G., 1990, *AJ* **99**, 1715.  
 Hutchings, J.B., 1995, *AJ*, **109**, 928.  
 Hutchings, J.B., Crampton, D., Morris, S.L., Durand, D., Steinbring, E., 1999, *AJ* **117**, 1109.  
 Kauffmann, G., Haehnelt, M., 2000, *MNRAS* **311**, 576.  
 Kotilainen J.K., Falomo R., 2000, *A&A*, in press.  
 Kotilainen J.K., Falomo R., Scarpa R., 1998, *A&A* **332**, 503.  
 Lehnert, M.D., Heckman, T.M., Chambers, K.C., Miley, G.K., 1992, *ApJ* **393**, 68.  
 Lucy, L., 1991, *ST-ECF Newsletter* **16**, 6.  
 McLeod, K.K., Rieke, G.H., 1994, *ApJ* **431**, 137.  
 McLeod, K.K., Rieke, G.H., 1995, *ApJ* **454**, L77.  
 McLure, R.J., Kukula, M.J., Dunlop, J.S. et al. 1999, *MNRAS* **308**, 377.  
 Mobasher, B., Sharples, R.M., Ellis, R.S., 1993, *MNRAS* **263**, 560.  
 Moorwood, A. et al. 1998, *The Messenger* **94**, 7.  
 Percival, W.J., Miller, L., McLure, R.J., Dunlop, J.S., 2000, *MNRAS*, in press.  
 Poggianti, B.M., 1997, *A&AS* **122**, 399.  
 Ridgway, S., Heckman, T., Calzetti, D., Lehnert, M. 1999, *Lifecycles of Radio Galaxies* (eds. J. Biretta. et al.), New Astronomy Reviews (astro-ph/9911049).  
 Surdej, J., Swings, J.P., 1981, *A&AS* **46**, 305.  
 Taylor, G.L., Dunlop, J.S., Hughes, D.H., Robson, E.I., 1996, *MNRAS* **283**, 930.  
 Thuan, T.X., Puschell, J.J., 1989, *ApJ* **346**, 34.  
 Wright, A., Ables, J.G., Allen, D.A. 1983, *MNRAS* **205**, 793.

# Type Ia Supernovae, Cosmology and the VLT

C. LIDMAN, *European Southern Observatory, Santiago, Chile*

A. GOOBAR, *University of Stockholm*

R. PAIN, *LPNHE, CNRS-IN2P3 and University of Paris VI & VII*

## 1. Type Ia Supernovae and Cosmology

Over the last decade, two international teams have used the magnitude-redshift relation of type Ia supernovae (SNe) to measure the mass density  $M$  and the cosmological constant of the universe. Both teams, using largely independent data sets and independent analysis methods, reach the conclusion that the cosmological constant is non-zero and that the expansion of the universe is accelerating (Riess et al. 1998, Perlmutter et al. 1999).

These results were derived from observations of 56 distant type Ia SNe, spanning a redshift range from  $z = 0.16$  to  $z = 0.97$ . The mean redshift of the combined sample is around  $z = 0.5$ . In what is an excellent example of international collaboration, the observations have been taken with 13 different telescopes spread over 7 different sites in both the Northern and Southern Hemispheres.

The SNe are discovered by observing blank fields over two epochs, which are separated by about three weeks. The fields are observed before and after full moon. In this way, the SNe are discovered while still brightening (Perlmutter et al. 1995), and follow-up observations can start during the following new moon. A final photometric point is taken after the SNe has faded, which is usually one year later.

The confirmation of the SN type has mostly been done by obtaining low-resolution spectra with the Keck 10-m telescope, but about 10 type Ia SNe have been confirmed from spectra taken with 4-m-class telescopes, such as the MMT and the ESO 3.6-m. As an example, the spectrum of SN 1997L ( $z = 0.55$ ), which was observed with EFOSC1 on the ESO 3.6-m, is shown in Figure 1.

Up until 1998, the photometric monitoring was mostly done with 4-m-class telescopes, including the ESO 3.6-m telescope and the ESO NTT. The ESO

3.6-m has been used to follow over 60 high redshift type Ia SNe. Now, with both groups finding more distant SNe ( $z \approx 1$ ), the photometry is done either from space with HST or with the largest ground-based telescopes, such as the VLT.

With the VLT now in operation and with other large 8-m telescopes coming on line, it is perhaps timely to review how these telescopes can contribute to the study of type Ia SNe, not only in terms of measuring the cosmological parameters but also measuring the evolution of type Ia properties as a function of redshift.

## 2. VLT Observations of a Type Ia SN at $z = 0.54$

Discovering type Ia SNe beyond  $z = 0.3$  is now routine and both groups combined have now observed over 100 such SNe. The SNe are discovered by using the largest wide field imagers available on 4-m-class telescopes. Both the BTC camera on the 4-m Blanco Telescope in Chile and the CFH12k on the CFHT in Hawaii have been used to discover distant type Ia SNe.

During our most recent run on the CFHT, we discovered a type Ia SNe well before maximum light. This SNe, which we nicknamed Beethoven<sup>1</sup>, has a redshift of  $z = 0.54$ , which is similar to the mean redshift of all the SNe that have been used to conclude that the universe is accelerating. A preliminary analysis of our data on SN Beethoven suggests that the CFHT discovery image was taken 14 days (in the rest frame of Beethoven) before maximum, and that the spectrum subsequently taken with FORS1 was taken 12 days before maximum. The early discovery of Beethoven enabled us to plan and execute relatively high signal-to-noise ratio target of opportunity observations with FORS1 and ISAAC with the aim of testing whether SN Beethoven is a normal type Ia SNe or not.

The observations with FORS1 on ANTU (UT1) were done on May 12, 2000. The observing conditions were very good, with a mean seeing of 0.55" and a clear sky. We used FORS1

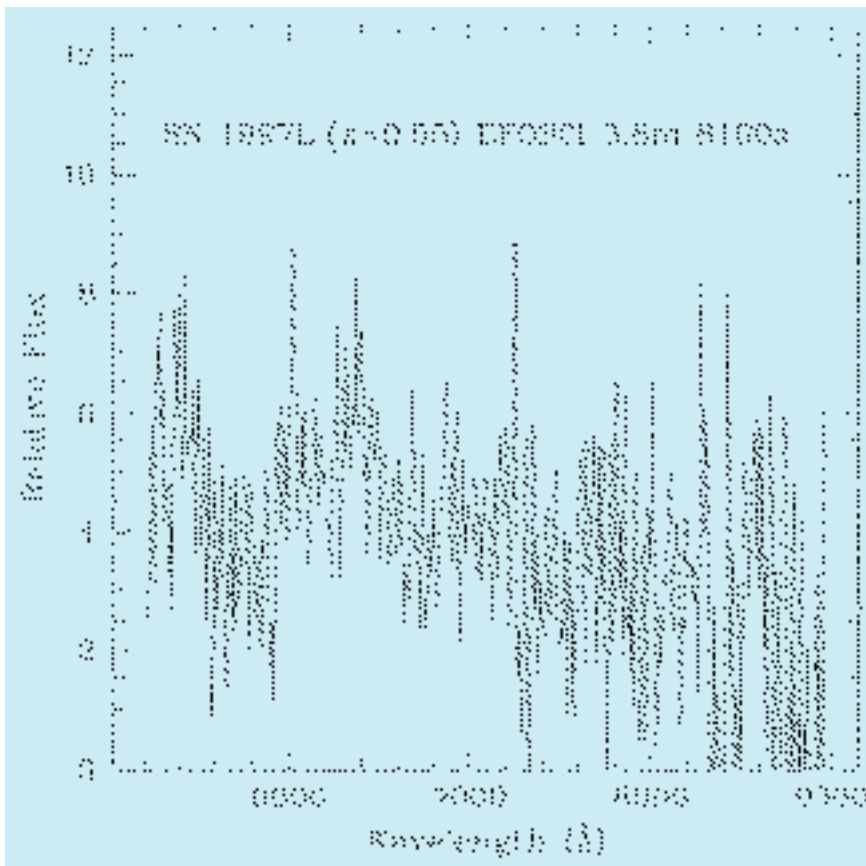


Figure 1: An unsmoothed spectrum of 1997L taken with EFOSC1 on the 3.6-m.

<sup>1</sup>We give a temporary name, for use within the team, to every candidate we find during a campaign. This time the names were composers. Once a SN candidate has been confirmed, we write an IAU circular and an official name is given to the SN following the IAU nomenclature.

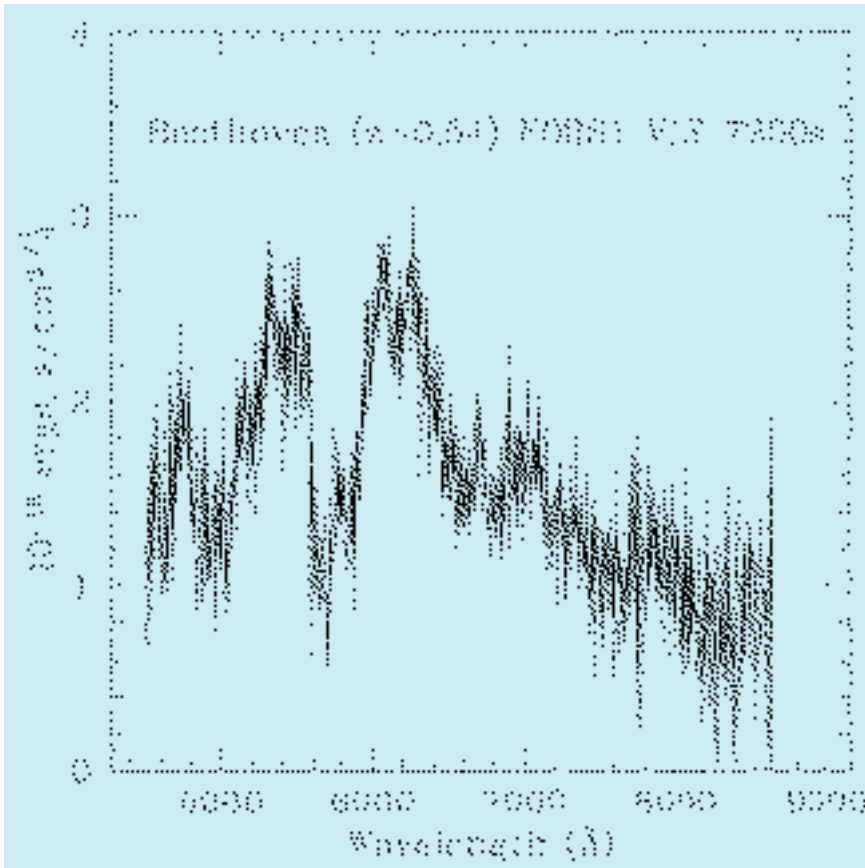


Figure 2: An unsmoothed spectrum of SN Beethoven ( $z = 0.54$ ) taken with FORS1 on ANTU UT1. The signal-to-noise ratio of the SN Beethoven spectrum is six times larger than the signal-to-noise ratio of the spectrum of 1997L.

in long-slit mode and with the 300 V grism. The total integration time was two hours.

The spectrum of SN Beethoven is shown in Figure 2. The signal-to-noise ratio is around 10 per pixel ( $2.6\text{\AA}$ ) or 20 per resolution element (which is 5 pixels and corresponds to the width of the slit). This is an exceptionally high signal-to-noise ratio for a SN at  $z = 0.54$  and it allows us to clearly see that SN Beethoven is a type Ia that was observed about a week (rest frame) before maximum light.

A comparison with spectrum SN 1997L in Figure 1 shows the dramatic improvement in the signal-to-noise ratio. Both SNe have similar redshifts and both have been observed about one week before maximum light. The VLT clearly allows us to make the transition from qualitative statements, such as "It looks like a SN Ia", to quantitative measurements of line strengths and comparisons with nearby SNe.

SN Beethoven was also observed with ISAAC on three separate occasions, which approximately correspond to the epoch of maximum light, and to 16 and 32 rest frame days after maximum light. SN Beethoven was observed with the Js filter, which, in SN Beethoven's rest frame, corresponds to the I-band. The conditions at the time of the observations were again

very good, with a median seeing of 0.6 and clear skies.

There are two reasons for observing moderately distant type Ia SNe with near-IR instruments such as ISAAC. As discussed by Riess et al. (2000), near-

IR observations provide a longer wavelength baseline to test for the presence of near-grey dust. They also provide a test which is not accessible at optical wavelengths. In the I-band, nearby SNe exhibit a second maximum approximately one month after the first. For SNe at  $z \approx 0.5$ , this second maximum occurs in the near-IR and has been observed in SN 1999Q (Riess et al. 2000).

The images from individual epochs and an image that combines all three epochs, which totals almost 10,000 seconds of integration time, are shown in Figure 3. SN Beethoven, which is marked by the arrows, is visible, with moderate signal-to-noise, about 1 arcsec away from the host galaxy. The FWHM of the star images in the final frame is 0.55 .

From a visual inspection of the images, it can be seen that at 32 days after the first maximum SN Beethoven is still visible with approximately the same intensity as it had at 16 days after maximum. However, at this preliminary stage of the analysis it is not clear if this is consistent with a second maximum or if a plateau better describes the observations.

### 3. The Near Future: the Role of the VLT

The use of type Ia SNe as standard candles has led to the proposition that the universe is dominated by an unknown form of dark energy, which is most commonly interpreted as a non-zero cosmological constant and that, at the present epoch, the expansion of the universe is accelerating. This is revolutionary and it is important

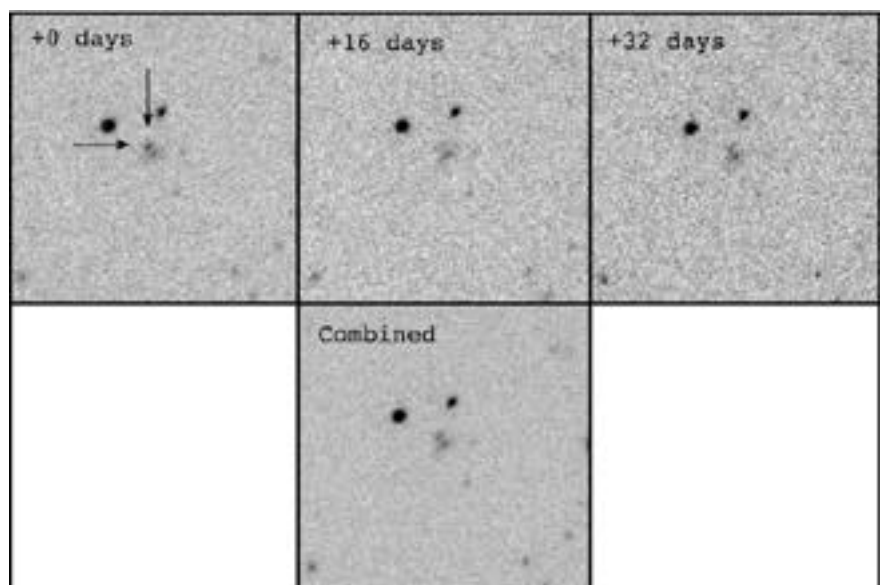


Figure 3: In the top row, a series of ISAAC images taken at different epochs. SN Beethoven is indicated by the arrows. In these images, North is down and East is to the right. FWHM of star images, 0.55 arcsec. The combined image is shown in the bottom row. To get an accurate measure of the underlying flux of the galaxy, a fourth and final image will be taken one year from now.

to make sure that the observed dimming of type Ia SNe with  $z$  is not caused by evolution, which has been the downfall of all standard candles to date, nor by grey dust.

We can test this proposition by conducting an intense optical and IR study of a dozen type Ia SNe at  $z = 0.5$ , the redshift at which the acceleration of the universe was derived. As we have demonstrated with SN Beethoven, the VLT, with ISAAC and the two FORS instruments, is well suited to contribute significantly to this necessary work.

Both groups of observers are now regularly finding SNe at redshifts of order one, and with instruments like VIMOS on UT3 becoming available soon, the number of such SNe will increase. With VIMOS, it will also be possible to detect lensed (highly magnified) SNe at even higher redshifts.

At  $z \approx 0.5$ , type Ia SNe can only be used to place joint limits on  $M$  and  $\Omega$ . They cannot be used to test whether or not the universe is flat. However, with a relatively small sample of SNe at  $z \approx 1$ , one can very significantly improve the

determination of  $M$  and  $\Omega$  separately and of the equation of state of the dark energy.

However, follow-up observations of type Ia SNe at  $z \approx 1$  are both difficult and time consuming. At these redshifts, the restframe B-band, where the light-curve of type Ia SNe are best understood, is shifted into the near-IR, where the sky background from the ground is relatively high. The R-band, where the background is more favourable, corresponds to restframe U. But observations of nearby type Ia SNe in the restframe U-band are scarce and their properties in that band are not yet accurately known. It is not clear, at present, whether from U band observations alone type Ia SNe can be used as distance indicators.

SN Beethoven, at a redshift of  $z = 0.54$  and SN 1999Q at a redshift of  $z = 0.46$  (Riess et al. 2000) have both been successfully observed with state-of-the-art infrared instrumentation on the largest telescopes. Near-IR follow-up observations of type Ia SNe at  $z \approx 1$  and beyond will probably have to wait

for the next generation of IR instruments that use adaptive optics, like NAOS and CONICA, which will be installed on the VLT next year.

In the meantime, the VLT will continue to be used to confirm and follow up type Ia SNe at more moderate redshifts,  $z \approx 0.8$ . Its performance will be strengthened further if the planned upgrade of FORS2 with red sensitive CCDs goes ahead.

#### 4. Acknowledgements

The authors thank Peter Nugent, Bruno Leibundgut and Jason Spyromilio for their critical review of the manuscript.

#### References

- Perlmutter et al. 1995, in *Thermonuclear Supernovae*, ed. P. Ruiz-Lapuente, R. Canal & J. Isern (NATO ASO ser. C, 486) (Dordrecht: Kluwer), 749.  
 Perlmutter et al. 1999, *ApJ*, **517**, 565.  
 Riess et al. 1998, *AJ*, **116**, 1009.  
 Riess et al. 2000, *ApJ*, **536**, 62.

## Lensed Quasars: A Matter of Resolution

F. COURBIN<sup>1</sup>, C. LIDMAN<sup>2</sup>, I. BURUD<sup>3</sup>, J. HJORTH<sup>4</sup>, P. MAGAIN<sup>3</sup>, G. GOLSE<sup>5</sup>,  
 F. CASTANDER<sup>5</sup>

<sup>1</sup>*Pontificia Universidad Católica de Chile, Departamento de Astronomía y Astrofísica, Santiago, Chile*

<sup>2</sup>*European Southern Observatory, Santiago, Chile;* <sup>3</sup>*Institut d'Astrophysique de Liège, Liège, Belgium*

<sup>4</sup>*Astronomical Observatory, University of Copenhagen, Copenhagen, Denmark*

<sup>5</sup>*Laboratoire d'Astrophysique, Observatoire Midi-Pyrénées, Toulouse, France*

### 1. Lensed Quasars

The interest in studying lensed quasars amongst the astronomical community has always been somewhat fluctuating. Periods of great enthusiasm and of profound disappointment have regularly followed one another.

Precisely described in the context of Einstein's Theory of General Relativity, the phenomenon of light deflection was first seen as a pure theoretical curiosity. It was however observed by Dyson et al. (1920), who measured, during a total solar eclipse, the angular displacement of a star by the sun's gravitational field. Gravitational lensing was thus established as an observed phenomenon, but the next important observational step was not made until 1979, with the discovery by Walsh et al. of the first lensed quasar, which had an angular separation of 6 arcsec between the two components. On the theoretical side, Refsdal (1964) proposed, well before Walsh's discovery, to use

multiply imaged quasars to constrain cosmological parameters. As the travel times of photons along the light path to each quasar image are different, an intrinsic intensity variation of the quasar is seen at different moments in each lensed image. The so-called time delay between the detection of the intensity variation in each image is directly related to the cosmological parameter,  $H_0$  and to the position and shape of the deflecting mass. One can therefore infer an estimate of  $H_0$  by measuring the time delay, provided the gravitational potential responsible for light splitting is known. Conversely, one might as well want to assume a "preferred" value for  $H_0$  and use the time delay to constrain a lens model, i.e., to study the mass distribution in distant lens galaxies. Both issues are undoubtedly of capital importance. They both require high spatial resolution observations. With the Hubble Space Telescope (HST) or, better, with large ground-based telescopes located in privileged sites, it is now possible to

perform in a routine manner observations which were impossible only 10 years ago. As an illustration of this, we present in this report recent VLT FORS2 observations of HE 1104-1805, a doubly imaged quasar at  $z = 2.319$  discovered in the framework of the Hamburg-ESO survey for bright quasars (Wisotzki et al. 1993). The choice of HE 1104-1805 is not intended to be representative of the importance of this particular object, but rather reflects how old observationally intractable problems can be tackled in a new way. We also present more recent results, obtained at the 1.54-m Danish telescope for another Hamburg-ESO quasar: HE 2149-2745.

### 2. The First Step: The Lens Geometry and the Time Delay

Resolving the blended images of multiply imaged quasars is one way to confirm or rule out their lensed nature.

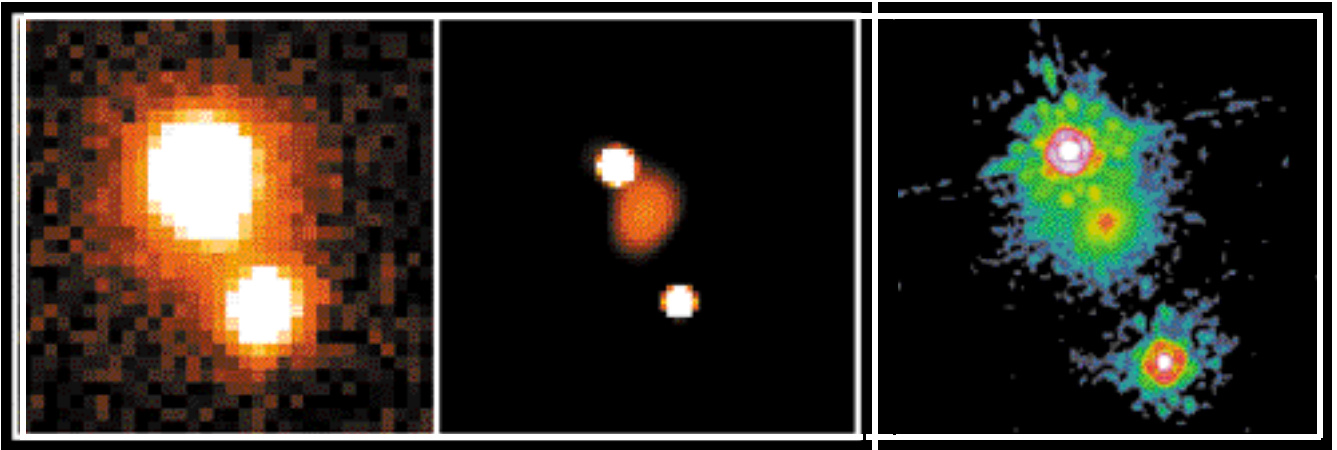


Figure 1: AJ-band image of HE 1104-1805 obtained at the ESO/MPI 2.2-m telescope with IRAC2b (Courbin et al., 1998). The seeing is about 0.8 arcsec and the pixel size is 0.28 arcsec. The middle panel shows a deconvolved version of the image, with a resolution (FWHM) of 0.28 arcsec and clearly revealing the lensing galaxy. An HST H-band image obtained later (PI: Emilio Falco) is displayed on the right panel and confirms the ground-based observation.

If each component of a system shows the same colour, or even better the same spectral energy distribution, the quasar has a good chance of being lensed. However, dust along the line of sight, microlensing, and even intrinsic variability of the quasar can affect the spectral energy distribution of the components. Finding the faint lensing galaxy between the quasar images is a much more reliable criterion. We show in Figure 1, left panel, the discovery image of the lens in HE 1104-1805 (Courbin et al. 1998). This J-band image was taken at the ESO/MPI 2.2-m with IRAC2b, which by today's standards has a relatively small field of view, 1 arc minute on a side, with coarse sampling, 0.28 arcseconds per pixel. It is difficult to see the lens in this image. However, with deconvolution (Magain et al. 1998; MCS) it can be detected at a distance of 1 arcsec from the bright quasar image (Fig. 1, middle). The HST-NICMOS2 image obtained by Lehar et al. 2000 in the H-band is also displayed (Fig. 1, right). Comparison with the deconvolved image confirms not only the position of the lens, but also its ellipticity and orientation. The seeing at the time the data were taken was 0.8, which is average for La Silla. With more modern instrumentation and larger telescopes one can do better. On Paranal, the seeing is often better than 0.5 and the pixel scale of modern detectors is usually of the order of 0.1.

The measurement of the time delay itself remains challenging. Precise light curves with good temporal sampling have to be obtained for each component. It can take several years of continuous monitoring to obtain the time delay of a single lens. HE 1104-1805 was spectrophotometrically monitored at ESO for four years by Wisotzki et al. (1998), and the

time delay was estimated to be 0.73 years. We are currently using the Danish 1.54-m and the 3.5-m NTT to monitor on a weekly basis almost all multiply imaged quasars visible from the Southern Hemisphere (PI: P. Magain for ESO time, J. Hjorth for Danish time).

The image quality is usually between 0.8 and 1.5 arcsec, which, with deconvolution, still allows accurate photometry of objects with angular separations of less than 1 arcsec, down to  $R \sim 19-20$ . One of the first results from this monitoring, the light curve for HE 2149-2745 (Lopez et al. 1998) is shown in Figure 2 (Burud et al. 2001). In this case, the two images of the quasar at  $z = 2.03$  are separated by 1.7 arcsec.

The monitoring data of HE 2149-2745 have been obtained during a wide variety of observing

conditions, even during full moon or through thin cirrus, and very few epochs have been missed. Loosing too many data points due to instrument scheduling or to excessively restrictive observing constraints would be fatal. Therefore, all available data have been used, even those taken under poor conditions.

We would like to point out that none of this would have been possible without the excellent collaboration of the 2.2-m and NTT teams and of the large number of visiting astronomers who performed observations for this programme. We are extremely grateful to all these people.

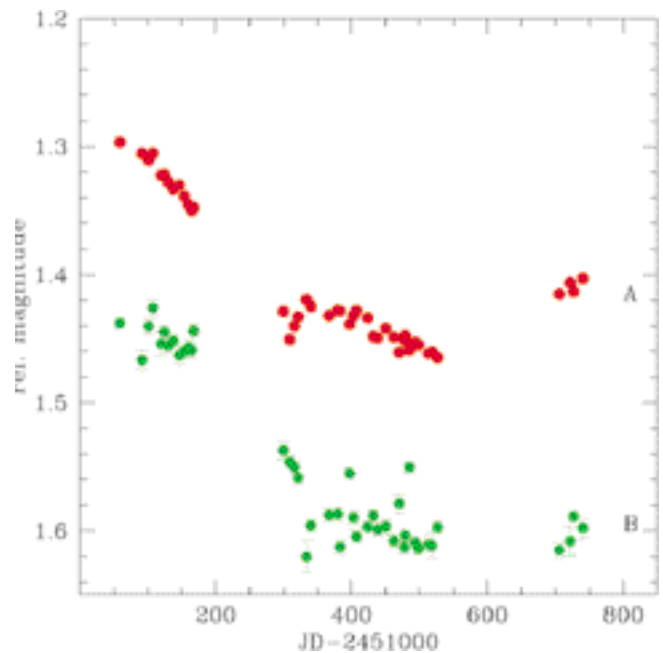


Figure 2: Example of light curve obtained at ESO in the framework of the lens monitoring programme. These light curves, for the two quasar images of HE 2149-2745 (Burud et al., 2001) have been constructed from data obtained at the 1.54-m Danish telescope under average weather conditions. The red curve shows the variation of the brightest quasar image while the green one corresponds to the fainter component, heavily blended with the lensing galaxy. The shift in time between the curves is the time delay. The present data suggest a very rough estimate of  $\sim 100$  days. Future monitoring will provide a better measurement of the delay.

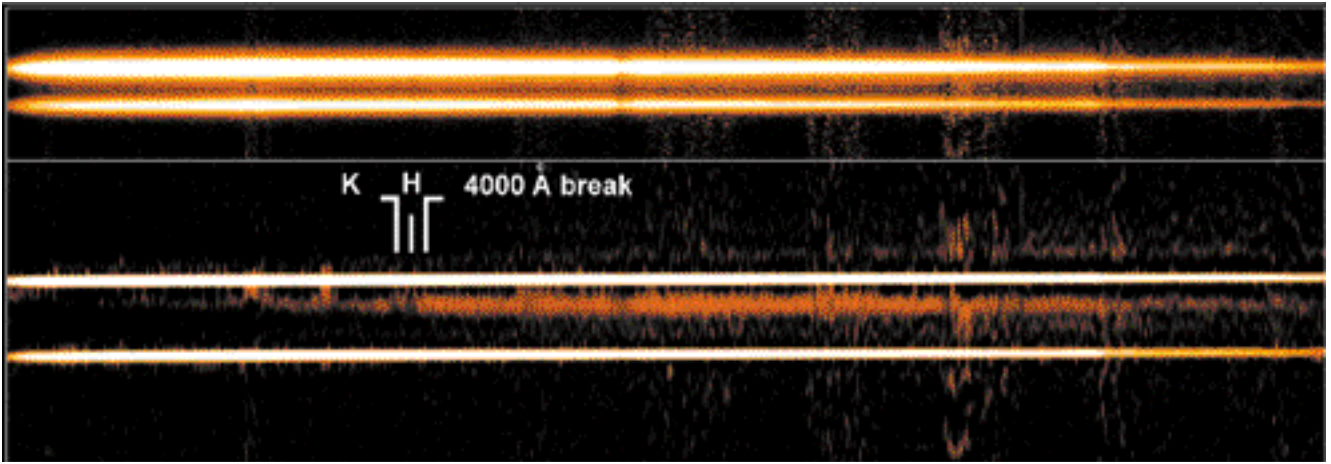


Figure 3: The two-dimensional spectrum of HE 1104-1805 (Lidman et al., 2000). The image at the top is the spectrum of the lens after bias subtraction, flat fielding, and sky subtraction, with the 2 quasar spectra separated by 3.14 arcsec. The image at the bottom is the spatially deconvolved spectrum, with a (spatial) pixel size twice as small as in the original data (this is why the height of the deconvolved spectrum is twice that of the raw spectrum). The lens galaxy, including the H and K bands and the 4000Å break, is clearly visible. The spatial resolution in this spectrum is 0.2 arcsec.

### 3. A Second, More Challenging Step: Spectroscopy of the Lens

Imaging the lensing galaxy is difficult, but obtaining its spectrum is even more so. Accurate modelling was therefore often hampered by the lack of the lens redshift. Lens galaxies are heavily blended with the bright quasar images and are often too faint for the HST. The solution to the problem might be, here again, to use good-quality ground-based data. Using the spectroscopic version of the MCS deconvolution (Courbin et al. 2000a, Courbin et al. 1999) and VLT data, we have obtained a spectrum of the lensing galaxy in HE 1104-1805 (Lidman et al. 2000) and determined its redshift.

Apart from the many unpublished attempts to measure it, the redshift of the lens had been estimated from indirect means. From IR and optical photometry, Courbin et al. (2000b) estimated a redshift in the range  $z = 0.8$  to  $z = 1.2$ . From the time delay measured at the ESO 3.6-m and a model of the lens, Wisotzki et al. (1998) estimated a redshift of  $z = 0.79$  and from the position of the lens on the fundamental plane, Kochanek et al. (2000) gave a redshift of  $z = 0.73$ .

Given these redshift estimates, a deep spectrum in the optical was likely to settle the issue. The VLT spectroscopic observations were taken with FORS2 on Kueyen at the Cerro Paranal Observatory on April 1, 2000 as part of ESO programme 65.0-0566(A). The observations consisted of three 1080-second exposures with the G200I grism and the high-resolution collimator.

This gives a scale of 0.1 per pixel in the spatial direction, which is excellent for deconvolution purposes. The corresponding scale in the spectral direction is approximately 4Å per pixel. The ob-

serving conditions were clear and the external seeing varied between 0.5 and 0.9 .

We used the movable slits in the FORS2 focal plane to select targets and to correct for telluric absorption, one slit was placed on a random object and the remaining slits were closed. Indeed, the final configuration

the two components, three slits were placed on field stars that were used to determine the PSF for the deconvolution and to correct for telluric absorption, one slit was placed on a random object and the remaining slits were closed. Indeed, the final configuration

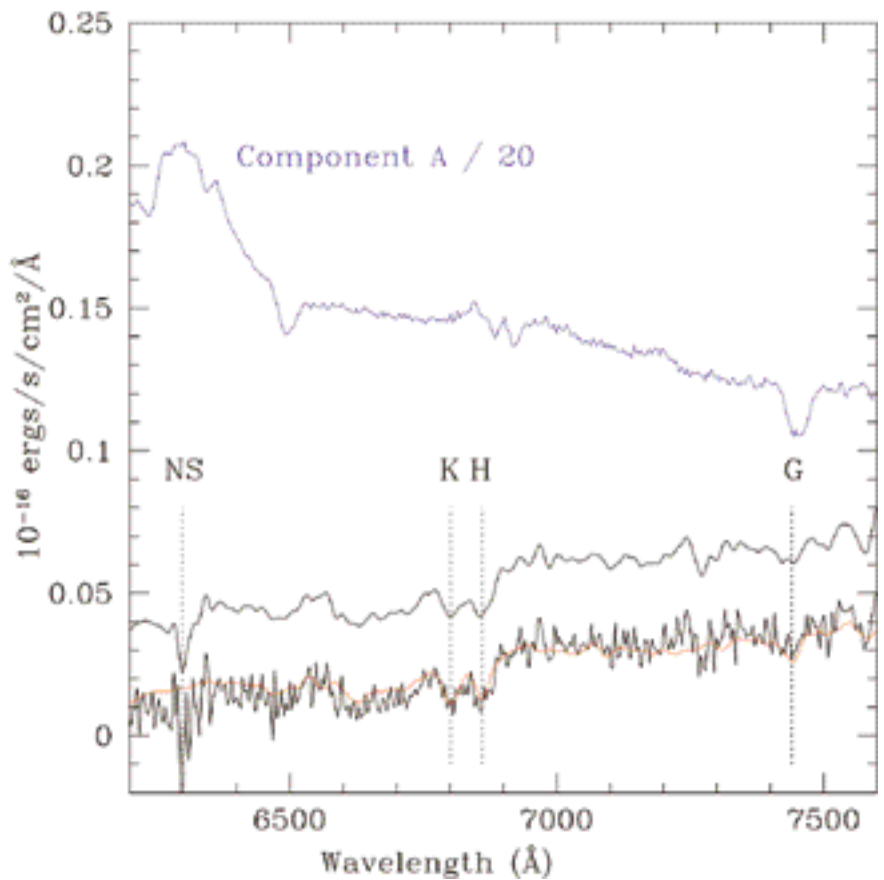


Figure 4: The spectrum of the lens in HE 1104-1805 (bottom). The major absorption lines are identified with the vertical dashed lines. Also plotted, but at 1/20th of the scale, is component A of the quasar (top). The red line is a template of an elliptical galaxy shifted to  $z = 0.729$  and not a smoothed version of the spectrum. The smoothed version of the spectrum has been shifted vertically by 0.03 units for clarity. The H and K Calcium bands and the G band are indicated. A strong sky line at about 6300 Å and introducing significant noise is also indicated.

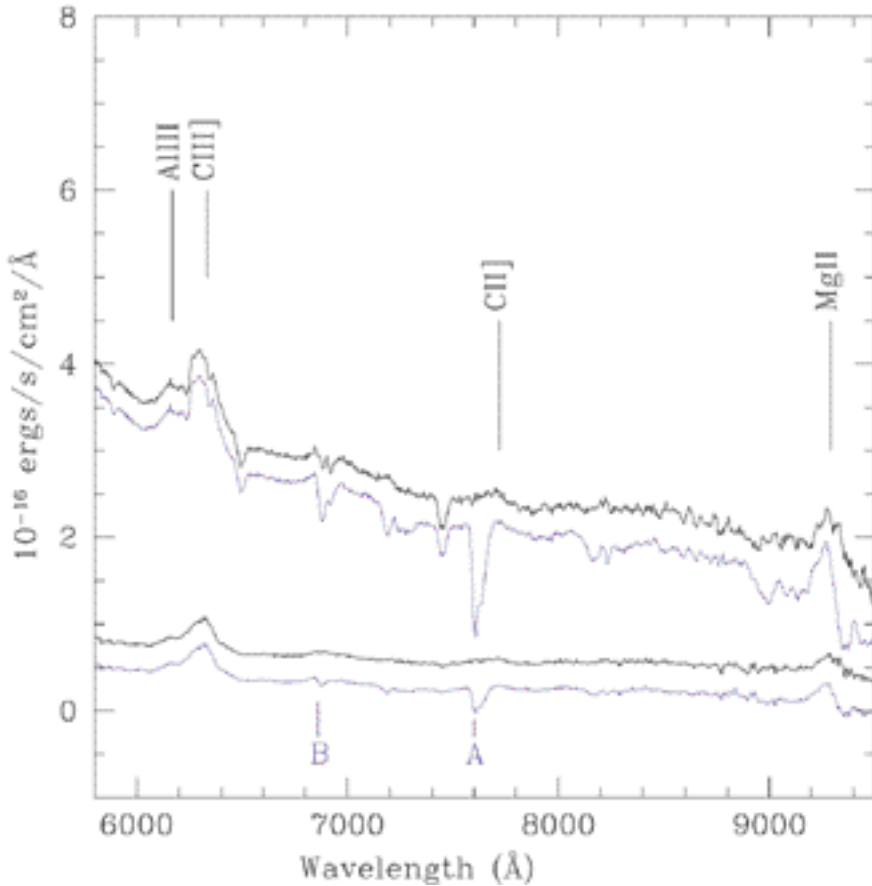


Figure 5: One-dimensional spectra of components A and B of HE 1104-1805. The blue lines are the spectra before the correction for telluric features was applied and the black lines are the spectra after the correction. For clarity, the blue lines have been shifted down by 0.3 units.

looks very similar to the configuration presented in right hand side of Figure 1 of Courbin et al. (1999).

The lensing galaxy is four to five magnitudes fainter than component A, which is located only one arc second away. Even with good seeing, the light of the galaxy is heavily blended with that of the quasar. To detect the lensing galaxy, extract its spectrum and measure the redshift, deconvolution in the spatial direction was essential.

The 2-D spectrum of the lens is shown in Figure 3. The lens is completely invisible in the raw data, shown in the top panel, while it is obvious, including absorption features, in the bottom panel. The 1-D extraction of the deconvolved lens spectrum is displayed in Figure 4. An unsmoothed version is shown at the bottom of the figure with a smoothed version, shifted by 0.03 units on the vertical scale. Also shown, but reduced by a factor of 20, is the spectrum of component A. Note that the lens spectrum shows no trace of contamination by the QSO emission lines. The Calcium H and K absorption lines are clearly detected in the lens and the G-band is marginally detected. A template spectrum of an elliptical galaxy shifted to  $z = 0.729$  (Kinney et al. 1996) is overplotted in red. Cross correlation of the data with this tem-

plate allows us to derive the redshift of the lens:  $z = 0.729 \pm 0.001$ .

The spectra of the two components of the quasar are shown in Figure 5. We plot the spectra before and after the telluric features have been removed. The PSF stars are fainter than the quasar, so the later spectrum is noisier. The main emission features of the quasar and the telluric A and B bands are indicated in the figure.

#### 4. On the Future of Quasar Lensing

Until recently, it was hard to resolve the lensed components of multiply imaged quasars. It is now relatively straightforward and it is becoming possible to extract the spectrum of the faint lensing galaxy. Measuring time delays is also becoming easier, since one can efficiently process data obtained with medium-size telescopes under average or poor weather conditions.

The remaining problem in using gravitational lenses for measuring the Hubble constant is now model degeneracy; several models can reproduce the available constraints for any given system. Observing many different lenses, with very different image configurations is one approach to reduce the degeneracy. Another approach is of

course to improve the accuracy of the observations for each individual system. Until now, one reconstructs the mass profile of the lens by probing the gravitational potential at only 2 or 4 positions, i.e., the position of the quasar images. Systems with more images are probably extremely rare, so the only way to use more constraints is to observe the distorted images of other objects behind the lensing galaxy. The host galaxy of the lensed quasar is an obvious candidate (e.g., Kochanek et al. 2000). With the very high angular resolution soon achievable with adaptive optics (AO) systems mounted on 8-m-class telescopes, it will be possible, in many objects, to see the quasar host galaxy as a lensed ring, hence providing new constraints for the mass modelling. Advanced multi-conjugate AO systems will allow for similar resolutions but on a wider field of view (about 1 arcmin) and with good PSF quality. Small arclets, as presently observed in lower-resolution observations of rich galaxy clusters, should be seen in the immediate vicinity of the lens, providing us with measurements of the lensing potential at many positions.

It is very tempting to speculate further on what we may be doing in a few years from now. Although such an exercise is always somewhat dangerous, it is not foolish to predict that a spectrograph mounted on an AO system will allow us to measure the rotation curve of lens galaxies, making it possible to compare, for the first time, the mass derived from direct velocity curve measurement, with the mass inferred from lensing. In the longer term, one may be using 2-D spectrographs on OWL to map the velocity field of lens galaxies, lensed quasar hosts, and lensed arclets in order to derive very precise lens models which will probably be fully non-parametric (e.g., like those described by Williams & Saha, 2000).

In conclusion, leadership of ESO in the field of lensed quasars can be maintained, by using both the small telescopes to measure time delays, and the larger ones to conduct imaging/spectroscopic observations with unprecedented quality. It will be interesting to see how lensed quasars will be used in the future. Will we derive  $H_0$  from quasar time delays, using the very detailed observations of lens galaxies, or will we use the value of  $H_0$  derived from other techniques to infer the mass profile for distant galaxies using lensing? In either case, there is a great deal to be learnt from the study of lensed quasars.

#### 5. Acknowledgements

It is a pleasure to thank Thomas Szeifert for his expert support on FORS2 at VLT-UT2. We also thank all

those observers – and there are many – who helped us to obtain data on the NTT and the Danish 1.54-m. We also specially thank the NTT and 2.2-m teams, whose professional and courteous support has made the monitoring programme a success. Frédéric Courbin acknowledges financial support through the Chilean grant FONDECYT/3990024. Additional support from the European Southern Observatory and through CNRS/CONICYT grant 8730 “Mirages gravitationnels avec le VLT: distribution de matière noire et contraintes cosmologiques” is also gratefully acknowledged.

## References

- Burud, I., et al. 2001, in preparation.  
 Courbin, F., Lidman, C., Magain, P. 1998, *A&A*, **330**, 57.  
 Courbin, F., Magain, P., Sohy, S., Lidman, C., and Meylan, G., 1999 *The Messenger*, **97**, 26.  
 Courbin, F., Magain, P., Kirkove, M., Sohy, S. 2000a, *ApJ*, **529**, 1136.  
 Courbin, F., Lidman, C., Meylan, G., Kneib, J.-P., Magain, P., 2000b, *A&A*, in press.  
 Dyson, F. W., Eddington, A. S., Davidson, C. R., 1920, *Mem. Roy. Astr. Soc.*, **62**, 291.  
 Lehar, J., Falco, E., Kochanek, C. et al. 2000, *ApJ*, **536**, 584.  
 Lidman, C., Courbin, F., Kneib, J.-P., et al., 2000, *A&A*, submitted.  
 Lopez, S., Wucknitz, O., Wisotzki, L., 1998, *A&A*, **339**, L13.  
 Kinney, A.L., Calzetti, D., Bohlin, R.C., et al., 1996, *ApJ*, **467**, 38.  
 Kochanek, C.S., Keeton, C.R., McLeod, B.A., et al. 2000, astro-ph/0006116.  
 Magain, P., Courbin, F., Sohy, S., 1998, *ApJ*, **494**, 472.  
 Refsdal, S., 1964, *MNRAS*, **128**, 295.  
 Walsh, D., Carswell, R. F., Weymann, R. J., 1979, *Nature*, **279**, 381.  
 Williams, L.L.R., Saha, P., 2000, *AJ*, **119**, 439.  
 Wisotzki, L., Koehler, T., Kayser, R., Reimers, D., 1993, *A&A*, **278**, L15.  
 Wisotzki, L., Wucknitz, O., Lopez, S., Sørensen, A., 1998, *A&A*, **339**, L73.

# 3D Structure and Dynamics of the Homunculus of Eta Carinae: an Application of the Fabry-Perot, ADONIS and AO Software

## I. MOTIONS IN HOMUNCULUS

D. CURRIE<sup>a</sup>, D. LE MIGNANT<sup>a</sup>, B. SVENSSON<sup>a</sup>, S. TORDO<sup>c</sup>, D. BONACCINI<sup>a</sup>

<sup>a</sup>European Southern Observatory, Garching, Germany

<sup>b</sup>Università di Bologna, Dipartimento di Astronomia, Bologna, Italy

<sup>c</sup>Osservatorio Astronomico di Bologna, Bologna, Italy

### Summary

Eta Carinae is an extremely massive and highly evolved member of the

Carinae starburst region. It has undergone numerous eruptions over the past millennium. In 1841, a giant eruption ejected several solar masses or more

of material. Most of this material is currently in the dusty nebula denoted as the “Homunculus”.

The Adaptive Optics Instrument of the ESO 3.6-m telescope, ADONIS, has been used in its Fabry-Perot interferometric mode to carry out observations of the nebula near the Brackett line at 2.16  $\mu\text{m}$ . These observations

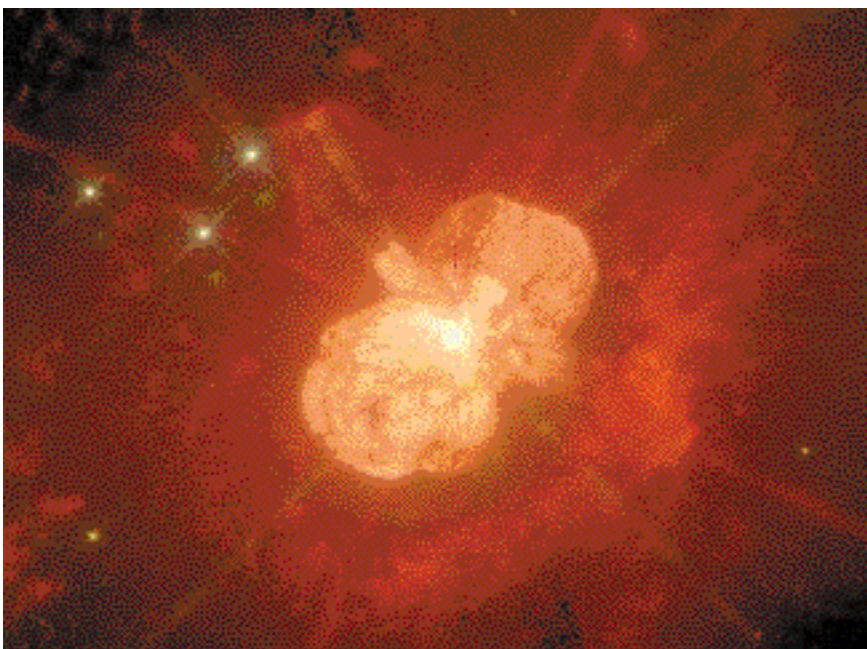


Figure 1: The Homunculus of  $\eta$  Carinae (i.e., the bright double-lobed structure) as observed with the WFPC2 of the Hubble Space Telescope. Data were obtained in a narrow-band filter centred at the emission line of  $H\alpha$ . The dynamic range of elements visible in this image is over one million. North is up, and the width of the image is about 45 arcseconds.

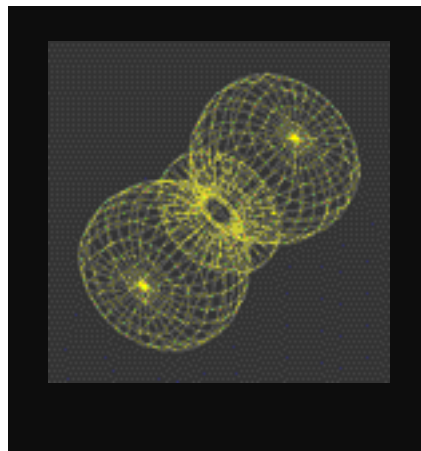


Figure 2: Three-Dimensional Representation of the Double-Flask Model<sup>3</sup> of the Homunculus, derived from the astrometric motion<sup>2</sup> and the Doppler velocities<sup>5</sup> of the clumps, and the assumption of rotational symmetry. This has the same scale and orientation as Figure 1.

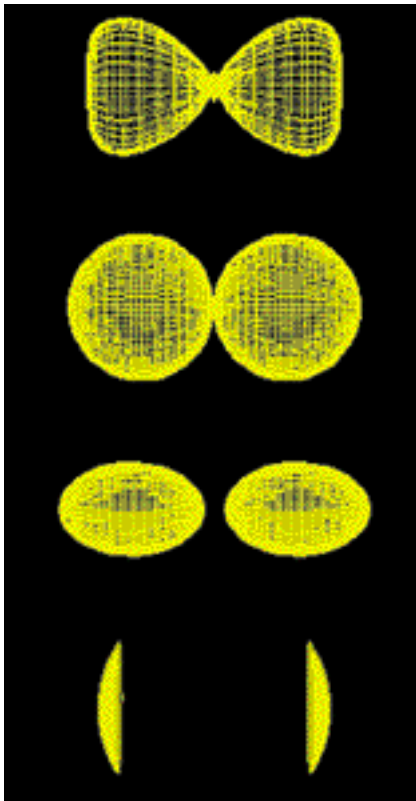


Figure 3: This figure shows the four models that have been published. The first is the Double-Flask presented by Currie *et al.* The second is the double sphere that has been the “standard” for many years. The third is the Double-Egg proposed by Meaburn *et al.*<sup>7</sup>. The fourth is the Double-Cap proposed by Allen and Hillier<sup>5</sup>. The Double Flask is the only model to satisfy both the requirements of the HST astrometry and the Doppler velocities in the Allen and Hillier<sup>5</sup> observations. (see Currie and Dowling<sup>1, 2</sup>).

have allowed probing the interior of the major elements of the Homunculus and, in particular, the back wall. These elements were not visible in our WFPC observations at visible wavelengths<sup>2, 3</sup>. The preliminary results of the analysis of the ADONIS data have confirmed the “Double-Flask” model of the Homunculus; a model that we proposed based upon the Hubble data<sup>3</sup> and spectroscopic data<sup>4, 5</sup>. This approach can also determine the opacity of the Homunculus walls, as well as the total mass and the grain structure of the dust. In the next issue of *The Messenger*, we shall present an analysis of small clumps of material ejected at velocities almost 1% of the speed of light<sup>1</sup>. These “bullets” and the material following the bullets, the “contrails”, called the “Spikes”, have been measured using the STARFINDER programme. This analysis has discovered about one hundred additional “Malin” bullets.

The ADONIS data, as well as other data taken in direct support of the PAPA0 programme<sup>6, 10</sup> (see June 2000 issue of *The Messenger*) pro-

vide new information on the structure of the Homunculus. Inter-comparison of the WFPC data and the ADONIS data is an integral part of the PAPA0 programme for the validation of diffuse-object astrometry and deconvolution software. Portions of these data will form the database for general community use for the calibration of different programmes.

### General Astrophysical Background

Eta Carinae is a star in the southern sky at a distance of about 8,000 light years. It is believed to be the most massive (> 100 solar masses) and most luminous object in our galaxy. In 1841, it underwent a cataclysmic eruption, becoming the second brightest extra-solar object in the sky. In the process, it ejected several solar masses of its outer envelope. Over the years the heavier elements of this ejected gas have cooled and condensed into an expanding dust cloud, resulting in the nebula shown in Figure 1.

By the detailed analysis of a sequence of HST images like Figure 1, we determined the motion of 178 individual clumps of dust that lie in the Homunculus. The analysis of these motions has shown that all of the clumps (i.e. the Homunculus, the NN and NS knots, and the south bar) were emitted by the central star in 1841<sup>1, 2, 3, 8</sup>. By the analysis of the spectra of the homunculus of Allen and Hillier<sup>4, 5</sup>, we may essentially determine the Doppler velocity of each of the clumps. Combining these data sets, we can define a three-dimensional model, at least for that portion of the Homunculus that we can see from earth<sup>1, 3</sup>. This analysis has allowed the definition of the Double-Flask Model, indicated in Figure 2, and the rejection of the other models that have been proposed in the literature in the past. The Double-Flask Model has recently been confirmed by polarisation measurements made with WFPC2 on the HST<sup>9</sup>. However, there are still questions as to the hidden portions of the Homunculus and we are interested in the structural and velocity details of the back wall. The back wall is invisible to HST because the visible radiation from the

back wall cannot penetrate the dust in the front wall. We report here our preliminary results on the motions of the back wall.

### Structure of the Homunculus

In order to observe the rear wall and determine its structure and velocity, we would need to observe in the infrared wavelengths. Observing at these wavelengths in the vicinity of the Br line, we see light that was emitted by the central star and reflected from a clump. Thus the observed brightness of an element of the image would consist of light originating near the central star, reflecting from the back wall and then proceeding toward the observer, as indicated in Figure 4. Since all of these clumps are moving radially away from the central star, the light reflected from the clumps is “red-shifted” with respect to the wavelength of the light as it leaves the central star. It is these shifts in wavelength that we will use to distinguish the light scattered from the rear wall as compared to the front wall.

However, three additional problems arise in attempting to accomplish these observations. In the first place, we need to have the angular resolution which is similar to that provided by the WFPC of HST to perceive the details of the structure. At the time of these observations, there was no infrared camera available on the HST. Even with the later proper operation of the HST infrared camera – NICMOS – it does not have the same resolution as our visible images. This is due to the diffraction limit of the relatively small aperture of the HST when used for observations at the relatively long wavelengths of two microns. For this reason, the ESO 3.6-metre telescope, with its Adaptive

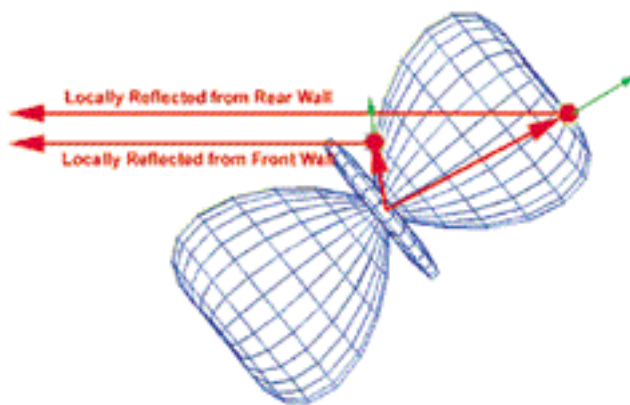


Figure 4: This figure illustrates the paths and the Doppler shifts of the Br $\gamma$  line-emission radiation that is emitted by the central star. This light reflects from the clumps in the walls of the Homunculus, experiencing a “double red shift”. The length of the green arrows is proportional to the radial velocity of the dust clumps. Each clump sees the arriving light as red-shifted by this radial velocity. Then since the clump is also moving away from the observer, there is a further red shift equal to the component of the velocity along the line of sight. Thus the Br $\gamma$  line proceeding along the red arrows to the observer has experienced a double Doppler shift of the wavelength that can be detected by the Fabry-Perot Interferometer.

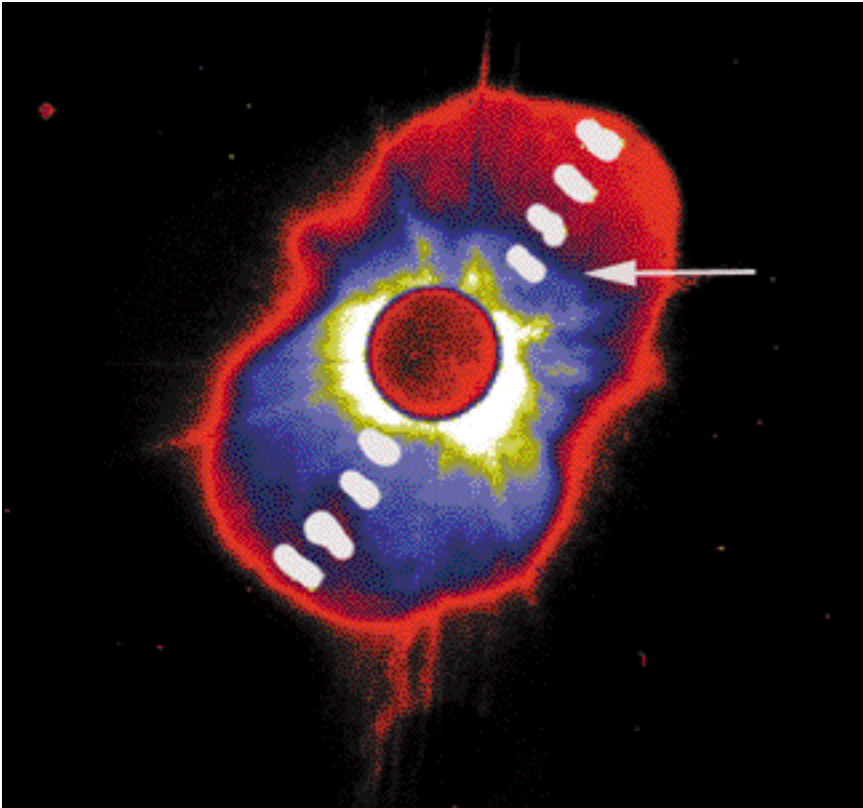


Figure 5: This is the image of the Homunculus, as seen with the Fabry-Perot of the Adaptive Optics System, ADONIS, attached to the ESO 3.6-m telescope. This is an average over the 13 individual images, each obtained at slightly different wavelengths. The disk in the centre is the image of the coronagraphic spot blocking the central star. Spectra are extracted at each of the 8 white spots, with some additional extractions of larger spots to reduce the noise. As an example of the type of spectra obtained at each patch in the image, we consider the patch indicated by the white arrow and shown in Figure 6. In this image, north is approximately up and the width of the image is about 25 arcseconds.

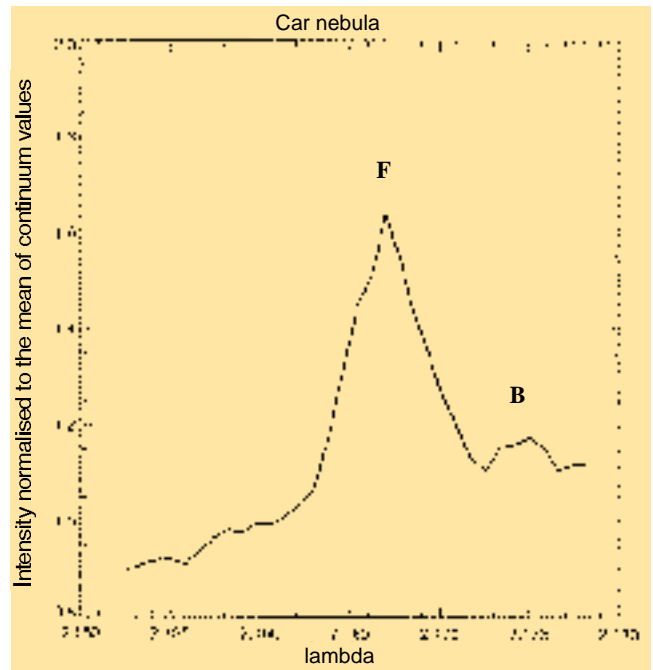
Optics System, ADONIS, is the only telescope (on earth or in space) that could satisfy the resolution requirements of this imaging.

However, this does not complete our requirements. We must have some method to distinguish between the radiation from the front wall and the back wall over the whole image. To this end, we have used the Fabry Perot Interferometer that is a part of the ADONIS system. We used this to provide images at different wavelengths in the vicinity of Br and with a spectral resolution of 1000. This implies that we have a velocity resolution of 300 km/sec, that is just enough to distinguish between the Doppler shift of the reflected radiation from the two walls. Finally, the central star is so bright that if it were placed on the detector, the array would be saturated. Therefore, we need to block the light from the central star. One could move the central star off the detector array, but then we need multiple exposures to cover the Homunculus.

Fortunately, ADONIS also has a coronagraphic occulting system. That is, an opaque blocking spot in the reimaged focal plane. This spot blocks the light of the central star, but allows

the light from the Homunculus to pass to the detector array.

Figure 6: Profile of the Br $\gamma$  line at the position of the patch indicated with an arrow in Figure 5. The peak at 2.167 microns (F) is the light that comes from the central star, reflects off a clump in the front wall and proceeds without further obscuration to the observer. The peak at 2.175 microns (B) represents the light that is emitted by the central star, and goes to the back wall and reflects toward the observer, as discussed in Figure 4. Since it then passes through the front wall, the intensity of the light from the back wall is much reduced. However, because the two walls may not have the same irradiation, and because the reflection occurs at different phase angles, we cannot directly interpret the ratio of the peak heights as the opacity of the front wall.



The Fabry-Perot can be used to scan over the wavelengths near the hydrogen emission line Br at 2.16 microns and obtain the line profile. The light from this line originates from the central star (or the stellar wind near the central star), and reflects off the clumps and then proceeds toward our telescope. The relative motion of the clump with respect to the source of the radiation and with respect to the earth causes Doppler shifts in the wavelengths. Thus the front and back wall have different wavelengths, which we can detect with the Fabry-Perot. The profile of the Br line of the patch shown with an arrow in Figure 5 is plotted in Figure 6.

Although we have data for the entire Homunculus, we here consider only the data from the axis of symmetry, that is, the plane that lies in the line of sight and includes the symmetry axis of the Homunculus. This is the most sensitive discriminator between the models.

We now use the Double-Flask Model to predict the position and velocity of each of the clumps. For each position in the Homunculus, we can predict the apparent wavelength (or shift in velocity) of the radiation sampled by the Fabry Perot Interferometer. For simplicity, we will consider only the effects along the "symmetry axis" of the Homunculus, along which the 8 spots are aligned in Figure 5. The red curve in Figure 7 shows the predicted velocities from the Double-Flask Model, and the red points show the measured offsets in the wavelength of Br.

Thus we see that this preliminary analysis yields a very good confirmation of the values of the velocities of the

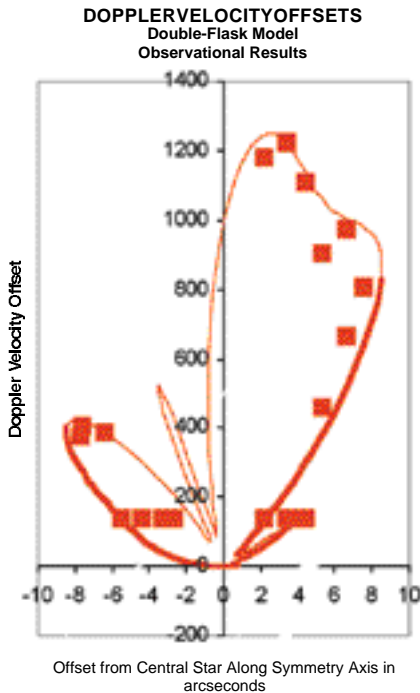


Figure 7: Velocity (in  $\text{km s}^{-1}$ ) as a function of the distance to the central star, along the symmetry axis. Comparison of the Fabry-Perot Observations and the Double-Flask Model. The red line illustrates the predicted Doppler velocities for the Double-Flask Model for the locally reflected  $\text{Br}\gamma$  line. This uses the published parameters (with no adjustable parameters) for the Double-Flask model. The thick red line indicates that part of the Homunculus that can be seen by an observer. The red boxes are the observations of the Doppler velocities, that is, the spectral peaks found in the set of 8 curves similar to Figure 6, for each of 8 patches along the symmetry axis of the Homunculus in Figure 5 (2 peaks per spatial position, corresponding to the front and the back wall).

### Conclusion

We have verified that the assumption of rotational symmetry, which was made in the earlier analysis<sup>3, 8</sup> is indeed correct. These data also illustrate that the Double-Flask Model is strongly preferred over the Double-Sphere and the Double-Cap models. Finally, this analysis also confirms the orientation of the symmetry axis with respect to the line of sight of  $40 \pm 2$  degrees. Further analysis will address the refinement of the Double-Flask parameters (rather than the discrimination between different models).

visible front wall that were derived from other data. In addition, for the first time, we can observe the structure and measure the velocities of the invisible back wall from the data obtained using the Fabry-Perot Interferometer and the coronagraphic spot of the ADONIS system.

### Acknowledgements

We wish to thank the 3.6-metre team at La Silla for support in the ADONIS observations.

### References

- <sup>1</sup>Currie, D.G. and D.M. Dowling. (1999) "Eta Carinae at the Millennium", ASP Conference Series, Vol. 179, 1999, J.A. Morse, R.M. Humphries, and A. Damineli, eds.
- <sup>2</sup>Currie D. G., D. M. Dowling, et. al., 1996, *AJ* **112**, 1115.
- <sup>3</sup>Currie, D.G., D.M. Dowling, E. Shaya, J.J. Hester (1996), "Role of Dust in the Formation of Stars", Garching bei München, Federal Republic of Germany, 11–14 September 1995. Proceedings of the ESO Workshop, Käuffl, H. U. and Siebenmorgen, R. (Ed.) Springer-Verlag, 89–94.
- <sup>4</sup>Allen, D.A. and D.J. Hillier, 1993. *Proc. Astron. Soc. Aust.*, **10** 338.
- <sup>5</sup>Allen, D.A. and D.J. Hillier, 1989, *MNRAS* **241**, 195–207.
- <sup>6</sup>Currie, D., E. Diolaiti, S. Tordo, K. Naesgarde, J. Liwing, O. Bendinelli, G. Parmeggiani, L. Close, D. Bonaccini, 2000, *SPIE*, 4007-73.
- <sup>7</sup>Dowling, D.M. (1996), "The Astrometric Expansion and 3-D Structure of eta Carinae" University of Maryland, Ph. D. Thesis.
- <sup>8</sup>Meaburn, J., J.R. Walsh and R. D. Wolstencroft (1993), *A&A* **213** 89.
- <sup>9</sup>Schulte-Ladbeck, R.E., A. Pasquali, M. Clampin, A. Nota, D.J. Hillier, O.L. Lupie (1999), *AJ* **118**, 1320.
- <sup>10</sup>Currie, D. et al. 2000. *The Messenger* **100**, 12.

# Unlocking the Past of Sakurai's Object Using FORS/VLT

F. KERBER<sup>1</sup>, R. PALSA<sup>2</sup>, J. KÖPPEN<sup>3,4,5</sup>, T. BLÖCKER<sup>6</sup>, M.R. ROSA<sup>1</sup>

<sup>1</sup>Space Telescope European Coordinating Facility; <sup>2</sup>European Southern Observatory; <sup>3</sup>Observatoire Astronomique, Strasbourg, France; <sup>4</sup>International Space University, Illkirch, France; <sup>5</sup>Universität Kiel, Germany; <sup>6</sup>Max-Planck-Institut für Radioastronomie, Bonn, Germany

## 1. Summary

Sakurai's object (V4334 Sgr) was discovered by Japanese amateur astronomer Y. Sakurai in February 1996 and first classified as a slow nova. Follow-up observations though immediately showed this to be a very special object indeed. It turned out to be a true stellar chameleon, perhaps the most rapidly evolving star ever witnessed. Details of its discovery and early observations are found in Duerbeck et al. (1996, 1997), Kerber et al. (1998) and Clayton & de Marco (1997). We have now used the combined power of FORS/VLT in order to deepen our insight into this object and its evolution.

Using FORS/VLT observations, we have obtained the best spectrum of the

old PN surrounding Sakurai's object. We have derived improved values for the interstellar reddening and we have been able to reliably measure additional diagnostic lines. In particular, the value found for the He II 4686 line is in excellent agreement with our earlier model calculations. We thereby confirm the previous result that the star was a hot, highly evolved PN nucleus before the flash.

## 2. The Nature of Sakurai's Object

Today astronomers think that Sakurai's object is undergoing a final helium flash. Helium (shell) flashes are common on the asymptotic giant branch (AGB) when stars burn hydrogen and

helium intermittently. While hydrogen burning can be gradually turned on, helium ignites in a thermo-nuclear runaway leading to a very abrupt increase in brightness, hence the term flash or thermal pulse. As a consequence of this behaviour, stars lose a very significant percentage of their mass within a short period of time leaving only a thin atmospheric layer on top of the former stellar core when it leaves the AGB. The post-AGB star heats up while shrinking physically and therefore moves horizontally in the HRD. Upon reaching 30,000 K, the matter lost previously (AGB wind) gets ionised and becomes visible as a planetary nebula (PN). This PN central star will quickly (few 1000 to 10,000 years) exhaust the remaining hydrogen fuel and then en-

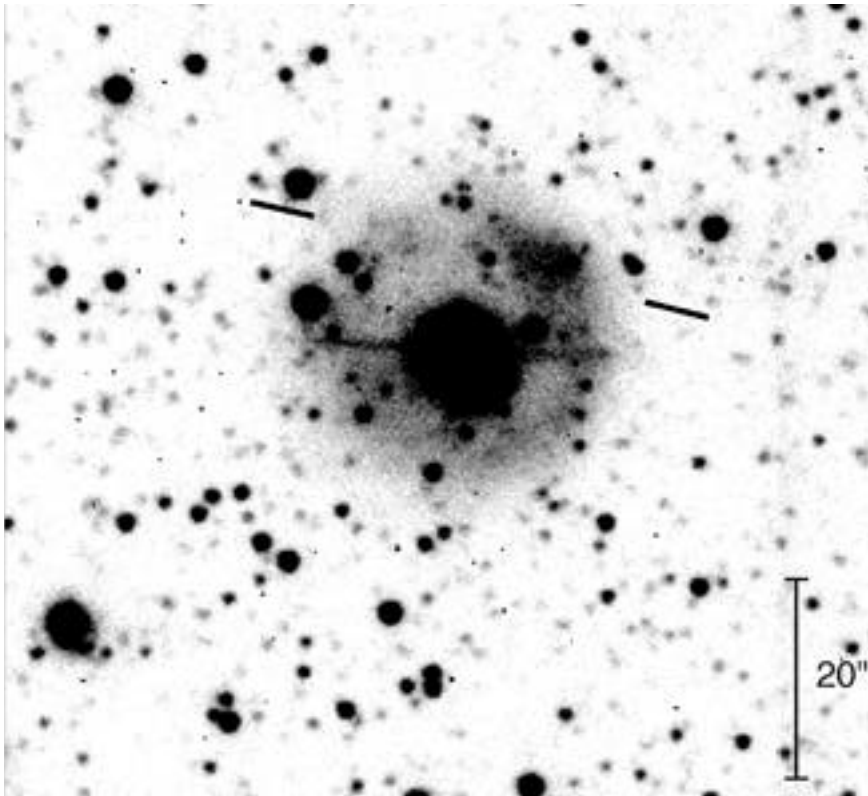


Figure 1:  $H\alpha$  image of the PN surrounding Sakurai's object. The slit position is indicated by the solid bars.

ters the white dwarf cooling track, while the PN quickly fades and mixes into the interstellar medium. Theory predicts though that for 10 to 20% of all low-mass stars one final, and delayed helium flash will occur with dramatic consequences: The renewed supply of energy balloons the star to giant dimensions, again sending it back to the AGB with a massive increase in brightness. The term born-again giant has been coined for such re-animated stars. The idea that Sakurai's object is indeed such a born-again giant is now based on several observational facts summarised below.

- The star is surrounded by a round nebula showing a spectrum typical for an evolved planetary nebula. This is strong evidence that the star must have been on the AGB previously and also had already evolved into a hot PN nucleus.

- V4334 Sgr's photosphere is highly deficient in hydrogen but enriched in heavier elements (Asplund et al. 1997, Kipper & Klochkova 1997). Furthermore, its composition has been found to change over time as hydrogen was further depleted, whereas s-process elements have increased in abundance (Asplund et al. 1999). This behaviour can be explained in terms of a very late helium flash during which the outer H-rich atmosphere is ingested into the helium burning shell while processed material from the stellar interior is mixed up to the surface resulting in the peculiar abundance pattern.

- The time evolution of the brightness is in general agreement with both the model (Iben et al. 1983) for a *very late* helium flash (i.e. after the end of H-burning, in contrast to a *late* flash which happens while H-burning is still active (suggested for FG Sge, by Blöcker & Schönberner 1997) and the other possible historic example for a very late helium flash, V605 Aql, the central star of A 58 (Seitter 1987).

- Another fact supporting the born-again hypothesis is the formation of molecular features (Asplund et al. 1997, Kerber et al. 1997) and of large amounts of hot dust as the star returns to the AGB. Our ISO observations covering four epochs over one year showed a tenfold increase in the 4 to 25  $\mu\text{m}$  range (Kerber et al. 1999b). We found a significant mass-loss rate, which also appears to vary. During the same period the visual light curve went through a series of deep declines as the dust became optically thick. This behaviour is similar to R CrB stars, a rare class of irregular variable stars, which form clouds of dust close to the photosphere blocking our line of sight. A similar process seems likely for Sakurai's object.

### 3. The VLT Observations

One crucial piece of evidence would be to know about the properties of Sakurai's object before the helium flash. Such information is hard to come

by directly as the only observations on record are Schmidt survey plates, which might just show it at the plates' limit of 21 mag in R. However, the density of the PN around the Sakurai's object is so low that it responds very slowly to the cut-off of UV photons, in fact, it will take hundreds of years to recombine. Therefore, the nebular plasma keeps a memory of the ionisation when the star was still hot enough to ionise it. With our VLT observation, we follow up earlier work by Pollacco (1999) and ourselves (Kerber et al. 1999a) in which we were able to confirm that Sakurai's object was indeed a highly evolved PN nucleus when the flash occurred.

The PN surrounding V4334 Sgr is an evolved round nebula of very low surface brightness which has a rather mottled appearance, and a brighter segment in the NW sector (Fig. 1). The angular diameter of 32 arcsec was given by Duerbeck & Benetti (1996). Jacoby et al. (1998) have clearly detected emission out to a diameter of 44 arcsec. In our 2D spectrum (Fig. 2) obtained with FORS 1 we can trace nebular emission to a maximum extent of about 39 arcsec. Since our slit only cuts through a section of the nebula, this is in agreement with the larger diameter reported.

As this is a photon-hungry enterprise, we decided to simply put to use the enormous light gathering capability of VLT's Antu in order to obtain a very deep spectrum of the PN. We therefore observed with FORS 1 using a single long slit on a single slit position that was centred on the brightest part of the nebula and covered a large fraction of the diameter but avoided V4334 Sgr itself, which was still a bright object at the time. No particular request in terms of seeing was made. The slit was 8 arcsec long and 2.5 arcsec wide. Specifically we aimed for a high signal-to-noise ratio and a large spectral coverage. To this end we used three different set-ups, Grism 300V (without filter), 300V with GG435 and Grism 300I with OG590. We had planned individual exposures of 2400 s each, which would then be combined during data reduction. Due to some technical problems, the observations were executed in a somewhat different manner, but that did not compromise their quality nor the scientific value. For 300V without filter, a total of 13,919 s were obtained in six exposures, for 300V+ GG435, 4800 s in two exposures, and for V300I+OG590 we integrated for 6961 s in four exposures, which gives a total integration time on the object of 25,680 s or just over seven hours in service mode.

A major part of the data reduction was performed using a developers release of the FORS pipeline software,

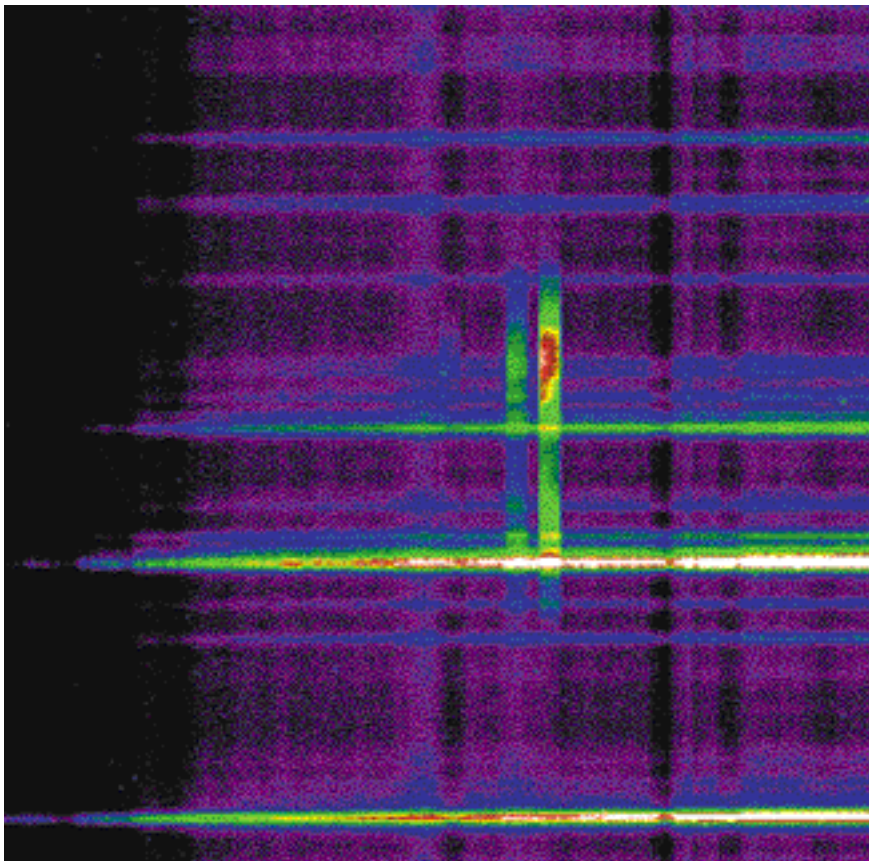


Figure 2: 2-D representation of a single FORS exposure with Grism 300V (2400 s). Shown is a region centred on 5000 Å with the two prominent [O III] lines. Slit width 2.5 arcsec.

which was made available to us by the Data Management and Operations Division (DMD) for evaluation. The FORS pipeline is implemented as a MIDAS context. In addition to the MIDAS package, we also had the chance to use the complete pipeline infrastructure (Data Organiser, Reduction Block Scheduler and Local Calibration Database) as it is used at the Paranal Observatory and by Data Flow Operations (DFO) in Garching. Usually, the pipeline infrastructure is not available to normal users. They have to use the MIDAS context RBS instead, which is part of the latest MIDAS release.

The pipeline was used to process the raw instrument calibration data (biases, flat fields) for each of the three instrument set-ups, which came bundled with the actual observations, to create master versions of the instrument calibration data. Also the dispersion relation was reliably determined by the pipeline for all instrument set-ups except for Grism 300I. It turned out that this was due to the emission-line catalogue used by the pipeline, which was not best suited for the combination of Grism 300I and 2.5 arcsec slit (a revision of the line catalogues used by the FORS pipeline is currently on its way). Therefore, a calibration-lamp exposure for the same instrument set-up, but for the FORS slit having a width of only 1.0

arcsec, was requested from the Science Archive for Grism 300I and processed by the pipeline. The obtained dispersion relation was then manually shifted by the appropriate offset which has been determined by cross correlating the line positions from the 2.5 arcsec slit exposure and the 1.0 arcsec slit exposure.

The science observations and the observations of the spectrophotometric standard stars were fed through the pipeline. As a final product we ob-

tained linearly rebinned, 2-dimensional spectra for the science data and sky subtracted, optimal extracted spectra for the spectrophotometric standards. Processing of spectrophotometric standards is still under evaluation by DFO and therefore not routinely used for pipeline reduction of service-mode data, but the results obtained with the developer's version of the FORS pipeline available to us are well within the limits set by our requirements.

Figure 2 shows a section of the 2D spectrum after bias subtraction and flat fielding have been performed. The dominant features are the emission lines from the night sky, many of which are much stronger than the nebular emission. After visual inspection, the spectrum was extracted and special care was taken to avoid contamination from brighter stars in the crowded field.

#### 4. Results

The spectrum of the PN around Sakurai's object we obtained with the combination of FORS/VLT has the highest S/N ever obtained. Furthermore, it extends the spectral coverage towards the red making additional lines available for analysis. From the Balmer decrement we derive a reddening  $E(BV)$  of 0.79, which is somewhat higher than earlier values derived from optical studies, but still within the error bars. This has some implications for the notoriously problematic distance determination. Highly discrepant values for the distance had been suggested by different methods (e.g. Duerbeck et al. 1997, Kimeswenger & Kerber 1998). The extinction distance method has yielded significantly lower values than other methods. With the new reddening value, distances larger than 2 kpc become possible and an improved reddening vs. distance relation is re-

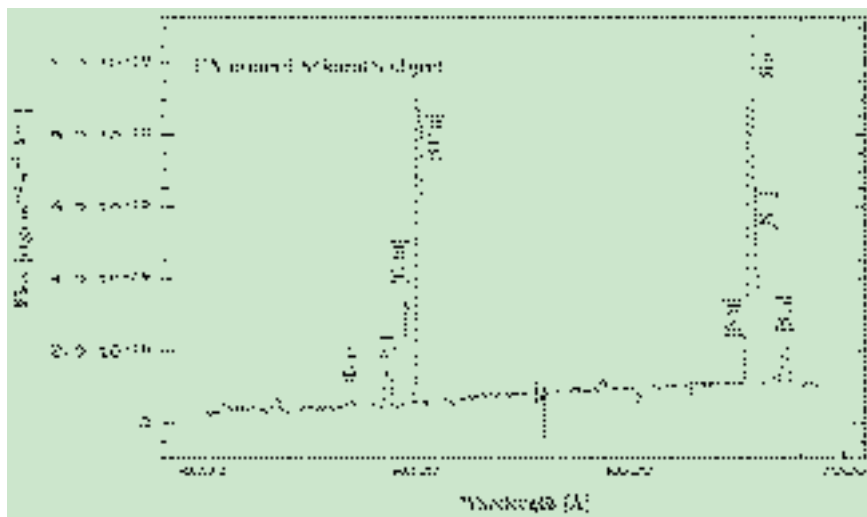


Figure 3: Spectrum extracted from a combination of the six Grism 300V exposures.

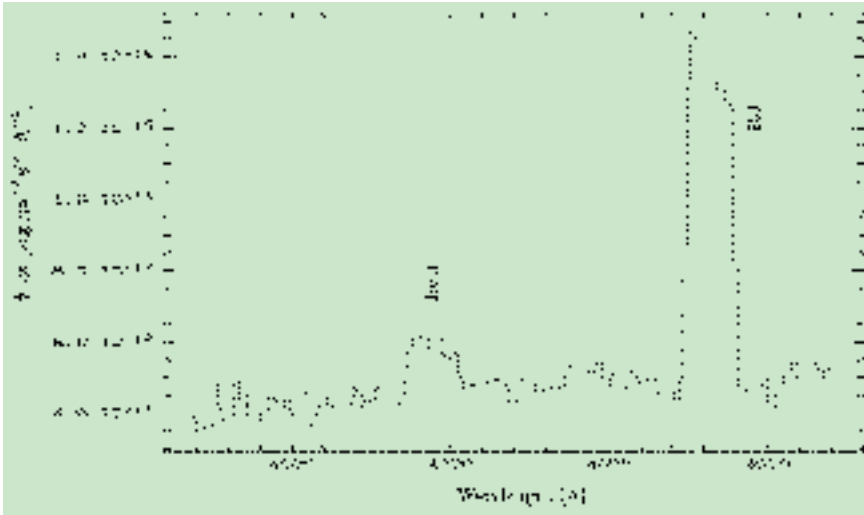


Figure 4: Expanded view of part of Figure 3 showing  $H\beta$  and the He II 4686 line.

Table 1: Intensities relative to  $I(H\beta) = 100$ , corrected with an extinction of  $c = 1.17$ .

[Å]	ID	$I/I(H\beta)$
4101	H	27.23
4340	H	58.5
4363	[O III]	5.9
4471	He I	9.2
4686	He II	19.0
4861	H	100
4959	[O III]	280.0
5007	[O III]	857.5
5875	He I	8.8
6548	[N II]	48.6
6563	H	304.3
6583	[N II]	171.0
6678	He I	5.0
6717	[S II]	31.7
6731	[S II]	22.2
7135	[Ar III]	14.1
7750	[Ar III]	3.1
9069	[S III]	27.4
9531	[S III]	78.1

quired to finalise the distance. From the nebular spectrum and the appropriate ionisation models alone a constraint on

$d$  cannot be obtained. Thus a reliable and accurate distance remains the greatest obstacle to a better understanding of Sakurai's object.

Preliminary analysis of the VLT data shows that most of the findings reported earlier can now be confirmed with a much higher level of confidence. In particular the best ionisation model in our previous study predicted an He II 4686 flux of about 20% of  $H\beta$ . This is beautifully corroborated by the new observations which show the helium line at a strength of 19% of  $H\beta$  (Table 1 and Figs. 3 and 4).

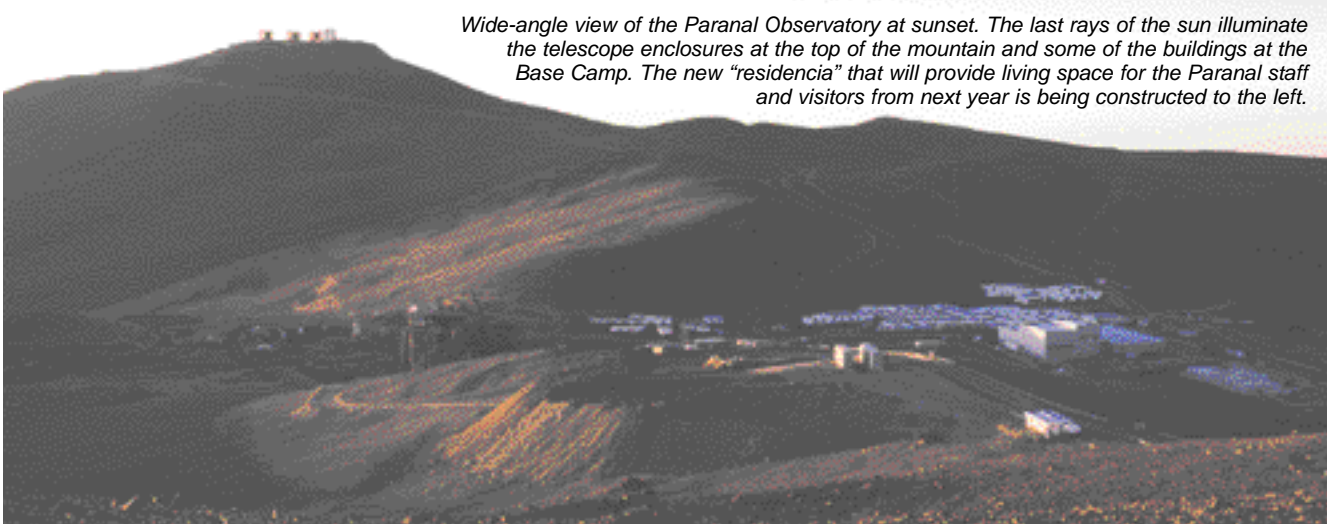
In our previous model we had assumed solar chemical composition, for which we had obtained a rather good fit. It has been demonstrated before that nebulae around hydrogen-deficient central stars have perfectly normal abundances. Examples are K 1-27 and LoTr 4 (Rauch et al. 1994, 1996).

With the photoionisation code GWYN (Köppen 1979; Rauch et al. 1996) we computed a grid of spherically symmetric models of solar composition nebulae, all having an angular di-

ameter of 32 arcsec at a distance of 1.5 kpc, with a density of  $100 \text{ cm}^{-3}$ . The best fit is given by  $T^* = 98,000 \pm 7000 \text{ K}$  and  $L^* = 25 \pm 5 L_{\odot}$ . For a distance of 5.5 kpc the best fit is at  $T^* = 95,000 \pm 7000 \text{ K}$  and  $L^* = 240 \pm 40 L_{\odot}$ . Our results show that Sakurai's pre-flash position in the HRD was indeed that of a highly evolved PN central star, entering the white dwarf cooling tracks. Thus, it is truly a case of a very late helium flash.

## References

- Asplund, M., Gustafsson, B., Lambert, D.L., Kameswara Rao, N., 1997, *A&A* **321**, L 17.
- Asplund, M., Lambert, D.L., Kipper, T., Pollacco, D., Shetrone, M.D., 1999, *A&A* **343**, 507.
- Blöcker, T., Schönberner D., 1997, *A&A* **423**, 991.
- Clayton, G.C., de Marco, O., 1997, *AJ* **114**, 2679.
- Duerbeck, H.W., Benetti, S., 1996, *ApJ* **468**, L111.
- Duerbeck, H.W., Benetti, S., Gautschi, A., van Genderen, A.M., Kemper, C., Liller, W., Thomas, T., 1997, *AJ* **114**, 1657.
- Iben, I., Kaler, J.B., Truran, J.W., Renzini, A., 1983, *ApJ* **265**, 605.
- Jacoby, G.H., de Marco, O., Swayer, D.G., 1998a, *AJ* **116**, 1367.
- Kerber F., Gratl H., Roth M., 1997, *IAU Circ.* 6601.
- Kerber, F., Gratl, H., Kimeswenger, S., Roth, M., 1998, *Ap&SS* **255**, 279.
- Kerber, F., Blommaert, J.D.A.L., Groenewegen, M.A.T., Kimeswenger S., Käuffl, H.-U., Asplund M., 1999a, *A&A* **350**, L27.
- Kerber F., Köppen J., Roth M., Trager S.C., 1999b, *A&A* **344**, L 79.
- Kimeswenger, S., Kerber, F., 1998, *A&A* **330**, L 41.
- Kipper, T., Klochkova, V.G., 1997, *A&A* **324**, L 65.
- Köppen, J., 1979, *A&AS* **35**, 111.
- Pollacco, D., 1999, *MNRAS* **304**, 127.
- Rauch, T., Köppen, J., Werner, K., 1994, *A&A* **286**, 543.
- Rauch, T., Köppen, J., Werner, K., 1996, *A&A* **310**, 613.
- Seitter, W.C., 1987, *The Messenger* **50**, 14.



Wide-angle view of the Paranal Observatory at sunset. The last rays of the sun illuminate the telescope enclosures at the top of the mountain and some of the buildings at the Base Camp. The new "residencia" that will provide living space for the Paranal staff and visitors from next year is being constructed to the left.



## The UVES Data Reduction Pipeline

P. BALLESTER<sup>1</sup>, A. MODIGLIANI<sup>1</sup>, O. BOITQUIN<sup>2</sup>,  
S. CRISTIANI<sup>1</sup>, R. HANUSCHIK<sup>1</sup>, A. KAUFER<sup>1</sup>, S. WOLF<sup>3</sup>

<sup>1</sup>European Southern Observatory; <sup>2</sup>Royal Observatory of Belgium, Brussels; <sup>3</sup>Science Computing GmbH, Munich

### 1. Introduction

The Ultraviolet-Visible Echelle Spectrograph (UVES) was the first instrument installed at the second VLT Unit Telescope KUEYEN at the end of 1999. UVES is a high-resolution cross-dispersed echelle spectrograph covering the wavelength domain from the ultraviolet at 300 nm to the near-infrared at 1100 nm with two optical arms, which can be used in dichroic mode for parallel observations (Dekker et al., 2000). Its large-size echelle gratings, each 84 cm long, make it possible to achieve a spectral resolution of up to 80,000 in the blue arm and 115,000 in the red. It is equipped with 3 CCD detectors each of size 4K × 2K pixels, one EEV CCD in the blue arm, and an EEV/MIT CCD mosaic in the red arm. Commissioning observations have shown the high intrinsic efficiency of this instrument, particularly in the ultraviolet domain (13% at 360 nm). More than 200 hours of scientific observations from UVES commissioning and science verification time have been released for public use. The instrument started regular operation in visitor and service mode on April 1, 2000, and is used for about 75% of the telescope time (D'Odorico, 2000).

The need to provide quick-look reduction of the data at the telescope, to monitor the instrument performance and to prepare the data distributed to service mode observers are the major drivers for VLT instrument pipelines. In the case of UVES, with the 500 spectral formats supported by the instrument and the expected 2.5 Gbytes of daily data, special emphasis was put into designing methods for automated spectral format calibration supported by physical models. These methods were prepared in 1998 and the pipeline integration started in 1999. After the initial phases of integration in Europe and commissioning of the instrument, the pipeline was first installed at the telescope during the second commissioning of the instrument in December 1999. It was then used for technical verification, and during the Science Verification that took place in February 2000. It was upgraded in March 2000 with a robust version, improved optimal extraction, support for

image slicer mode, an improved background estimation procedure and a complete update of the calibration database. The pipeline was then adapted to meet the needs of the Data Flow Operations (DFO) group in Garching, which delivers reduced data to service mode observers. A further upgrade with increased checks of quality control parameters was done in August 2000. Extended-source extraction, as well as the extension to support the FLAMES fibre port of UVES are under development.

### 2. Pipeline Operations

The UVES pipeline is tuned primarily to support operations in Paranal and Garching. The main difference between Paranal and Garching use of the pipeline lies mostly in the operational objective of the reduction. In Paranal it is used to have a quick look at the on-going observations and monitor the instrument health. DFO operations aim at providing the best-possible reduced products and at controlling their quality. As a consequence, the update rate of the calibration solutions differs between the two sites: daily in Garching, monthly at Paranal.

The Paranal pipeline is the one available to visiting observers at the telescope. It supports all standard settings of the instrument (11 central wavelengths and 4 detector modes) and makes use of pre-determined calibration solutions established for a reference configuration. The accuracy of this calibration is therefore limited by possible instrumental drifts for example due to temperature variations or earthquakes. The data-reduction software is robust to shifts of up to about ten pixels, and the spectral format is regularly compared at the telescope with reference calibration solutions. If a deviation is noticed that goes beyond the limit of robustness of the pipeline, it is necessary either to realign the instrument to the reference configuration or to update the database. Non-standard settings are also supported at the telescope. These solutions are however not stored in the calibration database, but in a temporary area and are removed at the end of an observing run.

The Garching pipeline is the one used by the Quality Control Scientists to prepare the reduced data distributed to service mode observers. The best possible accuracy is achieved drawing from the pool of available calibration data – either produced during the observing run, or as part of regular calibration programmes – the ones judged most suitable by the DFO Quality Control Scientist. The Garching pipeline applies the same pre-defined reduction strategy to all science data, independent of the scientific purpose of the observations. The quality of the calibration solutions is also measured and stored for trend analysis.

### 3. Reduction Procedures

To work its way through the many configurations, the pipeline makes use not only of the FITS header information, but also of the specific knowledge of the optical design of the instrument by means of a physical model. The model is involved at many stages of the calibration to provide reference values and initial solutions for the current configuration making the data reduction completely automatic. In addition to the calibration solutions, the pipeline delivers quality control information to help the user in assessing the proper execution of the data reduction process.

The UVES pipeline is able to provide good-quality science-data reduction for low to medium signal-to-noise data under the assumption that the object is a point-source, centred on the slit. The standard spectra extraction in the course of the reduction at Paranal or in Garching is made in optimal extraction mode which provides a maximal signal-to-noise ratio per bin, automatic sky background correction and cosmic ray rejection. Different reduction strategies can be implemented by using directly the data reduction package, which provides additional extraction methods and data reduction options.

#### 3.1 Predictive format calibration

The geometric calibration is a complete definition of the spectral format including the order position and the

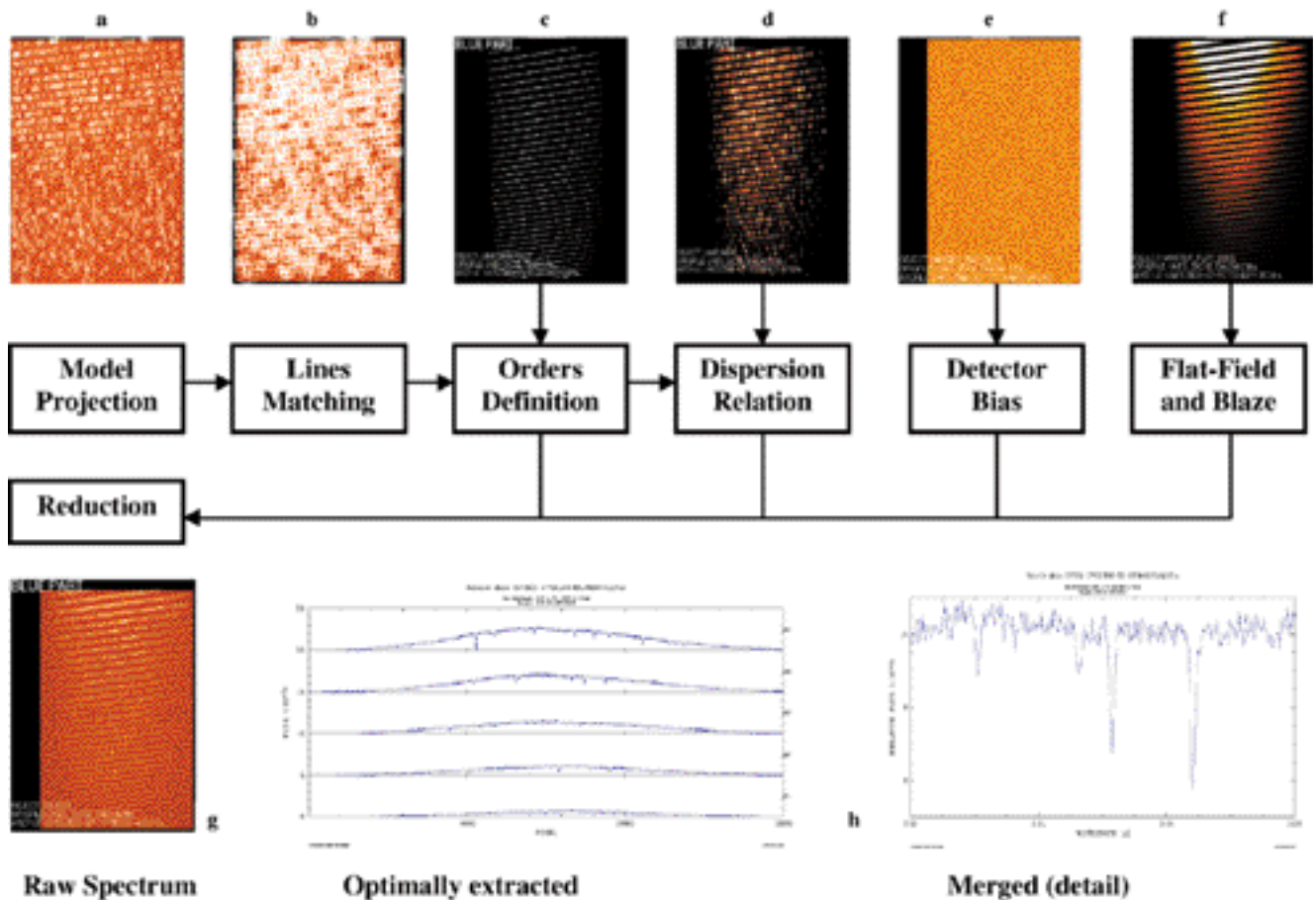


Figure 1: The general reduction scheme of the UVES pipeline. Model predicted positions of wavelength calibration lines are projected onto a format-check frame (a). The predicted positions are adjusted to the observed positions and an initial dispersion relation solution is produced (b). The order position is automatically defined on a narrow flat-field exposure using the physical model and a Hough Transform procedure (c). The initial dispersion relation is refined on a Th-Ar frame in order to fully take into account the slit curvature (d). Bias exposures are averaged to produce a master bias frame (e). Flat-field exposures are processed to produce a master flat frame and to determine the blaze function (f). The science frames are automatically reduced using the previous calibration solutions (g). After optimal extraction and or-der merging, a one-dimensional spectrum is produced (h).

wavelength associated to each detector pixel. This step was traditionally carried out via visual identification of a few lines and for this reason many new methods had to be developed. The precision with which the geometric calibration is performed determines the accuracy of all successive steps, in particular the optimal extraction and the photometric calibration. Initial methods for an automated detection of the order position and the wavelength calibration were developed using the Hough Transform method (Ballester, 1994). In the case of UVES, the high non-linearity of the dispersion relation required the development of a physical model of dispersion in order to predict the dispersion relation and to efficiently calibrate the several hundreds of optical configurations (125 central orders in 4 detector modes) offered by the instrument (Ballester & Rosa, 1997).

A template is dedicated to acquire a “format-check” frame (Fig. 1a, b), namely a ThAr calibration taken with a short slit height. The positions of a few hundred well-separated ThAr lines contained in a reference table are predicted by the physical model and their

central positions are projected onto the format-check frame. The lines are found in the narrow Th-Ar frame by a two-dimensional centring procedure. The initial dispersion relation, usually based on about a hundred initial detections on the spectrum until most lines are found.

The format-check data-reduction step generates control plots which provide a quality check of the model and of the stability of the instrument configuration. The difference between the predicted and measured position of the reference calibration lamp lines are plotted as a function of the position on the detector or the wavelength. Typically, a thin, well-clustered distribution of the displayed points, with mean value near zero, is a direct indication of good model prediction (Fig. 2a). On the contrary, a randomly scattered distribution indicates a probable instrument configuration shift (Fig. 2b). In this case one could guess adjusted model parameters. Once a concentrated distribution is found again, usually by changing the offset along the cross-order direction, the plot will have a mean

value close to the actual shift of the instrument configuration in the corresponding direction (Fig 2c). After the May 12, 2000 earthquake event, the instrument control parameters have been readjusted to a reference configuration.

A preliminary step toward the reduction of echelle spectra is the definition of the order position (Fig. 1c). For the sake of accuracy and stability of the slit tracing, this operation is usually performed on contrasted, continuous spectra such as flat-fields or bright star exposures. A specific narrow flat-field template was defined for this purpose. It takes an exposure of the flat-field lamp with the shortest slit equal to 0.5 arcsec. This kind of exposure provides an accurate position of the spectrum along the cross-dispersion direction. In this step the physical model uses the information on the instrument configuration provided in the FITS header to estimate the number of orders present in the image. Hough Transform detection is then applied to find the central position of each order and an estimate of their slope at the centre. Finally the cross-order profile is centred along the order and a polynomial fit is performed.

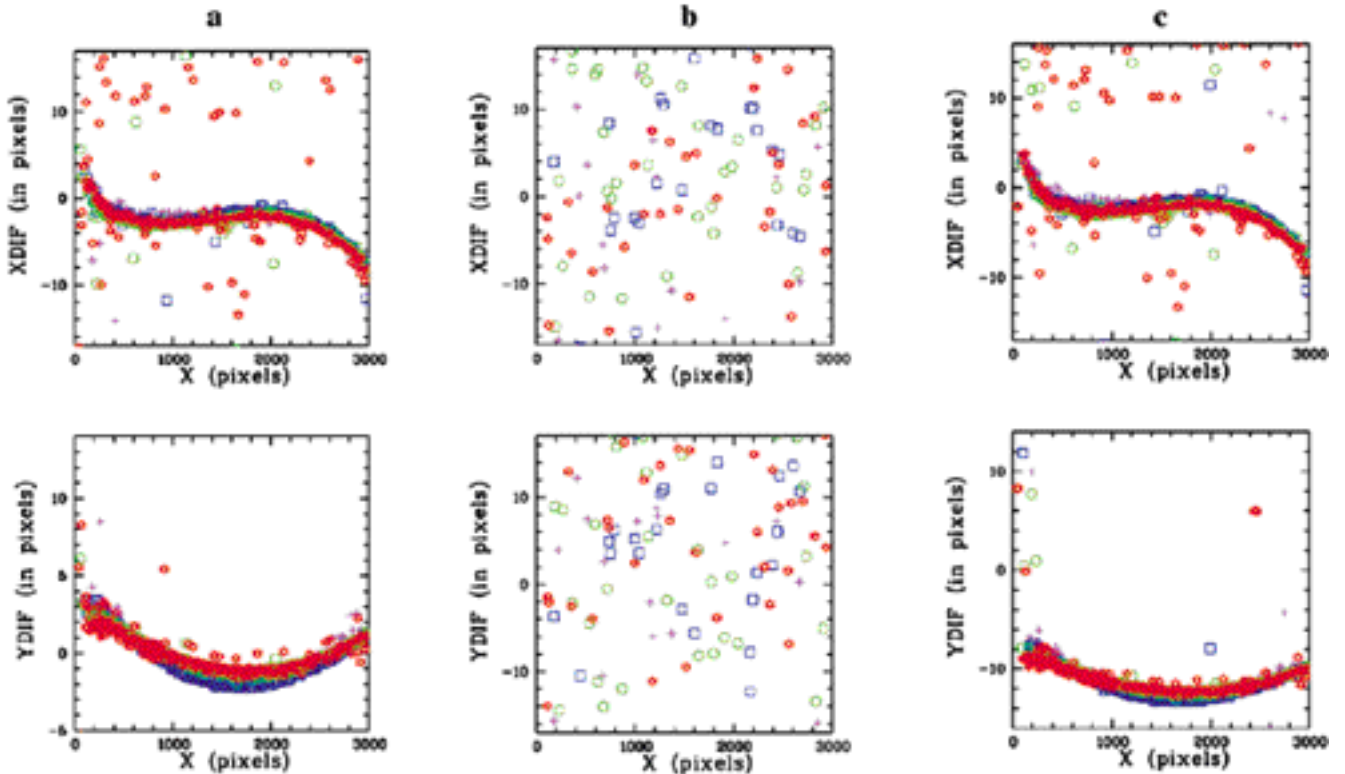


Figure 2: The May 12, 2000 earthquake event as detected from the physical model control plots. The normal result obtained after successful line matching (a) produces a well concentrated distribution with mean ordinate zero. The earthquake event causes the lines matching step to fail (b). Adjusting the model by  $-10$  pixels (along the cross-order direction) again matches the instrument configuration (c).

Three independent wavelength calibrations (Fig. 1d) are performed along the slit to take into account the potential effects of slit curvature. Three sub-windows are identified along the slit, one for the object and two for the sky, all equal in size. The initial dispersion relation produced with the format-check frame is refined on each sub-window.

From a set of bias exposures it is possible to produce a master bias image through a stacked mean (Fig. 1e). Similarly from a set of flat images it is possible to create a master flat image with master bias subtraction and background subtraction as well as to derive the blaze efficiency function for each order (Fig. 1f). Science raw data (Fig. 1g) can be processed using optimal or average extraction.

### 3.2 Optimal and average extraction

Optimal extraction is a minimal variance estimator of the flux at each wavelength. The algorithm introduced by Horne (1986) for long-slit data assumes that the illumination fractions of the spatial profile vary smoothly with the wavelength and can be adjusted by low-order polynomials. This assumption does not generally hold in echelle spectroscopy due to the inclination of the orders. Resampling the data along the spatial profiles would introduce periodic profile distortions and noise. Different methods have been devel-

oped for cross-dispersed spectroscopy (Marsh, 1989; Mukai, 1990) involving data resampling for the sole purpose of estimating the weights.

The optimal extraction algorithm of the UVES pipeline is based on profile fitting by chi-square minimisation. It estimates the object signal and sky background and performs cosmic ray rejection under the assumption of a Gaussian profile of the light distribution along the slit. The extraction is performed independently on each order. First the full-width at half-maximum and the position of the object is estimated for different subsections along the order. Next through a chi-square minimisation, the amplitude and the sky background are estimated. The Gaussian shape is a reasonable assumption for low to medium signal-to-noise data. Sky emission lines are removed during the extraction: they fill the whole slit and are accounted for by the constant term of the spatial profile. Tests have shown that the sky fine subtraction achieves an accuracy better than 5%. Strong sky emission lines may remain visible in the extracted spectrum as residual light and of course by the larger variance of the extracted spectrum. Cosmic rays are rejected by comparing the raw cross-order profile with the result of the fit. One of the common difficulties in optimal extraction schemes is to prevent the rejection of valid data samples by the cosmic ray rejection methods in particular on high signal-to-noise data. In the UVES pipeline, the

rejection threshold is therefore adjusted to the signal-to-noise so that the cosmic-ray rejection is relaxed for increasing signal-to-noise data, converging to an average extraction scheme for high signal-to-noise data. Presently, this method appears to be appropriate for data with a signal-to-noise per bin up to fifty. For higher signal-to-noise, an average extraction is recommended which is also provided in the data reduction software.

In the average extraction, the source is centred on the slit and sky windows are determined. The object contribution is summed in the object sub-window, and the sky contribution is averaged and subtracted from the object. Data acquired in image slicer mode are processed with average extraction and without sky subtraction.

Both extraction methods, average and optimal, support the propagation of variance. The initial variance is estimated on the raw images by a noise model including read-out and photon noise. The variance images are then transformed together with the data frames on each processing step. Finally this information is used to optimally merge the orders and to deliver error bar estimates on the result spectrum.

### 3.3 Standard pipeline processing and general reduction

The standard pipeline processing of science data starts with data preparation: the raw input frames are rotated

Central wavelength: 580.0 nm, slit: 0.5 arcsec, CCD: EEV, 11.7 °C  
 Filename : UVES\_DIC1R\_CAL0723.fits, Observ. date: 2000-03-12T10:45:36  
 Median(DX) = 2.971 pix , Mean(DX) = 3.1 pix ,  $\sigma$ (DX) = 0.6 pix  
 Median(RES) = 80370.273 , Mean(RES) = 78713.703 ,  $\sigma$ (RES) = 7959.0

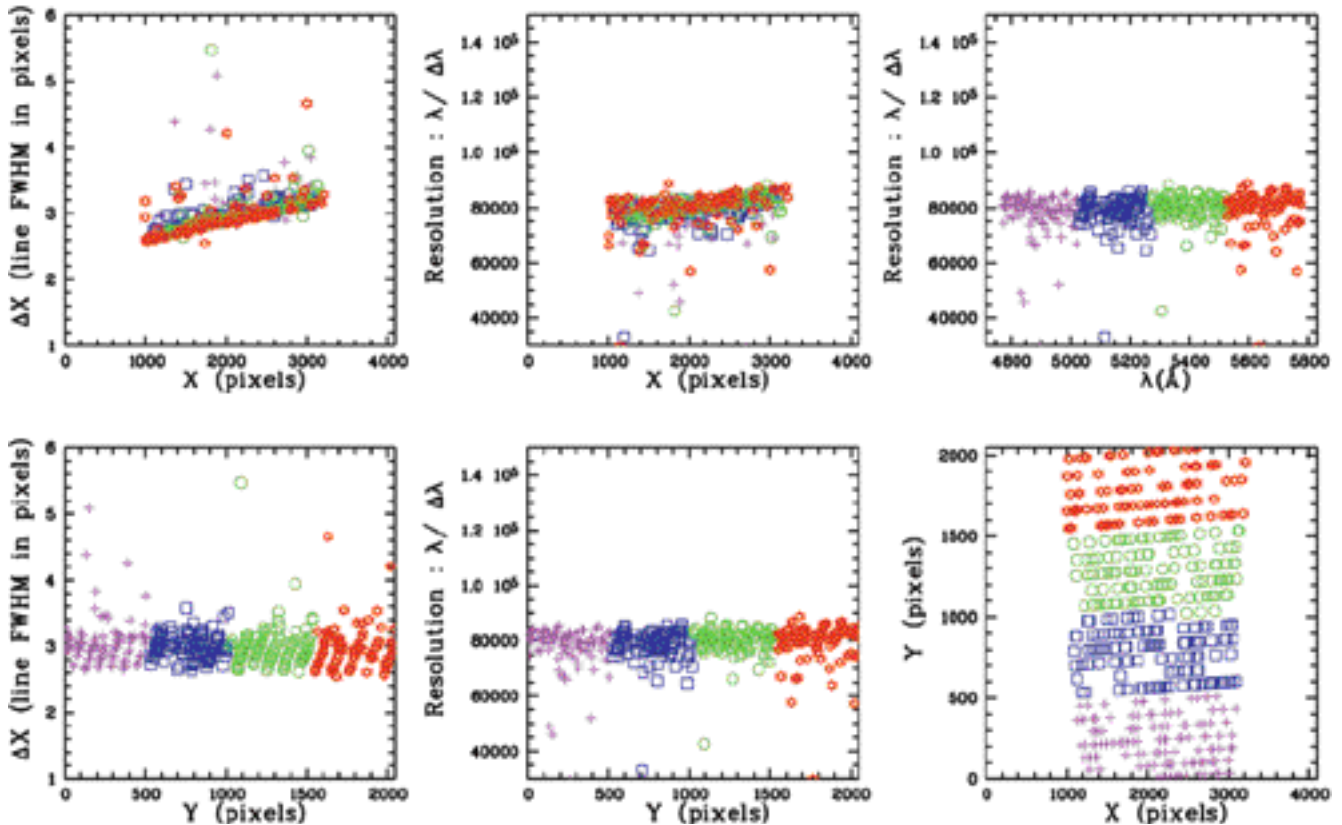


Figure 3: These plots show the FWHM of ThAr lines (left) and the instrument resolution (centre) as a function of the position on the detector along the X and Y directions, and finally the resolution versus wavelength (upper right) and the distribution of measured lines over the detector (bottom right).

and in the case of the red mosaic data, split for each detector. The instrument's background light is corrected in two steps: a master bias frame is subtracted and the inter-order background light is estimated by a minimum filter. The optimal extraction provides the object signal and its variance. The flat-field correction is performed in the standard reduction scheme in pixel-order space on the extracted data. The signal is then resampled to constant wavelength bins and the orders are merged into a single spectrum. The most time-consuming steps in the science reduction process are the inter-order background subtraction and the optimal extraction of the spectra. On Paranal, a  $4K \times 2K$  science exposure produced by one red detector is fully reduced in about six to twelve minutes depending on the machine.

In echelle spectroscopy, for a proper merging of the adjacent orders, a prerequisite is the correction of the blaze function. The UVES pipeline makes possible to estimate the blaze function from a spectrophotometry standard or from a flat-field exposure. The analysis of standard stars makes use of the target coordinates to look up in the database the appropriate flux reference table, reduces the star spectrum and determines the conversion factor for

each order. In standard pipeline reduction, the blaze function is estimated from a flat-field exposure, which after extraction, wavelength calibration and smoothing enables merging of adjacent orders with an accuracy of a few per cent.

The data reduction software and pipeline procedures are distributed as a MIDAS context on the 99NOV CD-ROM. It includes all the pipeline procedures for data reduction and on-line quality control, documentation, step-by-step examples and a tutorial demonstrating the complete calibration and reduction process for blue arm data. With this package, any user can interactively reduce the data, changing the options or the data selection with respect to the observatory pipeline. The user can interactively produce for all UVES configurations the calibration solutions necessary to properly reduce the raw science data.

#### 4. Pipeline Quality Control Procedures

Almost as important as data reduction is quality control. A number of procedures have been written to verify the instrument performance in terms of stability, efficiency and resolution. With format-check exposures a stability check can be performed. Using the

physical model, the line position on the actual format-check frame and on a reference format-check frame are measured and then the mean and standard deviation of the relative difference are determined. This quality control procedure has been particularly important to track the stability of the spectral formats since the beginning of operations (Figs. 2, 4).

During wavelength calibration, the mean, median, and standard deviation of line FWHM, and of the spectral resolving power are monitored as a function of the position on the detector. The resolution plot (Fig. 3) shows information on the instrument spectral resolution derived during the process of wavelength calibration.

On Paranal, the UVES pipeline records the quality control parameters in log files. Spectral resolution, instrument stability and efficiency parameters are tracked and stored together with environmental parameters measured by UVES sensors. These log files are archived for long-term trend analysis, and parsed for the generation of graphs accessible within the observatory to the operations teams. Figure 4 shows the evolution of the frame shift along the dispersion as a function of the observing date. This variation is correlated with the evolution of the temperature in

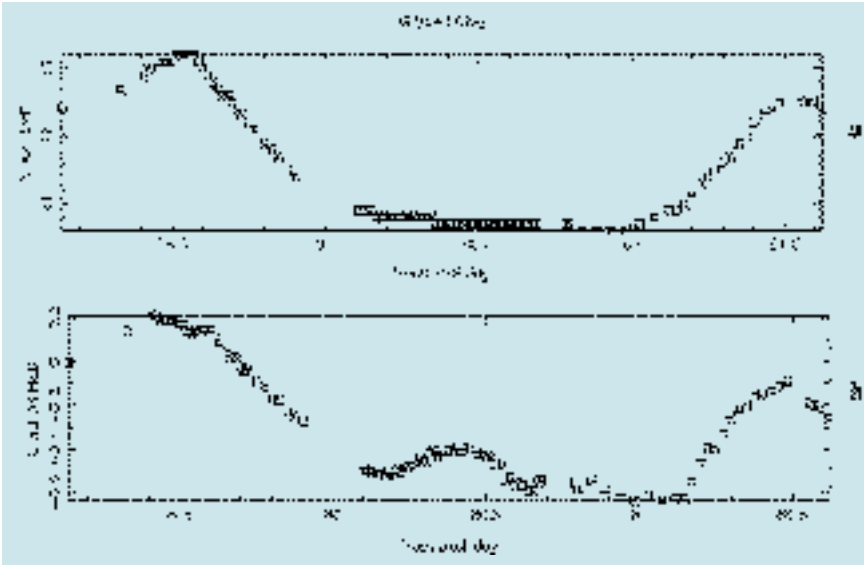


Figure 4: Evolution of the temperature in the instrument enclosure (a) and average shift in the dispersion direction (b) as a function of time over a period of 2.5 days. The two graphs show a strong correlation.

the instrument enclosure. The QC logs provide highly valuable information to the observatory to monitor the performance of the instrument and, if necessary, to recover or improve its quality.

The efficiency for each order at the blaze wavelength is monitored. The overall efficiency of the observation system, consisting of the telescope, instrument and detector, is determined as a function of wavelength by reducing spectrophotometry standards for which a flux table is available. It delivers an efficiency curve which makes it possible to directly track the reflectivity of optics coatings in the different wavelength domains and to verify the instrument performance predicted by the Exposure Time Calculators (<http://www.eso.org/observing/etc>).

The procedures for CCD characterisation are based on the MIDAS CCD package. Bias and flat-field exposures with different illumination levels are analysed to verify the CCD sensitivity and linearity maps. Usually a set of twenty-four exposures, six biases and nine pairs of screen flats exposures, each pair taken with the same exposure time, are used to determine several CCD parameters. For the 1×1 binned flat-field exposures, the intensities are measured in nine reference

sub-windows, uniformly distributed on the detector to detect possible edge contamination. One field is taken as reference. The relative intensities with respect to this reference field are logged for quality control.

### 5. Quality Checks by QC Garching

Although planned as an automatic data reduction ‘machine’, the UVES pipeline is also used by the Quality Control (QC) Scientist in Garching in a semi-interactive way to derive best-

possible calibration solutions and for reducing science data obtained in Service Mode. Procedures checking on the quality of pipeline results are essential here. They have been developed as post-pipeline procedures by the UVES QC Scientist to evaluate many of the pipeline-generated results.

As an example, Figure 5 shows the evolution of the spectral format in cross-dispersion direction (Y) for the blue (top) and red (bottom) gratings. These shifts are determined from flat-field exposures against a reference flat frame. They clearly correlate with UVES temperature. In addition, the May 12, 2000 earthquake has shifted the detector of the blue arm by more than 10 pixels.

Figure 6 shows a typical example of how the quality of a reduced (blue) spectrum is assessed.

1. The central row and column of the raw exposure are plotted. Here one can monitor any anomaly of the detector signal, e.g. unusual bias level.
2. A close-up of a central column (actually of 20 averaged columns) shows the (instrumental plus object) profile in cross dispersion direction. Here the exposure level, the centring and the sky background are controlled. These parameters are essential for assessing the quality of the optimum extraction.
3. Lower-left diagram: the full spectrum (S), its variance (N) and the signal-to-noise ratio (S/N) are plotted. The extreme left ends of S and N are shown at two different scales to fit in the graphic window. These

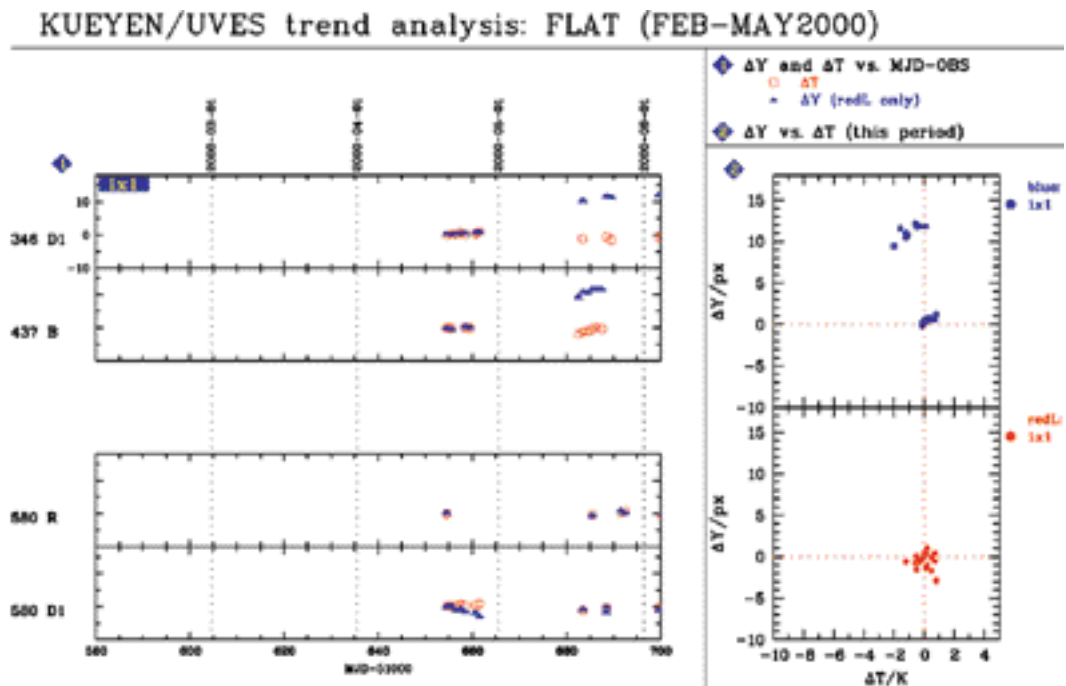


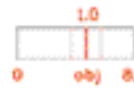
Figure 5: Left-hand-side panels: Vertical (cross-dispersion) shifts  $\Delta Y$  against temperature  $\Delta T$  for the blue (top) and red (bottom) gratings. For four of the  $2 \times 11$  standard settings,  $\Delta Y$  (blue triangles) and  $\Delta T$  (red circles) are plotted over time to monitor their trending. Right-hand-side panels: A composite diagram includes the two boxes on the right to visualise the thermal drifts of all gratings. The sudden non-thermal shift by more than 10 pixels on the detector of the blue arm was caused by the May 12, 2000 earthquake.

central wavelength: 3900.0; bin: 2x2; mode: D11

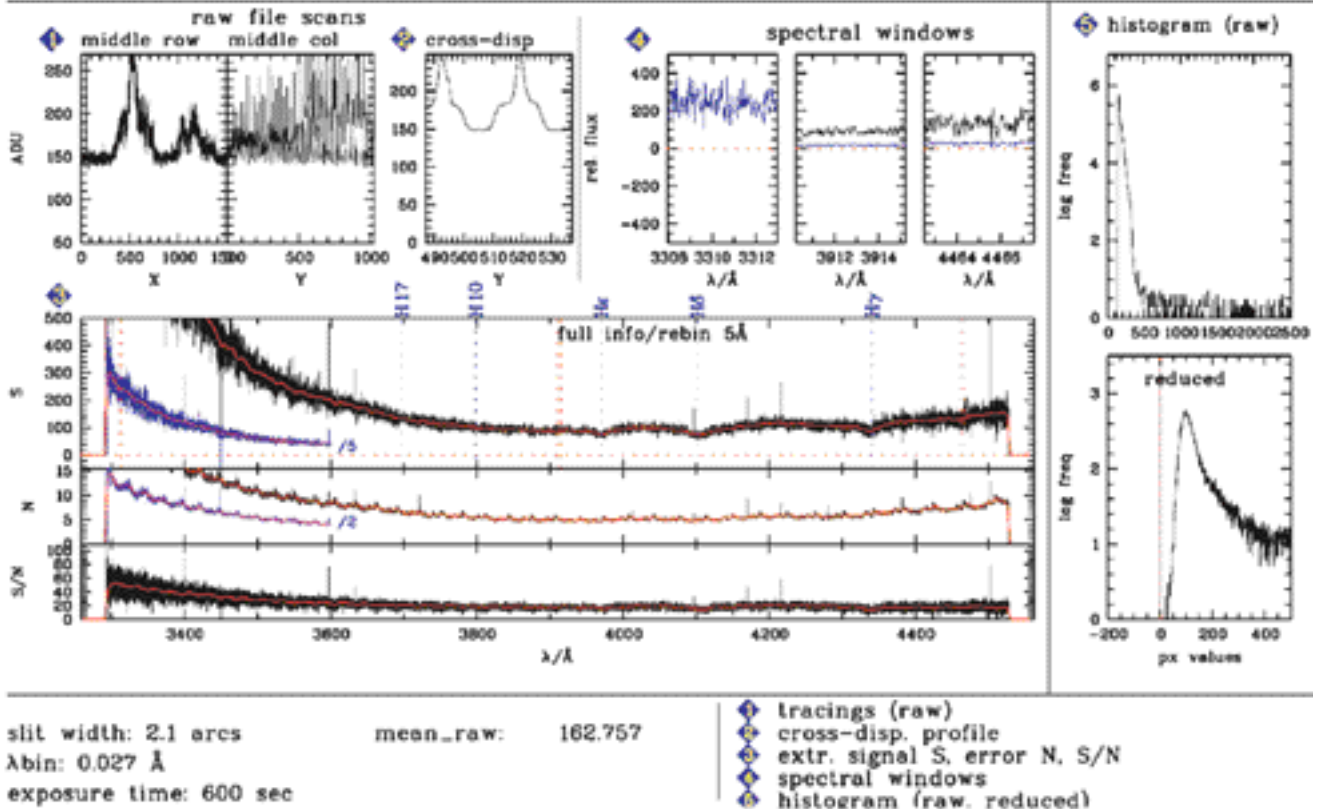
reduced: r.UVES.2000-07-16T09:15:59.939\_0000.fits

LINE2: PLI2\_000715A\_BLUE390d1\_2x2.tfits

ORDER: PORD\_000709A\_BLUE390d1\_2x2.tfits



mean T4 (Sci/Wave): 10.4/10  
 slit height: 8.0 arcsec  
 OBJ center: 4.7 arcsec  
 S/N: 21.3 (mean)



slit width: 2.1 arcs  
 $\lambda$ bin: 0.027 Å  
 exposure time: 600 sec

mean\_raw: 162.757

- tracings (raw)
- cross-disp. profile
- extr. signal S, error N, S/N
- spectral windows
- histogram (raw, reduced)

Figure 6: QC plot for a blue reduced science frame. See text in Section 5 for details of the plot.

- tracings permit an immediate check on the quality of the extraction.
- 4. Three spectral windows show enlarged portions of the full spectrum to check single bins.
- 5. Histograms of the raw and the reduced data provide further checks on anomalies.

Finally, three check-boxes (Fig. 6, upper right) raise alarm flags when

- the temperature difference between science and ThAr calibration frame is larger than a threshold value,
- the object is closer than 20% to the ends of the slit (check on centring). To the left of the middle check-box is a sketch of the slit showing the object position and the seeing FWHM.
- the signal-to-noise ratio is higher than a threshold value (then optimum extraction becomes unsafe).

Currently these plots are used to build up a trending database and to gain expertise for the quality assessment. It is planned to deliver these plots to the Service Mode observers. The UVES results from Quality Control Garching will be soon made public on the web (<http://www.eso.org/observing/dfo/quality/>).

During the first four months of operations, from April 1st to July 31st, 2000, more than 14,000 UVES raw files were produced representing about 153

Gbytes of data and including more than 4000 science frames. About half of these frames have been taken in service mode, resulting in 2640 reduced science spectra and 3852 calibration files produced with the pipeline.

### Conclusion

The UVES pipeline illustrates the increased efficiency and stability to be gained by the systematic use of instrument models and variance propagation in the reduction process. The cost of establishing new calibration solutions has been dramatically reduced, so that quick-look data reduction at the telescope is supported for most of the several hundreds instrument configurations. The instrument performance is monitored by comparing the calibration results with respect to the model and by measuring the effect of environmental parameters (temperature, earthquakes). All standard configurations of the instrument are supported in service mode and data packages are regularly shipped. A quality control database is being established for trend analysis.

### Acknowledgements

Many thanks to the UVES Principal Investigator, S. D'Odorico, the

project responsible, H. Dekker, and the UVES optical designer, B. Delabre, who provided many essential contributions to the design of this package since the beginning of the project in 1995.

### References

Ballester, P., 1994, Hough Transform for robust regression and automated detection, *Astron. Astrophys.*, **286**, 1011-1018.  
 Ballester, P., Rosa, M.R., 1997, Modeling echelle spectrographs, *Astron. Astrophys. Suppl.*, **126**, 563-571.  
 Dekker, H., D'Odorico, S., Kaufer, A., Delabre, B., and Kotzłowski, H., 2000, Design, construction and operation at the telescope of UVES, the Echelle spectrograph for the UT2 Kueyen Telescope at the ESO Paranal Observatory, Proc. Conf. SPIE 4008-61.  
 D'Odorico, S., 2000, UVES at Kueyen: Bright prospects for high-resolution Spectroscopy at the VLT, *The Messenger* **99**, March 2000, 2.  
 Horne, K., 1986, An optimal extraction for CCD spectroscopy, *PASP*, **98**, 609-617.  
 Marsh, T.R., 1989, The extraction of highly distorted spectra, *PASP*, **101**, 1032-1037.  
 Mukai, K., 1990, Optimal extraction of cross-dispersed spectra, *PASP*, **102**, 183-189.

## The ESO Observing Programmes Committee – an Evolving Process

CHRISTOFFEL WAELKENS, *Chairman of the OPC*

The Universe and its contents are evolving, but our tools to study the heavens at ESO are evolving at a much more rapid pace. The task of the Observing Programmes Committee (OPC) is each semester to recommend to the Director General among the typically 700 proposals introduced by the community those which are thought to lead to the best science with the available instrumentation. It is a challenging task, but also a gratifying one, since it continually confronts one with the rich scientific imagination of the ESO community. This community also frequently expresses its curiosity about the OPC procedures and criteria to rank the observing proposals. The information which is currently posted on the ESO web site might not be detailed enough on the procedures, which in fact recently underwent some changes which needed discussion within the committee before being implemented. The purpose of this contribution is then to explain to the community in some detail how the OPC currently operates.

Cosmologists need the cosmological principle to make sense of the evolving Universe. A credible assessment of observing proposals also needs isotropy and homogeneity: it is essential that every proposal gets a fair chance, and also that adequate ways are found to gauge proposals which cover a wide range of science domains. Aiming at a fair distribution of observing time has of course always been the main goal of the OPC, but putting this into practice within an environment characterised by changing possibilities and constraints, has induced rethinking of the process at about every OPC meeting. Nevertheless, the change has been a continuous one, which builds on the experience of several generations of OPC members.

### Composition of the OPC

The OPC consists of national delegates and members at large, who normally serve for three years. Each ESO member state designates one national delegate. In order to ensure that the expertise of these delegates is well spread over the different scientific sub-disciplines, Council has agreed in its June 1999 meeting that member states present a short list of candidates, and that the final designation is co-ordinated with ESO. The OPC chair is chosen among these national delegates. Members at large are chosen by ESO, after

consultation of the OPC chair, in order to complete the coverage of the different fields within OPC. Panels are organised according to scientific sub-disciplines, and contain – besides OPC members – experts, the number of which is determined by the typical workload of the panel. Panel experts are nominated for two years, and thus serve during four semesters. The length of their mandate is felt as a good compromise between the need for continuity in the process and a healthy rotation inside the ESO community.

The composition of the OPC is published every year in ESO's Annual Report and can be consulted on the ESO web site. The more rapidly changing composition of the panels is not made public, in order to maximally ensure the independence of the panel members and to avoid them being exposed to external pressure. In fact, in the renewed system (see below) it cannot be known beforehand to which sub-panel a particular proposal will be assigned, hence it is of little practical value to know the sub-panel composition. In the HST system, the composition of the panels is published after the time allocation for each cycle has been decided, but such a system is not practical to implement within the ESO system, where panel members serve for four periods.

### The New Panel System

The creation of OPC panels according to scientific domains was elaborated when the present Director General was OPC chair and was intended to relieve the workload on the OPC, which faced a steady increase of the number of proposals, and to actively involve a large number of experts from the community. There has been a continuous need to redefine the attribution of sub-categories to the different panels, essentially because of the evolution of the proposals when new instrumentation became available. For example, the availability of larger telescopes triggered the creation of a new extragalactic panel in 1997. It also significantly increased the potential for 'stellar work' in external galaxies, and thus had consequences for the overlap of sub-categories between 'stellar' and 'extragalactic' panels..

During the OPC meeting of December 1999 it was agreed that a major redefinition was in order. The evolution of the proposals was such that the work-

load had become quite unevenly distributed over the panels. On the other hand, it was felt that a further increase of the number of independent panels would too much narrow the scope of the panels and thus conflict with the healthy intertwinement of scientific questions which is at the heart of astronomy. The Sun is born in the Interstellar Medium panel, spends most of its life in the Cool Star panel, but ends as a white dwarf in the Hot Star panel, after a brief return in the Interstellar Medium panel during the planetary nebula stage! With this example in mind, it is not hard to imagine that with too narrow a panel definition, many proposals present severe overlap between aspects which formally belong to different panels.

The compromise which was agreed upon, is a new structure with four panels: A: *Cosmology*, B: *Galaxies and Galactic Nuclei*, C: *ISM, Star Formation and Planetary Systems*, and D: *Stellar Evolution*; thus the panels are not too specialised, a fact that applicants should take into account when writing their proposals. In order to achieve a reasonable workload, each panel is subdivided into two sub-panels, both covering the same scientific categories, which are listed in more detail on the web. There is thus not any more an independent *Solar System* panel; in fact, recent breakthroughs, e.g. on the study of cosmic dust, circumstellar disks and exoplanets, are truly interdisciplinary, and strengthen the general interest for solar-system research (now part of panel C). Also, the distinction between stellar projects on the basis of the evolutionary stage of the object removes much of the vexing overlap which often occurred in the old system, as well between star formation and stellar structure as between hot and cool versus massive and low-mass stars.

The assignment of a proposal to one of the two relevant sub-panels is done more or less at random, 'more or less' meaning that advantage is taken from the system to avoid conflict-of-interest issues, by systematically attributing a programme in which a sub-panel member is involved to the other sub-panel. A potential problem which immediately arises, is whether the procedure is optimal to judge similar projects which occur in different sub-panels. Therefore, after the panel meetings, unnecessary overlap of subjects and objects is identified, and the results of the deliberations are compared. Experience shows that the

issue is more academic than real. Moreover, it is a fact of life that individual biases affect any kind of evaluation if one wants this evaluation to be done by experts. The only solution is to average out these biases by rotating panel members regularly, and a dual panel system also effectively contributes to this.

### Activities Before the OPC Meeting

Despite the facts that applicants tend to wait until the very last minutes before the deadline expires and that some 700 proposals typically have to be treated, the Visiting Astronomers Office continues to manage to ship the proposals to the OPC and panel members within two weeks after the deadline. To each proposal three referees are assigned, from which the primary referee is expected to summarise the proposal at the meeting; all proposals in a sub-panel are expected to be read by every member, however. Two weeks are then given to the referees to identify unnoticed conflicts of interest and proposals that have been submitted to the wrong panel. When the replies have been received, corrections are made, and report cards are mailed to the referees on which these should write their grades and comments.

Before the meeting, documents are produced which summarise the evaluations by the referees. It should be stressed that these documents are of a preliminary nature: they essentially serve to prepare the panel meetings, during which all panel members are expected to intervene on every proposal. In order to minimise the bias introduced by a specific referee, it is recommended to the panel chairs not to discuss the proposals in the order of the average preliminary grades. Technical assessment about proposals is provided by ESO staff upon request by suspicious referees.

### Working Procedure for Large Programmes and Target of Opportunity Programmes

The VLT Science Policy document recommends that up to 30% of the telescope time should be attributed to large programmes, and this policy has since been extended to the La Silla telescopes. The idea behind is that experience with HST has shown that real breakthroughs often result from programmes, such as the Hubble Deep Field and the Hubble constant projects, to which large amounts of time have been devoted. Large programmes are also felt as a way to foster collaborations within the ESO community: not only many data but also much expertise helps to make progress! For the 2.2-m telescope, which is particularly demanded for surveys and other programmes which are preparatory for VLT science, more than 30% of the time may be awarded to large programmes.

Table 1. Time schedule for the OPC operations.

Date	Event
April 1, October 1 April 15, October 15 May 1, November 1 May 23, November 23 June 1, December 1 June 20, December 20	Deadline for submission of proposals Proposals arrive at the referees Proposal cards are issued to the referees Deadline for evaluations to be sent to ESO Start of OPC meeting Finalisation of comments on proposals

Before an OPC meeting, 30% of the time available on each telescope is set aside as a pool for large programmes, so as to make sure that the awarding of a large programme has no adverse effect on the fraction of time reserved for the regular programmes of a panel. The selection of large programmes is then the responsibility of the full OPC. On the other hand, a selection of such programmes by the OPC without the advice of the panels where the experts in the field reside, is clearly not wanted. Therefore, the first day of the OPC meeting is devoted to a discussion within OPC of the large-programme proposals, which results in a pre-selection which is then presented to the panels during days 2 and 3 of the meeting. During the last two days of the OPC week, the reports by the panels are discussed, and the OPC proceeds to the final selection of large programmes.

A similar procedure is followed for the selection of Target of Opportunity (ToO) proposals. Such programmes by definition get override status and thus need to be of high scientific priority in order to be recommended for scheduling. Moreover, by nature they most often concern the 'Stellar Evolution' panel, and if considered as regular programmes would bias too much the time allocation for this panel. During the first day of the OPC meeting, the ToO proposals are pre-discussed within OPC, and their final allocation is decided upon after they have been reviewed in the relevant panels.

### Working Procedure for Regular Programmes

The main task of the sub-panels is to provide grades and a ranking per telescope for the applications they received. During the two-day panel meetings, each proposal is summarised by the primary referee and then discussed by the whole panel. After the discussion of each proposal, a grade is given by every panel member, and the amount of time to be recommended is settled. Only when all proposals for a particular telescope are discussed, average grades are computed, and a listing of the proposals ordered according to their average grade is produced. On the basis of this listing, the panel is then free to discuss the achieved ranking and to change it.

Especially the unsuccessful applicants are eager to know what the ra-

tionale behind the recommendations was. An issue with which OPC has struggled for a long time, and which the Users Committee has often put on its agenda, is the redaction of exhaustive comments for every proposal. It may be useful information for brain researchers to know that it is not easy for the mind of a panelist to formulate a detailed comment immediately after the discussion of a proposal: analytical and synthetic thinking appears to reside in widely separate places in the brain! The redaction of comments slows the panel discussions, which already occur under some time pressure, considerably. But, clearly the request by the community of detailed explanations is sound. The solution which is now adopted, is to charge the primary referees with noting the remarks by the individual referees and to summarise them by writing comments after the meeting, in time for ESO to include them in the email messages to the applicants who did not get time.

While in principle panel members have an idea about the total observing time they can dispose on, the essential result of their deliberation is the ranking of the proposals. During the final selection of the proposals during days 4 and 5, the OPC respects the ranking of the proposals made by the panels. The main task of the OPC is then to determine the cut-off line which delimits recommended from not recommended proposals. The word 'recommended' deserves to be repeated, since the final attribution of time is the full responsibility of the Director General, who has to take into account scheduling constraints and other technical issues, application of the Agreement with Chile, etc. On the VLT, about half of the proposals require the service observing mode. The final execution of these proposals depends on the conditions on Paranal. The highest rated proposals are safe, but proposals lower in the list often can be executed only partially. Conversely, it is useful to know that service proposals not recommended in the first place, but which are not demanding on seeing constraints, have a fair chance to be partially successful after all.

The amount of time which is available for regular proposals in the different sub-panels, is initially set as proportional to the total time requested for the proposals in these sub-panels. Clearly, merely attributing telescope time to panels proportional to the total time requested, can appear to be an abdica-

tion with respect to discussing the real science issues in the OPC. Moreover, institutionalising such a procedure might contain an incentive to introduce fake proposals; experience shows, however, that our community is most reasonable in this respect, and that people understand that such an attitude would rapidly become self-destructive. Ideally, then, in order to recommend the highest-quality science, an OPC discussion should be held on the relative merits of the proposals in the sub-panels, and the cut-off lines should be modified accordingly. This final adjustment of the cut-off lines is not an easy issue, however. OPC members, who lively remember the thorough discussions they had in their panel, tend to refrain from reshaping the picture from much shorter discussions with less involvement from the experts in the field. Moreover, with eight sub-panels, any formal voting procedure which is systematically applied for each telescope, tends to be cumbersome, and for this very reason often hardly influences the result.

But it remains true that OPC members should strive, to the extent possible, towards gauging the quality of the science in their (sub-)panel to that in the others. If this did not happen, the system might degenerate into four or even eight independent OPCs, a situation which should definitely be avoided! It should be pointed out, however, that thorough multidisciplinary scientific discussions occur within the OPC for the large and ToO proposals, which concern all OPC members. Also, at the OPC meeting that follows the panel meeting, each panel presents its highlights to the whole OPC. In general, the very fact of living a full week together entails many opportunities for cross-fertilising. When more nights become available for regular programmes, because of the non-selection of large programmes, discussion naturally arises within OPC on which panel presents the best case for this additional time. Finally, if a panel definitely feels it

needs more time than the preliminary amount, it is able to fight for it and thus to trigger an agreement on some redistribution of time, involving a discussion within the OPC on the scientific quality of the cut-off proposals. The latter has often occurred, but was not felt as a stringent necessity during the last OPC meeting, which may reflect that the broad scope of the new panels also has a beneficial redistributing effect on quality. To conclude, my grateful experience is that the OPC consists of scientists who are open to abandon any corporative attitude with respect to the other panels, but that they are not reluctant to require specific discussions and formal voting in order to recommend the best science.

### Concluding Remarks

After the last OPC meeting, several panel and OPC members expressed their positive opinion about the procedure, and no dissenting voice was heard. The dual panel system, which was adopted with some hesitation, passed its first test very well. It would be naive, however, to anticipate that no new evolution of the procedures should occur in the future. Quite soon two more VLT units with new instrumentation will become available, probably again leading to an increase of the number and a widening of the scope of the proposals.

In order to cope with the steady increase of projects and particularly of data, not only the OPC but also the community should respond positively to the challenge of accepting to evolve. The large programme concept was designed to increase the efficiency with which the VLT could achieve the fundamental science issues for which it was built. Its success will also rely, however, on the capacity of the fairly dispersed ESO community to co-ordinate the expertise which exists in the member states. Some efforts are clearly needed to foster collaborations between institutes in the different countries, and the commu-

nity is large enough to achieve this while maintaining a healthy competition. It would be an expression of the strength of astronomy in Europe if the question would become actual to increase the fraction of time to be devoted to large programmes to more than 30%.

A major way to involve the ESO community in the rich potential of the telescope park in Chile, is the OPC itself. Several experts, asked to join a panel, decline the offer because they fear the high workload. They are right that the workload is high, but by declining they miss an opportunity to be part of a most inspiring process. There is no reserved time for OPC or panel members, but participating in the discussions is a unique way of enlarging one's scientific culture and is very helpful to learn how best use is made of the ESO instruments. This way, the panel members can exert a positive feedback on the dynamism of research in their home institutes and contribute to inspire their colleagues in their home country. Since the panel system, involving much more than before the community in the evaluation process, was installed, the average quality of the proposals has been increasing significantly indeed.

This is my last *Messenger* report as chairman of the OPC. I take advantage of this opportunity to express my gratitude to the many colleagues with whom it was so stimulating to work: to both ESO directors general Riccardo Giacconi and Catherine Cesarsky, to the Section Visiting Astronomers and other ESO staff involved, and of course to my colleagues in the OPC and the panels. In particular, we owe much to Jacques Breysacher, who is the living memory of the OPC and the practical mind which guarantees that the job can be done within one week, to Christa Euler, who for three decades now continues to produce logistic miracles before, during, and after the OPC meetings, to the ever efficient Elizabeth Hoppe, and to my predecessor Joachim Krautter, who made the new OPC system work.

## ANNOUNCEMENTS

### Scientific Preprints

(July – September 2000)

- 1381. S.A. Ehgamberdiev et al.: The Astroclimate of Maidanak Observatory in Uzbekistan. *A&A*.
- 1382. J. Breysacher and P. François: High-Resolution Spectroscopy of the SMC Eclipsing Binary HD 5989: the Hell 4686 Emission Line. *A&A*.
- 1383. I.M. van Bemmelen, P.D. Barthel and T. de Graauw: ISOPHOT Observations of 3CR Quasars and Radio Galaxies. *A&A*.
- 1384. A. Pasquali, M.S. Brigas and G. De Marchi: The Mass Function of NGC 288. *A&A*.
- 1385. T.H. Puzia, M. Kissler-Patig, J.P. Brodie and L.L. Schroeder: Globular Clusters in the dE,N Galaxy NGC 3115 DW1: New Insights from Spectroscopy and HST Photometry. *AJ*.
- 1386. R. Siebenmorgen, T. Prusti, A. Natta and T.G. Müller: Mid Infrared Emission of Nearby Herbig Ae/Be Stars. *A&A*.
- 1387. M. Chadid, D. Gillet and A.B. Fokin: Van Hoof Effect Between Metallic Lines in RR Lyrae. II. Comparison with Purely Radiative Models. *A&A*.
- 1388. F. Comerón, R. Neuhäuser and A.A. Kaas: Probing the Brown Dwarf Population of the Chamaeleon I Star Forming Region. *A&A*.
- 1389. S. Cristiani and V. D'Odorico: High-Resolution Spectroscopy from 3050 to 10000 Å of the HDF-S QSO J2233-606 with UVES at the ESO VLT. *AJ*.
- 1390. F.R. Ferraro, B. Paltrinieri, F. Paresce and G. De Marchi: Very Large Telescope Observations of the Peculiar Globular Cluster NGC 6712. Discovery of a UV, H Excess Star in the Core. *ApJ Letters*.
- 1391. G.A. Wade et al.: An Analysis of the Ap Binary HD 81009. *A&A*.
- 1392. F. Primas, P. Molaro, P. Bonifacio and V. Hill: First UVES Observations of Beryllium in Very Metal-Poor Stars. *A&A*.

ESO, the European Southern Observatory, was created in 1962 to "... establish and operate an astronomical observatory in the southern hemisphere, equipped with powerful instruments, with the aim of furthering and organising collaboration in astronomy ...". It is supported by eight countries: Belgium, Denmark, France, Germany, Italy, the Netherlands, Sweden and Switzerland. ESO operates at two sites. It operates the La Silla observatory in the Atacama desert, 600 km north of Santiago de Chile, at 2,400 m altitude, where several optical telescopes with diameters up to 3.6 m and a 15-m submillimetre radio telescope (SEST) are now in operation. In addition, ESO is in the process of building the Very Large Telescope (VLT) on Paranal, a 2,600 m high mountain approximately 130 km south of Antofagasta, in the driest part of the Atacama desert. The VLT consists of four 8.2-metre and three 1.8-metre telescopes. These telescopes can also be used in combination as a giant interferometer (VLTI). The first 8.2-metre telescope (called ANTU) is since April 1999 in regular operation, and also the second one (KUEYEN) has already delivered pictures of excellent quality. Over 1200 proposals are made each year for the use of the ESO telescopes. The ESO Headquarters are located in Garching, near Munich, Germany. This is the scientific, technical and administrative centre of ESO where technical development programmes are carried out to provide the La Silla and Paranal observatories with the most advanced instruments. There are also extensive astronomical data facilities. In Europe ESO employs about 200 international staff members, Fellows and Associates; in Chile about 70 and, in addition, about 130 local staff members.

The ESO MESSENGER is published four times a year: normally in March, June, September and December. ESO also publishes Conference Proceedings, Preprints, Technical Notes and other material connected to its activities. Press Releases inform the media about particular events. For further information, contact the ESO Education and Public Relations Department at the following address:

EUROPEAN  
SOUTHERN OBSERVATORY  
Karl-Schwarzschild-Str. 2  
D-85748 Garching bei München  
Germany  
Tel. (089) 320 06-0  
Telefax (089) 3202362  
ips@eso.org (internet)  
URL: <http://www.eso.org>  
<http://www.eso.org/gen-fac/pubs/messenger/>

The ESO Messenger:  
Editor: Marie-Hélène Demoulin  
Technical editor: Kurt Kjär

Printed by  
J. Gotteswinter GmbH  
Buch- und Offsetdruck  
Joseph-Dollinger-Bogen 22  
D-80807 München  
Germany

ISSN 0722-6691

# PERSONNEL MOVEMENTS

## International Staff

(July – September 2000)

### ARRIVALS

#### EUROPE

ARNOUITS, Stéphane (F), Fellow  
FYNBO, Johan (DK), Fellow  
LEDoux, Cédric (F), Fellow  
SOLLERMAN, Jesper (S), Fellow  
ZOCCALI, Manuela (I), Fellow

#### CHILE

BAGNULO, Stefano (I), Fellow  
BROOKS, Kate (AUS), Fellow  
ELLISON, Sara (UK), Fellow  
JAUNSEN, Andreas (N), Fellow  
JEHIN, Emmanuel (B), Fellow  
MARCO, Olivier (F), Operations, Staff  
Astronomer  
MENDEZ BUSSARD, Rene (RCH),  
Astronomer/2P2  
SCARPA, Riccardo (I), Operations  
Staff Astronomer  
SELMAN, Fernando (RCH),  
Operations Staff Astronomer

### DEPARTURES

#### EUROPE

ALBRECHT, Miguel (D), Head of  
Science Archive Group  
BENOIST, Christophe (F), Associate  
EIS  
BOITQUIN, Olivier (B), Scientific  
Application Developer  
CARBOGNANI, Franco (I), Software  
Engineer  
CURRIE, Douglas (USA), Support  
Engineer to Adaptive Optics Group

ROGON, Thomas (DK), Scientific  
Applications Developer  
TELANDER WEISS, Christine (S),  
Division Secretary  
WIEDEMANN, Günter (D),  
Instrumentation Scientist

#### CHILE

BREWER, James (UK), Operations  
Staff Astronomer  
ELS, Sebastian (D), Student  
ENDL, Michael (A), Student  
MARCHIS, Franck (F), Student

## Local Staff

(June – September 2000)

### ARRIVALS

BAEZ, José, Electro Mechanical  
Maintenance Technician, Paranal  
CASTEX, Duncan, Telescope  
Instruments Operator, La Silla  
CERON, Cecilia, Data Handling  
Administrator, Paranal  
CORTES, José Ignacio, Telescope  
Instruments Operator, La Silla  
HADDAD, Juan Pablo, Electronics  
Technician, Paranal  
LOBOS, Claudio, Optical Technician,  
Paranal  
MARTINEZ, Mauricio, Telescope  
Instruments Operator, La Silla  
PINO, Andres Iván, Instrument  
Technician, Paranal

### DEPARTURES

GONZALEZ, José Luis, Cook,  
Guesthouse  
ROJAS, Luis, Cook, Guesthouse

# Contents

C. Cesarsky: Successful Completion of an Ambitious Project – A Midwinter Night's Dream .....	1
J.G. Cuby et al.: ISAAC: 18 Months of Paranal Science Operations ..	2
Message to the ESO Community: Opening of the VLT Visitor Focus ..	8

## THE LA SILLA NEWS PAGE

2p2 Team News .....	9
---------------------	---

## REPORTS FROM OBSERVERS

R. Maoli et al.: Cosmic Shear with ANTU/FORS1: An Optimal Use of Service Mode Observation .....	10
R. Falomo et al.: VLT/ISAAC Images of Quasar Hosts at $z \sim 1.5$ .....	15
C. Lidman et al.: Type Ia Supernovae, Cosmology and the VLT .....	18
F. Courbin et al.: Lensed Quasars: A Matter of Resolution .....	20
D. Currie et al.: 3D Structure and Dynamics of the Homunculus of Eta Carinae: an Application of the Fabry-Perot, ADONIS and AO Software. I. Motions in Homunculus .....	24
F. Kerber et al.: Unlocking the past of Sakurai's Object Using FORS/VLT	27

## DATA MANAGEMENT & OPERATIONS DIVISION

P. Ballester et al.: The UVES Data Reduction Pipeline .....	31
---	----

## OTHER ASTRONOMICAL NEWS

C. Waelkens: The Observing Programmes Committee – an Evolving Process.....	37
---	----

## ANNOUNCEMENTS

Scientific Preprints (July–September 2000) .....	39
Personnel Movements.....	40